



Investigation of minor groove binders (MGB),
non-ionic surfactant vesicles (NIV) delivery
systems and IL-4i1 as novel pathogen- and
host-directed drug therapy for tuberculosis

by

Lerato Hlaka

SUBMITTED TO THE UNIVERSITY OF CAPE TOWN

In fulfilment of the requirements for the degree

Doctor of Philosophy

Faculty of Health Sciences

UNIVERSITY OF CAPE TOWN

Supervisor: A/Prof. Reto Guler

Co-supervisors: Prof. Frank Brombacher

Dr. Mumin Ozturk

Cytokines and Disease Group,
International Centre for Genetic Engineering and Biotechnology
(ICGEB), Cape Town Component and Institute of Infectious Diseases
and Molecular Medicine (IDM), Division of Immunology,
Faculty of Health Sciences, University of Cape Town,
Cape Town, South Africa.

The copyright of this thesis vests in the author. No quotation from it or information derived from it is to be published without full acknowledgement of the source. The thesis is to be used for private study or non-commercial research purposes only.

Published by the University of Cape Town (UCT) in terms of the non-exclusive license granted to UCT by the author.

Table of Contents

TITLE PAGE	1
DECLARATION	4
ACKNOWLEDGEMENTS	5
LIST OF PUBLICATIONS	6
LIST OF ABBREVIATIONS	8
ABSTRACT	11
CHAPTER 1	13
LITERATURE REVIEW	13
1.1 TUBERCULOSIS	13
1.2 CURRENT TREATMENT CHALLENGES	13
1.3 TREATMENT STRATEGIES.....	14
1.4 MINOR GROOVE BINDERS AS PATHOGEN DIRECT THERAPY FOR TB.....	15
1.4.1 <i>Structure and binding selectivity</i>	15
1.4.2 <i>Minor groove binders against parasitic diseases</i>	16
1.4.3 <i>Minor groove binders against fungal diseases</i>	16
1.4.4 <i>Minor groove binders against bacterial diseases</i>	17
1.4.5 <i>Minor groove binders against antimycobacterial tuberculosis diseases</i>	17
1.5 DRUG DELIVERY SYSTEMS.....	18
1.5.1 <i>Nanoparticles</i>	18
1.5.2 <i>Liposomes</i>	18
1.5.3 <i>Non-Ionic Surfactant Vesicles (NIVs)</i>	20
1.6 HOST TARGETS FOR HOST-DIRECTED THERAPY	22
1.6.1 <i>Pathogenesis and Immunity of Mtb</i>	22
1.6.2 <i>Mycobacterium tuberculosis in macrophages</i>	23
1.6.2.1 <i>Macrophage activation</i>	23
1.6.2.2 <i>Classically activated macrophages (caMph/M1)</i>	24
1.6.2.3 <i>Alternatively activated macrophages (aaMph/M2)</i>	25
1.6.2.4 <i>Candidate genes upregulate in alternatively activated macrophages during Mtb infection: IL4i1.</i>	26
1.6.2.5 <i>IL-4i1 expression and activity</i>	28
1.6.2.6 <i>Functional role of IL-4i1 in immune responses</i>	30
1.7 STUDY AIM, OBJECTIVES OVERALL STUDY AIM:	32
PATHOGEN-DIRECTED DRUG TARGETS FOR TUBERCULOSIS THERAPY	33
CHAPTER 2 PUBLISHED MANUSCRIPT	34
SUMMARY	35
EVALUATION OF MINOR GROOVE BINDERS (MGBS) AS NOVEL ANTI-MYCOBACTERIAL AGENTS, AND THE EFFECT OF USING NON-IONIC SURFACTANT VESICLES AS A DELIVERY SYSTEM TO IMPROVE THEIR EFFICACY	36
2.1 ABSTRACT	37
2.2 INTRODUCTION.....	38
2.3 MATERIALS AND METHODS	41
2.5 DISCUSSION	45
2.6 ACKNOWLEDGEMENTS	47
2.7 FUNDING.....	47
2.8 TRANSPARENCY DECLARATIONS	47
CHAPTER 3 MANUSCRIPT IN PREPARATION	53
SUMMARY	54
EVALUATION OF <i>IN VIVO</i> EFFICACY OF MINOR GROOVE BINDERS (MGBS) AND NON-IONIC SURFACTANT VESICLES	

(NIVS) ENCAPSULATION AGAINST <i>MYCOBACTERIUM TUBERCULOSIS</i> VIA INTRANASAL ADMINISTRATION	55
3.1 ABSTRACT	56
3.2 INTRODUCTION.....	57
3.3 MATERIALS AND METHODS.....	59
3.4 RESULTS.....	63
3.5 DISCUSSION	65
3.6 ACKNOWLEDGEMENTS	67
3.7 FUNDING.....	67
3.8 TRANSPARENCY DECLARATIONS	67
HOST-DIRECTED DRUG TARGETS FOR TUBERCULOSIS THERAPY	76
THE ROLE OF IL-411 ON IMMUNE HOMEOSTASIS DURING STEADY-STEADY AND <i>MYCOBACTERIUM TUBERCULOSIS</i> INFECTION	76
CHAPTER 4	77
MANUSCRIPT IN PREPARATION	77
SUMMARY	78
CHAPTER 4	79
IL-411 REGULATES IN VIVO LOCAL T-CELL ACTIVATION AND PROLIFERATION AT STEADY- STATE	79
4.1 ABSTRACT	80
4.2 INTRODUCTION.....	82
4.3 MATERIALS AND METHODS.....	84
4.4 RESULTS.....	88
4.5 DISCUSSION	93
4.6 CONCLUSION.....	95
4.7 SUMMARY	101
4.8 ACKNOWLEDGEMENTS	101
4.9 FUNDING.....	101
4.10 TRANSPARENCY DECLARATIONS	102
CHAPTER 5	103
MANUSCRIPT IN PREPARATION	103
SUMMARY	104
CHAPTER 5	105
IL-411 REGULATES MACROPHAGE MEDIATED IMMUNE RESPONSES DURING ACUTE	105
<i>MYCOBACTERIUM TUBERCULOSIS</i> INFECTION.....	105
5.1 ABSTRACT	106
5.2 INTRODUCTION.....	107
5.3 MATERIALS AND METHODS.....	108
5.4 RESULTS.....	111
5.5 DISCUSSION	114
5.6 SUMMARY	114
5.7 ACKNOWLEDGEMENTS	115
5.8 FUNDING.....	115
5.9 TRANSPARENCY DECLARATIONS	115
CHAPTER 6	116
CONCLUSIONS.....	116
REFERENCES	120
APPENDIX.....	130

Declaration

I, Lerato Hlaka, hereby declare that the work on which this dissertation/thesis is based is my original work (except where acknowledgements indicate otherwise) and that neither the whole work nor any part of it has been, is being, or is to be submitted for another degree in this or any other university. I empower the university to reproduce for the purpose of research either the whole or any portion of the contents in any manner whatsoever.

Signature:

Signed by candidate

Date: 02.07.2019

Acknowledgements

I would like to express my heartfelt gratitude to the following people who have made this PhD thesis possible:

My deepest gratitude goes to my supervisors, A/Prof Reto Guler for allowing me an opportunity to work in his team and for his guidance, support, encouragement to be an independent thinker, always being open for discussion, providing constructive feedback and mostly for his patience throughout the study. Prof Frank Brombacher for allowing me an opportunity to work in his lab, his expert advice and encouragement. I would like to thank Dr Mumin Ozturk, who invested his time to teach me experimental microbiology, assist me with experiments; and for extensively reviewing this thesis.

I would like to thank Dr Justin Komgwap Nono for his guidance, mentorship and for investing his time to teach me experimental immunology.

Our collaborators: Dr Fraser Scott from University of Huddersfield, Huddersfield, England; Prof Collin Suckling, Dr Catherine Carter from University of Stathclyde, Glasgow, Scotland; Prof Harukazu Suzuki and Dr Sugata Roy from RIKEN Center for Integrative Medical Sciences, Yokohama, Japan.

My funders for making it possible: The South African Medical Research Council through its Division of Research Capacity Development under the SAMRC Internship Scholarship Programme from funding received from the South African National Treasury. The LOREAL-UNESCO For Women in Science Sub-Saharan Africa Programme for PhD grant. The Department of Science and Technology (DST) / South African National Research Foundation (NRF) Collaborative Postgraduate Training Programme under supervisor grant.

Ms Wendy Green, Mrs Dhuraiyah Abdullatief, Mrs Adri Wrickler, IDM finance office team and Ms Desne Jodamus from post-graduate funding office, for all their assistance with administrative issues.

The UCT Animal Unit staff, including, Ms Siziwe Xozwa, Mr Jabu Magagula, Mr Peter, Ms Julia, Mr Rodney Lucas and Dr Kim Tutt.

Dr Hlumani Ndlovu for his mentorship, motivation, encouragement and for always availing himself for advice and guidance

My fellow labmates from Brombacher lab. A special thanks to my "TB and Schisto

teams”, Dr Ousman Tamgue (my lab partner) for teaching PCR and qPCR, Mr Julius Chia (my Juju) for assistance with experiments, the advice and “the necessary evil”, Mr Nathan Kieswetter (Supernate), Dr Santosh Kumar, Dr Suraj Parihar, Ms Shelby Jones for assistance with experiments, Ms Shandre Pillay (“nayi le walk”) Ms Lorna Gcanga, Mr Jermaine Khumalo, Ms Paballo Mosala, Dr Nada Abdelaziz and Mr Thabo Mpotje, for all the lab assistance and friendships and to Dr Tiro Brombacher (sis T) for welcoming me into your home, the encouragement and the prayers. To my other friends and colleagues in the division and IDM Ms Khanyisile Kgoadi, Ms Nomfundo Sibiyi, thanks for sharing opportunities. To all of you, thank you for the laughs, the good times, the friendships, the discussions, the outings and the frustrations without you this thesis would have not been possible.

The former and current Brombacher lab staff: Ms Munadia Ansarie, Ms Raygaana Jacobs, Ms Nazilla Ghodzi for assistance with genotyping; Ms Fadwah Bowley, Ms Zarinah Sunday, Mr Marlon Petersen, Mr George Jacobs for technical assistance and Mr Ronnie Dreyer for assistance with flow cytometry. Ms Lizette Fick for assistance with histology.

I am indebted to Mr Edward George (Br V) and all my sponsors from the Catholic Institute of Education for all the invested support, prayers and guidance throughout my studies.

My friends and family thank you for the consistent motivation and support, especially Siphelile for being a guardian to my little girls (Enkosi maNzolo).

My prayer group, thank you for being my constant pillars of strength and encouragement.

To my dearest parents Mrs Stella Hlaka and my late father Mr Thabo Hlaka, thank you for allowing and always encouraging me to pursue my dreams. I thank you for believing in me even when it was hard for me to believe in myself, for the unconditional love, patience, motivation and endless support.

To my beloved precious little angels, Karabo and Naledi thank you for your patience, for being my motivation and my cheerleaders. Mommy loves you.

Lastly, I would like to thank the almighty God and my Lord and saviour Jesus Christ for the gift of life and His constant love and mercy for giving me the strength and courage to complete this study. Glory be to Him who reigns supreme.

This thesis is dedicated to my parents and my daughters.

“...I can do all things through Him who gives me strength...” Phillipians 4:13.

List of publications

1. **Hlaka L**, Rosslee MJ, Ozturk M, Kumar S, Parihar SP, Brombacher F, Khalaf AI, Carter KC, Scott FJ, Suckling CJ, Guler R. Evaluation of minor groove binders (MGBs) as novel anti-mycobacterial agents and the effect of using non-ionic surfactant vesicles as a delivery system to improve their efficacy. *The Journal of antimicrobial chemotherapy*. 2017;72:3334-41.
2. Scott FJ, Nichol RJO, Khalaf AI, Giordani F, Gillingwater K, Ramu S, Elliott A, Zuegg J, Duffy P, Rosslee MJ, **Hlaka L**, Kumar S, Ozturk M, Brombacher F, Barrett M, Guler R, Suckling CJ. An evaluation of minor groove binders as anti-fungal and anti-mycobacterial therapeutics. *European journal of medicinal chemistry*. 2017;136:561-72
3. Guler R, Mpotje T, Ozturk M, Nono JK, Parihar SP, Chia JE, Abdel Aziz N, **Hlaka L**, Kumar S, Roy S, Penn-Nicholson A, Hanekom WA, Zak DE, Scriba TJ, Suzuki H, Brombacher F. Batf2 differentially regulates tissue immunopathology in type 1 and type 2 diseases. *Mucosal immunology*. 2018;12:390-402.
4. Nono JK; Ndlovu H, Abdel Aziz N, Mpotje T, **Hlaka L**, Brombacher F. Interleukin-4 receptor alpha is still required after Th2 polarization for the maintenance and the recall of protective immunity to Nematode infection. *PLoS Neglected Tropical Diseases*. 2017; 11:1-17.
5. Nono JK, Ndlovu H, Abdel Aziz N, Mptoje T, **Hlaka L**, Brombacher F. Host regulation of liver fibroproliferative pathology during experimental schistosomiasis via interleukin-4 receptor alpha. *PLoS Neglected Tropical Diseases*. 2017;11.1-22.

List of abbreviations

aaMph- Alternatively Activated macrophages

AAT- Animal African Trypanosomiasis

APC- Antigen Presenting Cell

BMDM- Bone Marrow-Derived Macrophage

BSA- Bovine Serum Albumin

caMph- Classically Activated Macrophages

CFU- Colony Forming Unit

DMEM- Dulbecco's Modified Eagle Media

DOTS- Directly Observed Therapy Short Course

ESAT- 6- Early Secretory Antigen Target

EMB- Ethambutol

FCS- Fetal Calf Serum

GFP- Green Fluorescent Protein

HAT- Human Africa Trypanosomiasis

iNOS- Inducible Nitric Oxide Synthase

IFN- γ R- Interferon Gamma Receptor

INH- Isoniazid

KO- Knockout

MHC II- Major Histocompatibility Complex Class II

MTORC1- Mammalian Target of Rapamycin 1

MIC- Minimum Inhibitory Concentration

MGB- Minor Groove Binder

MDR- Multi-drug Resistant

Mmp- *Mycobacterium* membrane protein large

Mtb- *Mycobacterium tuberculosis*

NIV- Non-ionic Surfactant Vesicles

NFκB- Nuclear Factor kappa B

NO- Nitric Oxide

OADC- Oleic Albumin Dextrose Catalase

PBS- Phosphate-buffered Saline

PRR- Pathogen Recognition Receptor

PK/PD- Pharmacokinetic/Pharmacodynamic

PZA- Pyrazinamide

RIF- Rifampicin

RNI- Reactive Nitrogen Intermediates

SQ109- Sequella 109

TLR- Toll-like Receptor

TB- Tuberculosis

TNF- Tumour Necrosis Factor

TCR- T-cell Receptor

XDR- Extremely-drug Resistant

WT- Wildtype

Abstract

Tuberculosis (TB), caused by *Mycobacterium tuberculosis* is the leading infectious disease epidemic that claims over 1.6 million lives, while 10 million fell ill in 2017. South Africa is burdened with the third highest global incidences following India and China with high rates of co-infections with HIV and highest numbers of multi-drug resistant (MDR) and extremely resistant (XDR) TB per capita. The current treatment regimen is decades old and requires a prolonged period of 6 months. The lack of efficient TB therapy and the emergence of MDR and XDR TB, there is an urgent need to find new drug targets for TB therapy through understanding the complex host-pathogen interactions. This may then lead to pathogen, host-directed therapies (HDT) or adjunct therapies as well as the development of effective drugs and drug formulations for the treatment of TB.

Here we aimed to investigate potential targets for pathogen-and host-directed therapies for TB. We screened the anti-mycobacterial activity of 172 minor groove binder (MGB) compounds that selectively bind to AT-rich regions of the minor groove of bacterial DNA with the helical structure matching that of DNA in Mtb culture.

Of the 172 total compounds screened 17 hits were identified, of which 2, MGB 362 and MGB 364 displayed intracellular mycobactericidal activity against Mtb HN878 at an MIC₅₀ of 4.09 and 4.19 μ M, respectively, whilst being non-toxic. Encapsulation of MGBs into non-ionic surfactant vesicles (NIVs) demonstrated a 1.6- and 2.1-fold increased intracellular mycobacterial activity, similar to that of rifampicin when compared with MGB alone. Treatment with MGB 364 or MGB 364 formulation did not cause DNA damage in murine infected macrophages as displayed by low expression of γ -H2Ax compared to H₂O₂ and DMSO. Intranasal administration of MGB 364 and MGB-NIV 364 formulation showed one log reduction in bacterial burden with improved pathology and immune cytokine production when in formulation. However, intranasal administration of 10 mg/kg MGB 362 together with rifampicin had no effect on bacterial loads. In summary, the data demonstrate the potential of MGB as a novel class of drug/chemical entity in anti-TB therapy and NIVs as an effective delivery system in a novel anti-TB formulation.

Using deep CAGE and small RNA (CHIP-seq) technologies, International Center for Genetic Engineering and Biotechnology's Cytokines and Diseases lab in collaboration with the RIKEN Center for Integrative Medical Sciences (Yokohama, Japan) performed a novel transcriptomics study approach by conducting a genome-wide transcriptional analyses of RNA transcripts from classically activated macrophages (caMph) and alternatively activated macrophages (aaMph) during Mtb infection. We identified host

target genes that may play a role in host immune subverting mechanism by Mtb to hide away from host effector functions providing a possible target for host-directed therapy for tuberculosis. It is postulated that Mtb modulates the transcriptional landscape of IL-4/IL-13 alternatively activated macrophages (aaMph) to escape killing by reactive nitrogen intermediates (NO) and reactive oxygen species (ROS) functions by IFN- γ stimulated classically activated macrophages (caMph). Here we report on the immunoregulatory role of IL-4i1, a candidate gene that was upregulated in aaMph during Mtb infection. IL-4i1 is a secreted L-amino oxidase with antibacterial properties. The enzyme converts Phenylalanine (Phe) into phenylpyruvate releasing toxic products ammonia and hydrogen peroxide (H₂O₂) which in-turn cause immunosuppression of effector T-cells by directly inhibiting polarization, proliferation and function or by promoting the generation of Foxp3 T-regulatory cells. Thus suggesting that IL-4i1 is involved in immune-regulatory mechanisms and may be implicated in immune evasion mechanisms by the pathogen. Here we report on the role of IL-4i1 on tissue localized T-cell activation and proliferative status thus maintaining immune local immune homeostasis. Thus showing that the absence of IL-4i1 could cause autoimmunity. To determine the functional role of IL-4i1 during Mtb infection, IL-4i1 deficient mice and wild-type littermate controls were infected with H37Rv and hypervirulent HN878 Mtb strain. IL-4i1 deficient mice were highly resistant to both strains of Mtb at 12- and 21-days post-infection as denoted by significant reduction in bacterial loads, reduced inflammation, reduced tissue iNOS expression reduced recruitment of interstitial macrophages, pro-inflammatory cytokines showed a trend for reduction. Interestingly there was a significant increase in NO production in infected tissues. There was an increase in M1-like macrophages that correlated with increased pro-inflammatory cytokines and chemokines. These data suggested that IL-4i1 regulates macrophage-mediated inflammatory responses during acute Mtb infection thus showing potential as an immunomodulatory target for TB HDT therapy. The study thus provides a framework for new drug targets for the development of new effective drugs and vaccines for TB therapy.

CHAPTER 1

LITERATURE REVIEW

1.1 Tuberculosis

Tuberculosis (TB), a deadly epidemic caused by the widely spread pathogen, *Mycobacterium tuberculosis* (Mtb), remains a major global challenge responsible for many ill healths and deaths among millions of people each year [1]. Approximately one-third of the world's population is infected with Mtb. South Africa is burdened with the third highest global incidence of this deadly epidemic after India and China, high rates of co-infections with HIV and highest number of multi-resistant and extremely resistant tuberculosis per capita [1, 2]. An estimate of over 10 million of the world's population had developed TB in 2017, an estimated of 1.6 million deaths were due to the disease [1]. The high rates of multi-drug resistant (MDR) and extremely drug-resistant (XDR) TB development over the current TB regimen, propels an urgent need to find new therapeutic strategies for the treatment of TB [3, 4].

1.2 Current treatment challenges

The current regimen for drug-susceptible Mtb is decades-old. It involves a strict compliance phase to a cocktail of four drugs containing rifampicin (RIF), isoniazid (INH), pyrazinamide (PZA), and ethambutol (EMB), followed by a longer phase that involves RIF and INH [5]. The current regimen lasts up to six months and is effective provided full compliance by the patient [5, 6]. The major challenge associated with this regimen is the duration which makes it difficult for patient compliance, thus immensely contributing to the development of MDR and XDR Mtb strains because of dormant Mtb bacilli since the current regimen focuses on the target's bacterial replication [7]. To help facilitate the compliance to the current regimen, in 1991 WHO implemented the Directly Observed Therapy short course (DOTS) program [5, 6]. The program included case detection by sputum-smear microscopy, government commitment to TB control, regular supply of drugs, supervised treatment, and reports on the progress of the health system. However, due to inadequate diagnostics and treatments, DOTS was only effective to 45% of globally estimated TB cases [5]. Furthermore, HIV/AIDS and TB co-infections have contributed to an increased prevalence to TB incidences which increase the number of MDR cases. The current treatment for MDR can last up to 2 years and this involves the use of toxic less effective second- or third-line drugs that are not readily available in endemic areas [5, 7]. Thus, confirming an urgent need for new drug discoveries for the treatment of TB that ideally would have novel mechanism of action; rapid bactericidal activity; optimized

pharmacokinetic/pharmacodynamic (PK/PD); low potential for drug–drug interactions and an excellent safety profile [6].

1.3 Treatment strategies

Several advances are in the pipeline for the development of new drugs and vaccines for the treatment of TB. The complex interplay between host and pathogen has resulted in different approaches to identify drug targets for TB therapy. Using genomic and functional data analysis have identified host-pathogen inter and intra genes that could be potential drug targets for TB treatment [8]. Furthermore, several candidates of mycobacterial agents are on phase II and phase III of clinical trials. The STOP-TB partnership which was established in 2000 aims to eliminate tuberculosis as a public health problem through the development of new TB diagnostics, new drugs, new TB vaccines and new TB biomarkers [9]. In recent years the approval of bedaquiline and delamanid for treatment against MDR and XDR have shown promise for the development of more effective drugs [6, 10, 11]. However, some adverse effects were noted for these drugs including hERG toxicity which indicated the need for identification of different target agents for TB therapy [6]. Recent advances have used different strategies to identify useful targets through their different modes of actions through different screening methods [6]. For example, SQ109 an inhibitor of *Mycobacterial* membrane protein Large (Mmp) 3 which is an export protein important for the transportation of metabolites from the cytosol of Mtb [12]. Therefore, SQ109 acts by blocking the protein that is important for Mtb survival. One crucial step to achieving STOP-TB partnership 2050 goals is through the understanding host-pathogen interactions [4, 9]. The recent global complementary approach focuses on developing adjunct host-directed therapies [4, 13]. This aims at dissecting the immunological pathways involved in killing Mtb and how Mtb subverts and hides from this protective immune response for its survival [4, 13]. Targeting of host-factors may lead to identifying possible drug targets that may reduce inflammation, tissue damage, preserve lung function and enhance effectiveness of TB therapy leading to the development of effective drugs against Mtb and drug-resistant TB [4, 14]. Several classes of repurposed drugs have been identified as host-directed candidates for TB therapy. These include vitamin D, Metformin, Statins, Prostaglandin E2 among others [4, 15-18]. These drugs target a vast range of host immune responses against Mtb, including the release of innate antimicrobial peptides such as cathelicidin [19], enhancing autophagy, promoting phagosome maturation [20] and targeting host cholesterol/lipid metabolism [17]. Other host target candidates include various classes of coding and non-coding genes involved in host immunity Mtb. Examples include microRNAs, long non-coding RNA and transcription

factors which have important roles in regulating gene expression cellular pathways involved in immune regulation against Mtb or could be used as biomarkers for TB progression [4, 21-23].

1.4 Minor groove binders as pathogen direct therapy for TB

1.4.1 Structure and binding selectivity

Minor groove binders (MGBs) are a large class of compounds from the family Lexitropsins [24]. These are small molecules that have a helical structure that matches the curvature of DNA at the minor groove and thus strongly bind and form complexes with the minor groove of DNA [25]. Binding selectivity of the minor groove compounds with respect to the DNA base sequence it binds to depends on the structure of the compound [25, 26].

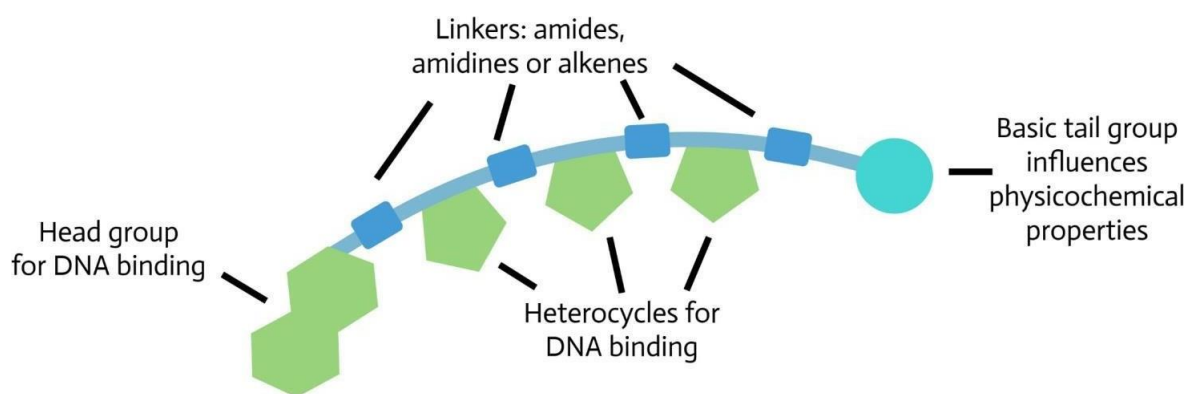


Figure 1.1 Graphical representation of a minor groove binder. [24]

Natural forms of MGBs such as the aromatic diamidines, pentamidine prefer binding at AT-rich regions of the minor grooves of DNA [27]. Their mechanism of action include interfering with gene transcription that controls DNA replication and topoisomerase inhibition [28]. The synthesis of several classes of minor groove binders from the University of Strathclyde (S-MGB) have shown activity against a range of infectious diseases [28]. Derived from the natural product distamycin, the many variations in the head to tail structure of S-MGB have shown successful selectivity against a wide range of infectious diseases [24, 28-30]. The current S-MGBs library which contains over 400 compounds, was made by varying several components of the structure of distamycin, these changes included a less basic functional group that replaces the amidine at the C-terminus (tail group). Methyl groups were replaced by larger alkyl side chains while body is made of and thiazole rings. The formyl group from distamycin was replaced by aromatic rings and the N-terminal amide has been replaced by its isosteric alkene [24, 28, 31] (Figure 1.1). The selectivity and activity against infective agents were linked to the structure and binding affinity to DNA. The different structural features based on charge and lipophilicity

are deemed essential for selectivity of penetration through cell walls of target organism. For example, *Trypanosoma congolense* was attributed to replacement of a pyrrolyl with phenyl/pyridyl [25], and for Gram-positive bacteria the isosteric replacement of an amide with an alkene, the replacement of a pyrrolyl with phenyl group and the inclusion of a less basic morpholine tail group were important [26].

1.4.2 Minor groove binders against parasitic diseases

Minor groove binders have been used against parasitic infections for decades. For example, the use of bisamidine, pentamidine and diminazene have been used for treatment against Human African Trypanosomiasis (HAT) and Animal African Trypanosomiasis (AAT) [32, 33]. The activity of furamidine and pentamidine against trypanosoma or plasmodia have been associated with DNA binding with specific affinity for AT-rich regions of parasitic minor groove of DNA [31]. The mechanism involved was linked to the destruction of the parasitic kinetoplast minicircles which are predominantly AT-rich, within 24 hours of exposure to pentamidines and furamidines [28, 33]. S-MGBs were studied for their activity against *Trypanosoma brucei brucei*. Modifications in the head and in the number of heterocycles were made upon synthesis to these compounds. The head group was linked by an amide, an amidine, or an alkene and the number of heterocycles between the head and the tail group was either two or three. Four compounds showed anti-trypanosoma activity in a nanomolar range and this was attributed to the alkene and amide linked head groups [34]. *In vivo* activities of these MGB compounds have been shown in mice infected with *T. congolense* [35]. MGBs with an alkene link between the two N-terminal building blocks showed nanomolar activity range against chloroquine sensitive (3D7) and resistant strains (Dd2) of *Plasmodium falciparum* infections. Most of the active compounds were those containing a C-alkylthiazole building block [36].

1.4.3 Minor groove binders against fungal diseases

Classes of MGBs have also been investigated against fungal infections by *Candida albicans* (*C. albicans*), *C. neoformans* and *Aspergillus fumigatus* (*A. fumigatus*). Many of which have shown cross reactivity with other anti-parasitic and anti-bacterial activities [28]. Analogues of pentamidines and di-cationic substituted bis-benzimidazoles, derived from classes of compounds that have excellent activity against several protozoan pathogenic organisms, showed potent fungal activity *C. albicans* and *C. neoformans* and other fungal species [37]. S-MGB compounds showed selective activity against *C. neoformans* over *C. albicans* and this activity was attributed to the insufficiency of the single interaction of cationic tail group from the tested compounds with the negatively charged phosphodiester

anion on the cell wall of *C. albicans* which allows the penetration of the MGB in the cell wall. Furthermore, the observed anti-fungal activities matched that against *Staphylococcus aureus* (*S. aureus*) [29]. Most of the active compounds were associated with the isoquinoline head group that potentially contributed to the threshold lipophilicity necessary for the observed activity [29]. Currently, these studies have advanced to *in vivo* “proof of concept” animal studies (unpublished data from Suckling and Scott groups).

1.4.4 Minor groove binders against bacterial diseases

Identification of an active molecular structure showing antibacterial properties requires a series of steps to verify a target as active. These steps include measurement of MIC and MBC; activity against a series of bacterial strains; measurement of static activity; potential to cause resistance and solubility, stability and formulation issues. A candidate successful of these steps is warranted for “proof of concept” studies that involve *in vivo* testing in animal models [28]. Distamycin A, GSQ 1530 has been reported for activity against gram-positive staphylococci species that include *S.aureus*; *S. epidermidis* and *S. haemolyticus* when tested against 73 clinical isolates [38]. *In vitro* killing kinetic study revealed a 3-log reduction of bacterial growth within 6h after exposure [38]. One S-MGB is currently undergoing phase IIa clinical trial for treatment of *Clostridium difficile* in partnership with MGB Biopharma. The compound consisting of a head group with a stilbene-like moiety and a body that consists of two N-methylpyrroles attached to an aminoethyl morpholine is active against Gram-positive bacteria [24, 26, 30].

1.4.5 Minor groove binders against antimycobacterial tuberculosis diseases

Distamycin analogues have been evaluated for their activity against *Mycobacterium tuberculosis*. Khalaf et al. [24] found that, replacing the N-terminal pyrrole-formamido moiety of Distamycin with biaryl units improved DNA sequence-selectivity binding for antimycobacterial activity [24]. Thiophene motif-containing polyamide exhibited a 10-fold increased Mtb compared to distamycin [39]. Our preliminary screenings of S-MGB compounds showed micromolar activity against Mtb without being toxic to mammal cells due to the substitution of the pyrrole group with a thiazole group which improved lipophilicity and increased binding affinity [29]. The identified structural features indicate an important class of minor groove binders that warrant hit to lead optimization for antimycobacterial activity [29].

1.5 Drug delivery systems

1.5.1 Nanoparticles

The use of nanoparticle drug delivery systems to the site of infection have been considered an important tool for the treatment of pulmonary TB in their advantage to encapsulate multiple hydrophilic and hydrophobic drugs. Nanoparticles are structures with sizes ranging from 1-100nm with unique physiochemical and chemical properties thus possessing favourable material for biomedical applications [40]. Strategic drug conjugation either through covalent linking or encapsulation is important for the outcome of targeted therapy. Cell-specific targeted approach through special carriers conjugated with recognition ligands at the surface of cells is aimed at retaining the drug longer at the site of infection [40, 41] mainly targeting alveolar macrophages which are used as a harbour by mycobacteria for prolonged survival. Furthermore, this would reduce systematic toxicity. A single dose of inhaled formulation would reduce the number of oral daily doses and thus improve patient compliance [42]. Oral therapy is still effective, but several patient relapses and drug resistance have been attributed to the high drug dose with multiple drugs. A single retainable prolonged low dose treatment shows potential for an effective treatment strategy.

1.5.2 Liposomes

Liposomes are the first class of drug carriers to be investigated. These are nano/macroparticles or colloidal spherical ranging from 80-300nm in size [40]. They are composed of phospholipids and steroids, bilayers and enclose a discreet aqueous spaces and other lipids which aids them to increase drug solubility and pharmacokinetic properties, cellular uptake and biodistribution to target sites *in vivo* [43, 44]. The major advantage of liposomes is that they can entrap both hydrophilic in the aqueous layer and hydrophobic molecules in the lipid bilayer. Their biocompatibility and self-assembly capability, ability to entrap several drug loads as well as the easy manipulation of their physiochemical and biophysical properties has shown favour towards their use as delivery systems for many biomedical applications [44]. Generally four classes of liposomes have been reported; conventional liposomes; sterically stabilized liposome; ligand-targeted and a combination of all types which are employed according to intended therapeutic use ranging from gene therapy, drug molecules, bioactive drugs, and adjunct therapy (Figure 1.2) [44]. Conventional liposomes face various defense challenges that are aimed at removing foreign particles from the body. These include reticuloendothelial system (RES); opsonization and immunogenicity [44]. To counter such challenges to improve permeability, effective treatment, reduce RES clearance and minimize toxicity, modified

forms of liposomes with changes in lipid composition, charges and the addition of cell surface ligands have been synthesized and investigated *in vitro* and *in vivo* for biomedical use [44]. For example, Antisense oligodeoxynucleotides (AsODN) with therapeutic efficiency against lung cancer when encapsulated into dendrosomes, a specialized form of liposomes, showed high suppression of target gene PKC- α in lung cancer cells with no apparent toxicity *in vitro* [45]. Mannosylated liposomes targeted at mannose receptor at alveolar macrophages have been used for the treatment of respiratory intracellular parasitic infection [46]. Mannosylated liposomes with 4-aminophenyl-a-d-mannopyranoside (particle size:1000nm) were used to encapsulate ciprofloxacin. Pulmonary administration of the mannosylated CPF-X-liposomes improved targeting efficiency was significantly greater than CPF-X in unmodified liposomes [46]. Liposomes have also been used for delivery of anti-TB for treatment *in vitro* and *in vivo* also following targeted approach [41, 42, 47, 48]. Encapsulation of first-line anti-TB drugs isoniazid and rifampicin into stealth liposomes improved Mtb clearance compared to free drugs following 6 weeks bi-weekly injections in mice. Liposome-encapsulated drugs at and below therapeutic levels reduced bacterial loads in lungs, spleen and liver significantly compared to free-drugs while being non-toxic [49]. Pandey et al. (2004) [50] reported on the efficiency of lung specific stealth liposomes encapsulated with rifampicin (RIF) and isoniazid (INH) intravenously administered to guinea pigs weekly for 6 weeks. Treatment with drug formulation sustained drug bioavailability for 96-168 hr in plasma, while tissue drug levels were retained for up to 7 days, a 2.9-4.2-fold increase compared to free drugs. Following 6 weekly treatments, Mtb clearance was improved in liposomal drugs compared to free drugs [50]. A single nebulization of liposomal INH and RIF maintained therapeutic plasma drug levels from 45mins to 48hrs and up to 5-days in lung tissue and alveolar macrophages, whereas drugs were cleared within 24hrs post-nebulization in free-drug treated guinea pigs [51]. Recently, Cheng and Schorey, (2019) used liposomes to deliver Mtb RNA derived from extracellular vesicles of Mtb-infected macrophages that activated RNA sensor signalling for IFN- β production, a mechanism that showed efficiency in adjunct therapy when combined with moxifloxacin *in vitro* and *in vivo* for Mtb treatment [48]. The shortfall for the use of liposomes as delivery systems in the clinical practice is associated with the technology and manufacturing costs, stability of formulations and quality assurance [42, 44, 47].

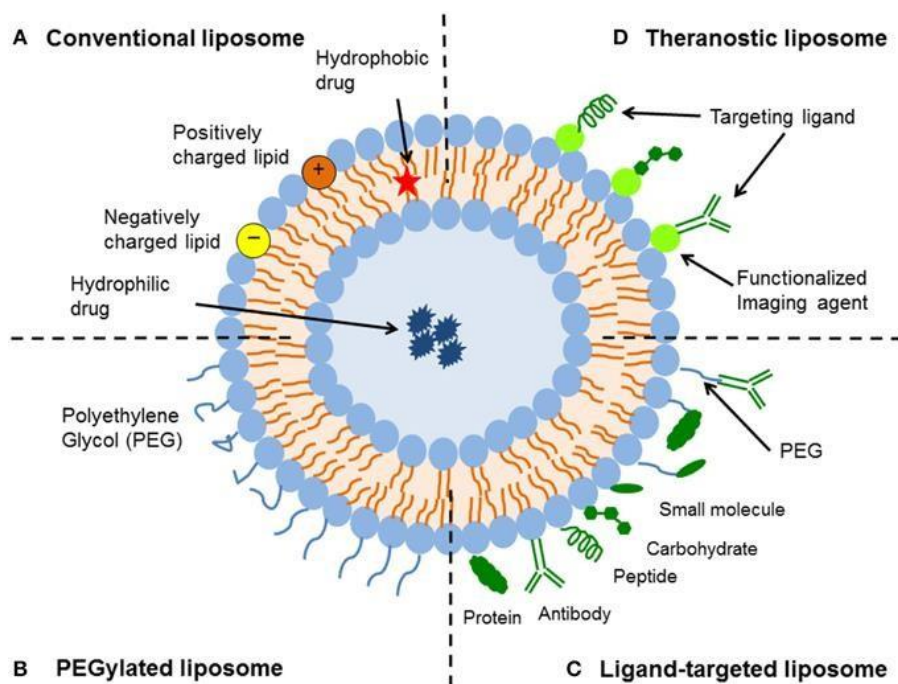


Figure 1.2: Representation of different types of liposomal drug delivery systems derived from [44]. There are four types of liposomes A) Conventional liposome B) PEGylated liposome C) Ligand-targeted liposome and D) Theranostic liposomes each with its own characteristics advantages and disadvantage.

1.5.3 Non-Ionic Surfactant Vesicles (NIVs)

Non-ionic surfactant vesicles (NIVs), small colloidal particles which are composed of a non-aqueous, non-ionic surfactant bilayer surrounding a central aqueous compartment are a better alternative to liposomes in that they are thermodynamically stable, they can be easily manufactured, size can be altered easily, they have flexible storage conditions and are cost-effective (Figure 1.3) [52]. Generally, they are less toxic, less hemolytic, less irritating to cell surfaces and stable at physiological pH in solution [52]. NIVs have been evaluated in several studies in the treatment of infectious diseases. A study to evaluate the use of NIVs as a delivery system on pulmonary treatment of fungal infection showed that amphotericin B (AMB), used for the treatment of fungal and leishmania infection had a significantly higher efficiency when encapsulated into NIVs. (AMB)-NIV delivered by nebulization, significantly reduced fungal lung burdens in rat model of invasive pulmonary Aspergillosis compared with carrier alone [53]. AMB-NIV reduced *Leishmania donovani* liver burden compared to AMB alone, however had no effect on the formation of cutaneous *Leishmania major* lesions without being toxic to host [54]. Single dose treatment with nonionic surfactant vesicle formulation of sodium stibogluconate (SSG-NIV) against visceral leishmaniasis significantly suppressed spleen and bone-marrow parasite burdens compared to SSG free drug in BALB/c mice [55]. In study to

evaluate the release efficiency of different types of NIVs that were encapsulated with Ciprofloxacin (CPFX) based on the methods of preparation, Akbari *et al.* (2015) showed that all formulations of CPFX had higher antibacterial activity compared to free CPFX solutions. However, there have not been studies on the use of NIVs as delivery systems in the treatment of Mtb infections [56].

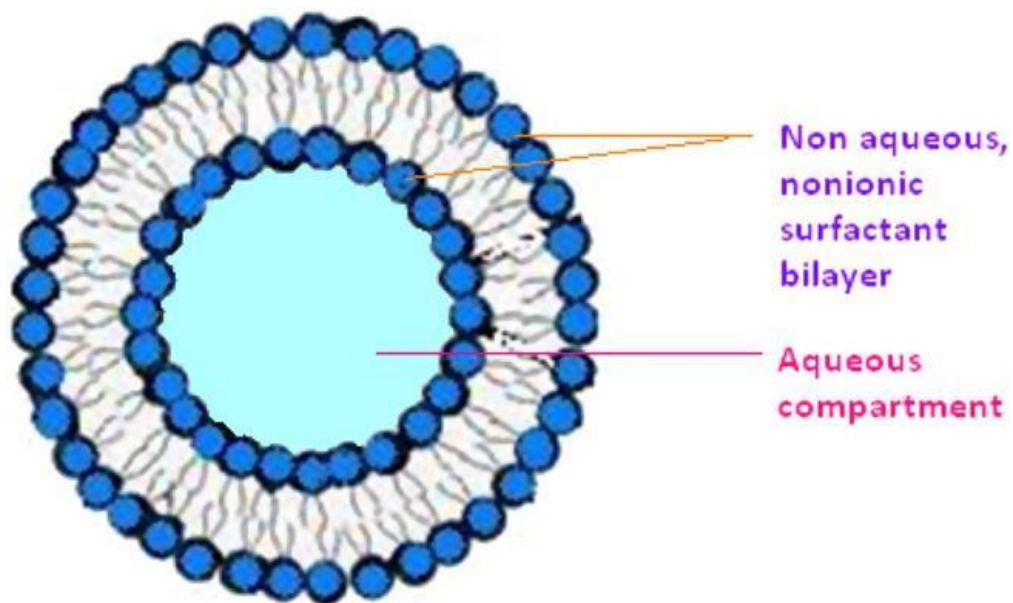


Figure 1.3: Schematic representation of a non-ionic surfactant vesicle (niosome) derived from [52]. Niosomes contain an inner and outer the compartment, the inside is made up of an aqueous compartment while the outer compartment is made up of a lipid bilayer.

1.6 Host targets for host-directed therapy

1.6.1 Pathogenesis and Immunity of *Mtb*

Mtb is transmitted through the inhalation of aerosol droplets containing tubercle bacilli from an individual with active pulmonary TB disease. The bacilli migrate to alveoli where they are encountered by alveolar macrophages [57]. The bacterium is rapidly phagocytosed by macrophages through recognition by pathogen recognition receptors (PRRs) and toll-like receptors (TLRs) ligands. The bacterium is then captured in phagosome which later fuses with the lysosome, matures and kills the bacterium [57, 58]. The host cell is then stimulated to produce pro-inflammatory cytokines such as tumour necrosis factor (TNF, IL-6, IL-1 α , IL-1 β , IL-12 and IL-18) and chemokines which drive the recruitment of more leukocytes to the site of infection via the MyD88 dependent and independent activation of NF κ B signalling [57]. Neutrophils and monocytes are recruited first to help form and organize foamy granulomas, followed by dendritic cells which also engulf and phagocytose the bacterium into antigen (Ag) which is crucial for antigen presentation. Dendritic cells then migrate to regional lymph nodes where they present the processed antigens to lymphocytes via the major histocompatibility complex class II (MHCII) [59]. Lymphocytes are then recruited to the site of infection following cues from antigen presentation and cytokine release [59-61]. This leads to the formation of organized granulomas for containment of infection, consisting of infected macrophages at the centre surrounded by epithelioid macrophages, foam cells and recruited lymphocytes and fibrous capsule [60, 62]. However, granulomas undergo necrosis over time, the dead macrophages form caseum at the centre allowing *Mtb* to survive within macrophages extracellularly within the granuloma [60, 63]. This increases the chances of *Mtb* escape and spread into airways and other areas of the body (Figure 1.4) [63].

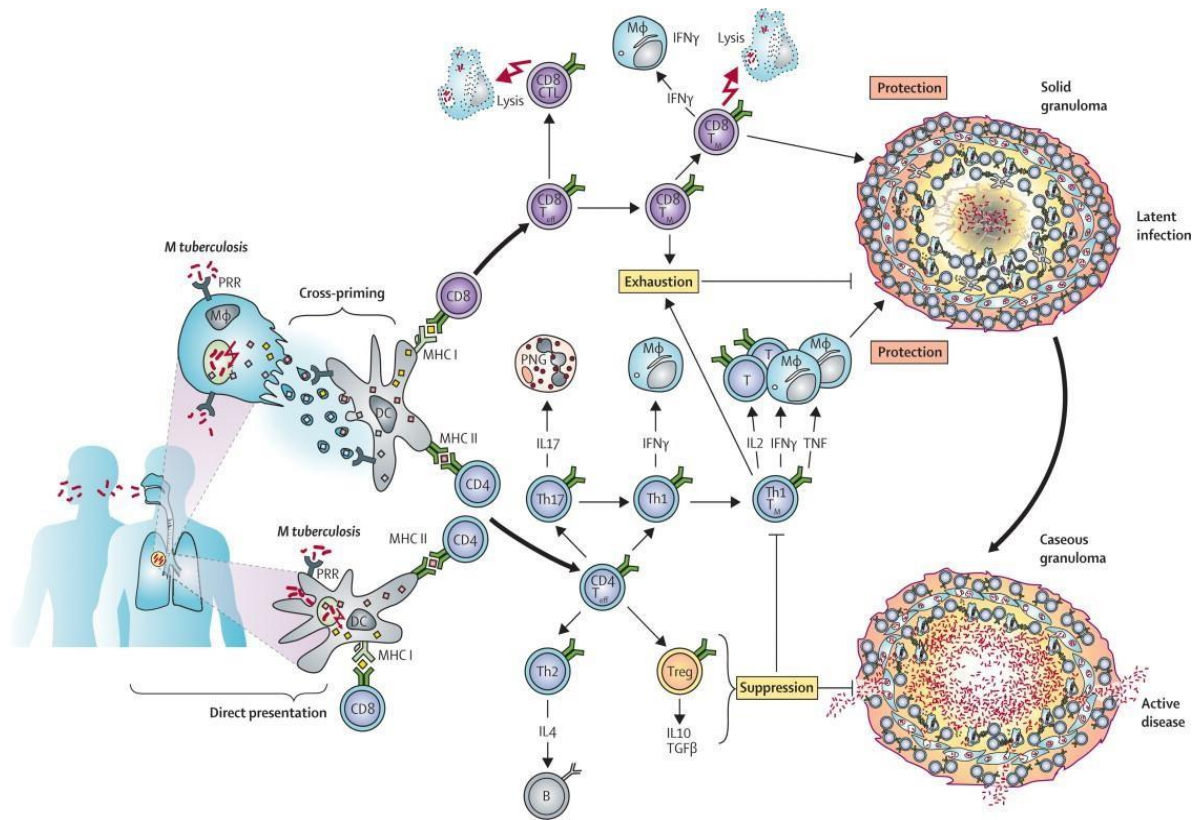


Figure 1.4: Pathogenesis, immunity and dynamics of granuloma formation upon Mtb infection. Adopted from [64]. Mtb transmission through aerosol droplets into alveolar macrophages. Pathogen recognition receptors (PRR) are stimulated through the recognition of pathogen associated molecular patterns (PAMPs). Macrophages are then stimulated to release chemokines and cytokines which drive the recruitment of leukocytes to site of infection to drive innate and adoptive immunity which leads to the formation of granulomas.

1.6.2 Mycobacterium tuberculosis in macrophages

1.6.2.1 Macrophage activation

Subsequent to phagocytosis of Mtb, macrophages are polarized into distinct subtypes, IFN- γ classically activated macrophages (caMph or M1) and IL-4/IL-13 alternatively activated macrophages (aaMph or M2) upon activation by different activation stimuli [65]. Thus, suggesting that the different subsets of macrophages engage in distinct induction pathways and responses to Mtb infection.

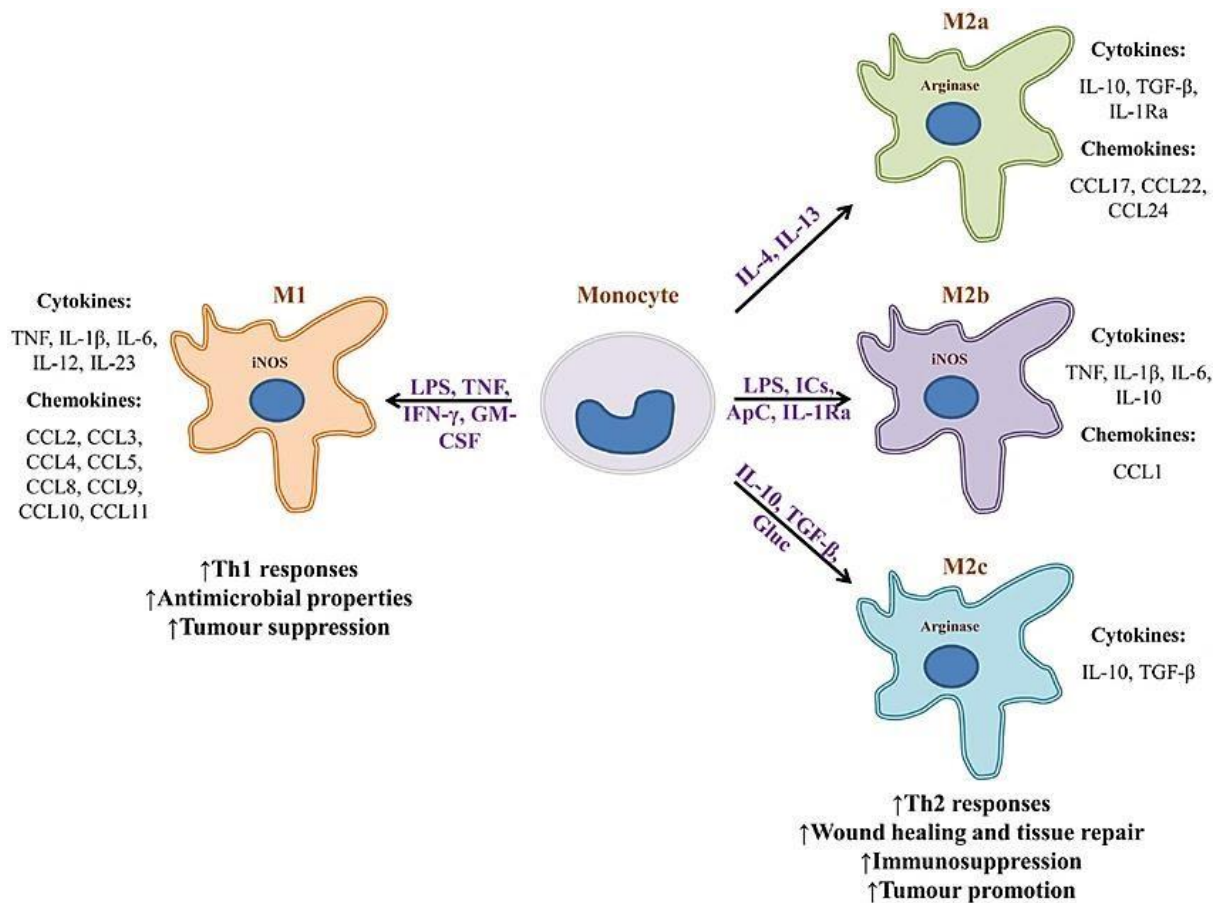


Figure 1.5: Macrophage polarization into distinct phenotypes following various stimuli. Adopted from [66]. Due to the cascade of various environmental and cytokine cues, monocytes turn into highly microbicidal classically activated (M1) or alternatively activated immunosuppressive (M2) phenotype.

1.6.2.2 Classically activated macrophages (caMph/M1)

Classically activated macrophages (caMph or M1) are characterised by increased microbicidal activity marked by the expression of nitric oxide synthase 2 (iNOS), high Ag presentation associated with increased MHC class II expression and the production of IL-12 [65]. This is dependent on nuclear factor κ B (NF- κ B) pathways in response to pro-inflammatory cytokines such as IFN- γ stimulus via IFN- γ receptor (IFN- γ R) together with the binding of microbial products such as lipopolysaccharides (LPS) leading to the production of nitric oxide (NO) through iNOS expression [65]. iNOS converts L-arginine into reactive nitrogen intermediates (RNI) resulting in NO bacterium and mycobacterium killing (Figure. 1.5) [65].

During Mtb infection, the production of pro-inflammatory cytokines and RNS is critical for the inhibition of growth and clearance of the pathogen [65]. Mice deficient of the proinflammatory cytokines such as TNF- α , IL-1 and IL-12 which are released by caMph and essential for granuloma formation, creating an environment for containment of infection, were reported to succumb to infection before wild-type (WT), had an increased disease burden and dissemination of bacteria to different organs [67-70].

Likewise, Scanga et al. reported an increased and rapid replication of Mtb in iNOS knockout mice compared to wild-type mice [71], implying a significant role for NO in host defence against Mtb. Furthermore, macrophages found at the centre of granulomas have a more proinflammatory phenotype compared to those at the periphery, with higher expression of iNOS compared to arginase-1 [72]. In the absence of NOS-2, mice deficient of NOS-2 developed large liver and spleen granulomas at four weeks post infection due to an accumulation of macrophages following infection with *Mycobacterium bovis*. However, these macrophages had a decreased acid phosphatase activity as well as decreased epithelioid differentiation compared to wild-type mice, suggesting a role for NO in macrophage activation [73]. At 6 weeks post infection, lung and spleen granulomas of nos-2 deficient mice had become larger compared to that of wild-type mice and had developed large central cavities surrounded by necrosis that were associated with a number of acid-fast bacilli, thus displaying an exacerbated yet inefficient cellular immune response due to the absence of NOS-2 which then led to tissue damage [74]. Taken together, essentially these findings emphasise the instrumental role of caMph and RNS in the eradication of mycobacterial infections.

1.6.2.3 Alternatively activated macrophages (aaMph/M2)

Alternatively activated macrophages are activated by anti-inflammatory cytokines produced generally in Th2 responses against allergic, cellular and humoral responses to parasitic and extracellular pathogens, IL-4 and IL-13 via the IL-4 receptor alpha chain (IL-4R α) and STAT 6 signalling (Figure. 1.5) [75-77]. Alternatively, activated macrophages are described as a mechanism by which Th2 responses reduce excessive inflammation resulting in moderate inhibition of proinflammatory responses, upregulation of mannose receptor and MHC II presentation and the production of Arginase 1 (Arg1) [75-77].

While the role of caMph against bacterial and mycobacterial infections like *Listeria monocytogenes* and Mtb infections is well established, the role of aaMph is less defined and requires further investigation. In contrast to the killing of Mtb as a result of NO production, aaMph induces the production of Arginase-1 (Arg-1) which competes with iNOS for L-arginine, resulting in decreased NO production [75, 77]. This suggests a

potential evasion mechanism by which Mtb hides in aaMph to avoid effector killing functions by caMph.

Other studies have shown the expression of Arg1 obtained from human macrophages and type II pneumocytes obtained from lung granulomas of TB patients and HN878 infected murine macrophages [78]. Other studies have also shown Mtb to interfere with the polarization of caMph by secreting virulence factor early secretory antigenic target 6 (ESAT6) which is employed in the lysis of phagolysosomal membrane causing translocation of Mtb to the cytoplasm of myeloid cells, thus restricting the MyD88-dependent TLR signalling [78, 79]. Recently Guler et al. showed that the virulent clinical Mtb strains induce Arg1 production in aaMph independent of the IL-4R α in aaMph¹[80].

While aaMph may be essential for host protection against parasitic and extracellular pathogens, Mtb strategically uses aaMph to hide from host protective functions. It is thus hypothesized that Mtb potentially modulates the transcriptional landscape of aaMph to escape and survive host-effector responses [80]. However, this subverting strategy mechanism is not well understood.

1.6.2.4 Candidate genes upregulate in alternatively activated macrophages during Mtb infection: IL4i1.

In collaboration with RIKEN Center for Integrative Medical Sciences (Yokohama, Japan), our lab conducted a novel transcriptomics study approach by performing a genome-wide transcriptional analyses of RNA transcripts using deep CAGE) technology aiming at identifying candidate genes that are upregulated in aaMph during Mtb infection as an evasion strategy by Mtb [81-83]. RNA transcripts obtained either from caMph or aaMph infected with HN878, a hypervirulent strain of Mtb responsible for high TB mortality rates and reduced host resistance, were used to identify the candidate genes (Figure 1.6). Among the identified candidate genes was the L-phenylalanine encoding gene, Interleukin 4 inducible (IL-4i1) gene 1 (Figure 1.7) [83].

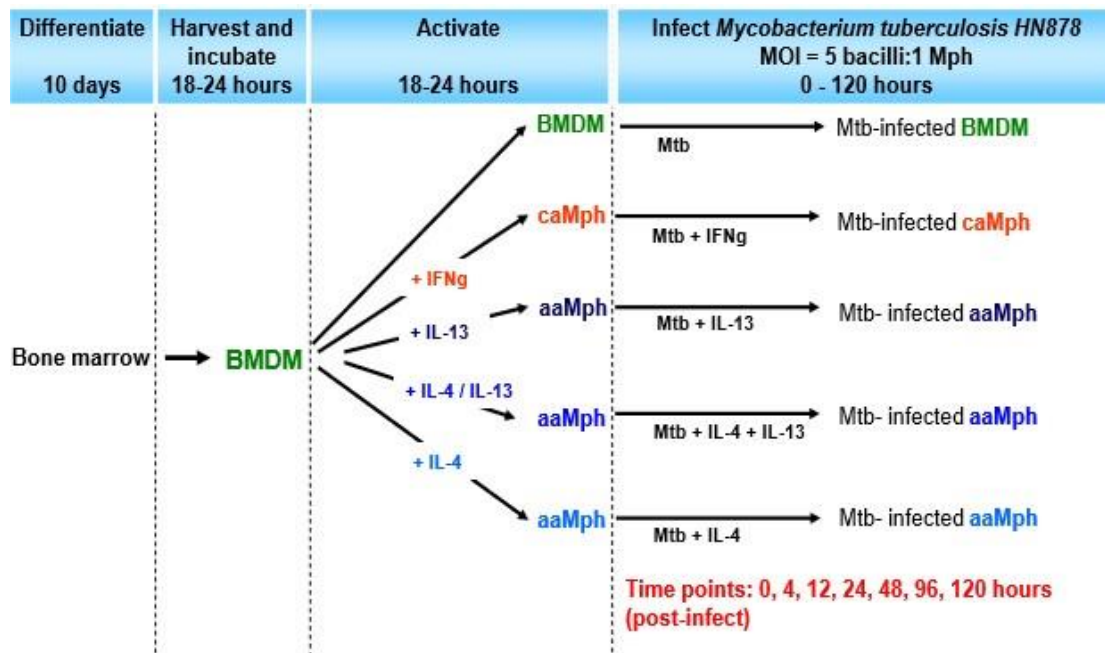


Figure 1.6: Layout of CAGE experiment. Bone marrow-derived macrophages (BMDM) were differentiated for 10 days in culture medium followed by treatment with either recombinant IFN- γ , IL-13, IL-4 or with a combination of IL-4/IL-13. Following stimulation, macrophages were incubated for 24 hours followed by restimulation and infection with HN878 Mtb strain at 4 hours post restimulation. RNA was then isolated at 0, 2, 4, 6, 12 and 24 hours post initial stimulation and 4, 12, 24, 48 and 96 hours post-infection to determine mRNA transcripts for IL-4i1 using CAGE tags. Top graphs in each replicate represent Mtb-infected macrophages while bottom represents uninfected macrophages.

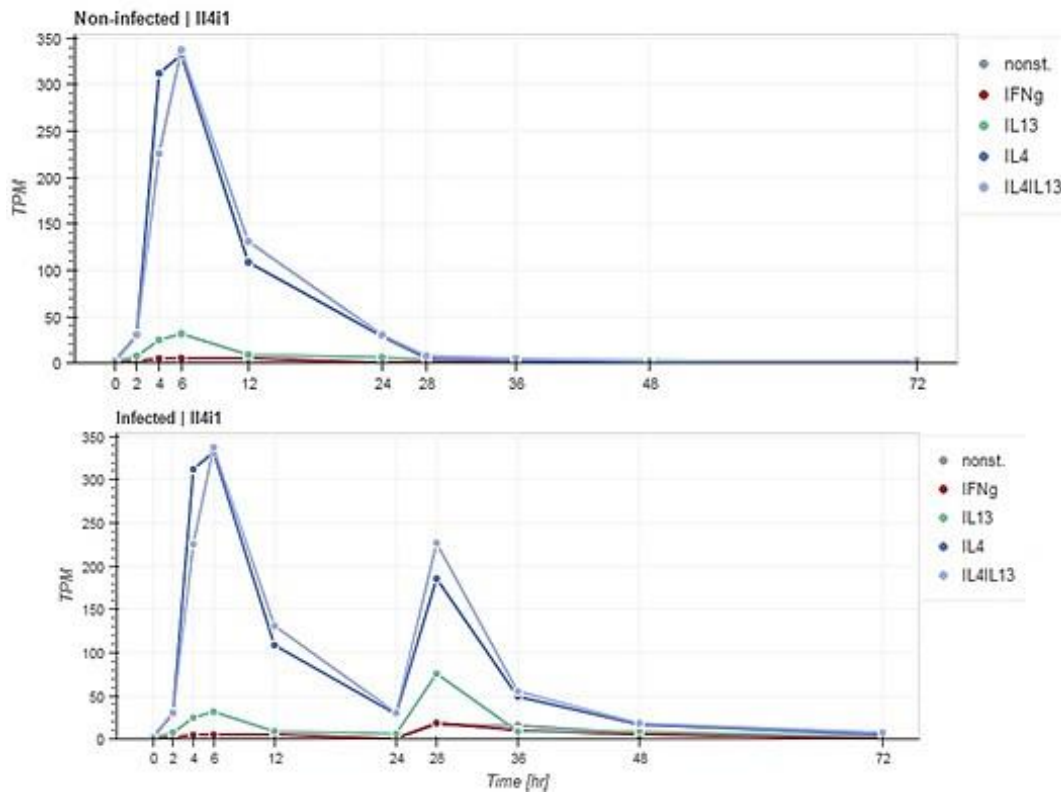


Figure 1.7: IL-4i1 mRNA expression profile in. Adopted from Cage data. IL-4i1 is highly upregulated in IL-4 of IL-4/IL-13 macrophages at 4-6hr post-stimulation and 4hr post-infection.

1.6.2.5 IL-4i1 expression and activity

IL-4 inducible gene 1 was primarily characterized as an IL-4 activated gene expressed in murine and subsequently in human B-cells [84]. High expression levels of the gene were further demonstrated in primary mediastinal B-cell lymphoma (PMBL) which was further described in professional antigen presenting cells (APCs), mature dendritic cells and macrophages [74, 84]. However, there has been contradicting evidence on the expression stimulus that triggers IL-4i1 expression on B-cells and that which triggers expression in APCs [85, 86]. Contrary to IL-4 stimulation in B-cells and results obtained from the CAGE data, IL-4i1 was shown to express under proinflammatory and Th1 (IFN- γ) mediators in macrophages and dendritic cells *in vitro* [86]. Human monocyte-derived macrophages and monocyte-derived dendritic cells displayed five-fold higher IL-4i1 expression and activity in response to IFN- γ and no activity when stimulated with IL-4 whereas B-cells displayed a two-fold activity in response to IL-4 [86]. Furthermore, immunohistochemistry of Th1 granulomas biopsies obtained from sarcoidosis or TB patients revealed 80% IL-4i1 expression in regions concentrated in macrophages and dendritic cells compared to Th2

granulomas obtained from schistosomiasis patients [86]. This suggests that IL-4i1 is implicated in the regulation of inflammatory responses [85, 87].

Most recently IL-4i1 expression was reported in Th17, conventional memory CD4+ T cells, and human inducible regulatory T (Foxp3+ iT-reg). The expression of IL-4i1 in Th17 cells was attributed to its role in the transdifferentiation of these cells to iT-regs in order to maintain cell-cycle progression of this cell type [88]. The expression of IL-4i1 in iT-regs was characterised by the expression of the transcription factor Aiolos, a member of the Ikaros family which is involved in the differentiation of Th17 and iT-regs cells [87]. However, IL-4i1 did not express in cells expressing Helios, another transcription factor of the Ikaros family which identifies natural Foxp3+ T-reg cells from thymocytes [87]. This suggests a close relationship between Th17 cells and iT-regs and thus a role for IL-4i1 under functional roles of these cell types. Because the murine IL-4i1 is an orthologue of the human IL-4i1 (hIL4i1), which map to chromosome 7 and 19 respectively, these genes share many similarities in their functional roles as demonstrated in most studies [74, 87]. The expression profile of IL-4i1 may provide insight on its immune regulatory function.

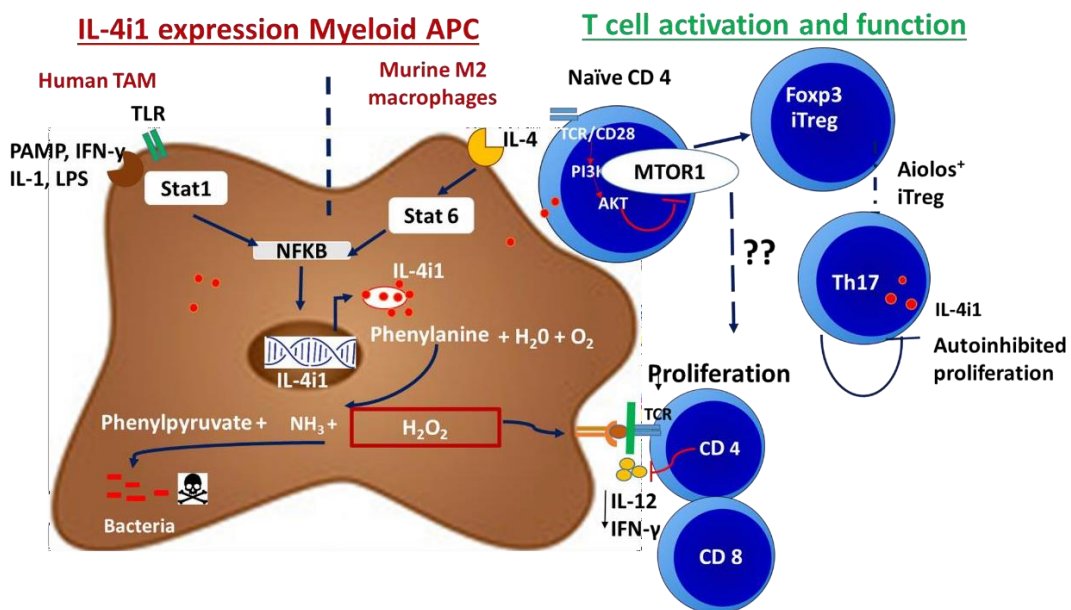


Figure 1.8: Functional role of IL-4i1 in immune regulation. Expression of IL-4i1 in macrophages is driven by different stimuli in human and murine macrophages. IL-4i1 is expressed under inflammatory conditions marked by IFN- γ , LPS and TLR mediated responses whereas in murine macrophages, IL-4i1 expression is stimulated through IL-4R α signaling via STAT-6 phosphorylation. The expression of the gene IL-4i1 codes for the secretion of the enzyme, which through its enzymatic activity presents antibacterial properties and immune regulatory properties.

1.6.2.6 Functional role of IL-4i1 in immune responses

IL-4i1 is a secreted L-amino acid oxidase which acts by degrading essential amino acid phenylalanine (Phe) to produce toxic products, phenylpyruvate, H₂O₂ and ammonia which provide a hostile environment for bacterial growth, presenting antibacterial properties at both physiological and acidic conditions [84, 85]. Mason et al. reported IL-4i1 to have an acidic pH and lysosomal localisation preference which was unusual for an L-amino acid oxidase which is normally most active at physiological pH [84]. However, Boulland et al. showed optimal IL-4i1 activity is at physiological pH and temperature similar to other L-amino acid oxidases [89]. This suggests colocalisation between lysosome and cytoplasm to confer an increased enzymatic activity and antibacterial properties.

On the other hand, this enzymatic activity has been implicated in immune suppression activities through the downregulation of TCR complex ζ chain expression via the production of H₂O₂ thus inhibiting T-cell proliferation [89]. Lasouadris et al. further reported this immunosuppressive effect in antitumor T-cell response *in vivo*. Transgenic mice injected with cells expressing IL-4i1 developed tumours more frequently than control mice and had a reduced number of IFN- γ producing cytotoxic antitumour cells [90]. In line with these findings, analysis of T-cell differentiation from conventional splenic CD4⁺ (GFP-CD25⁺CD62L⁺) cells from Foxp3-EGFP transgenic mice cultured with IL-4i1 expressing or HEK control cells and naive CD4⁺ cells from PBMC cultured with THP1 or THP1-IL-4i1, showed that IL-4i1 stimulates the generation of FoxP3⁺ regulatory (T-regs) from mouse and human T-cells through the ablation of mTORC1 kinase signaling pathways in activated CD4⁺ T cells while limiting the differentiation of T-effector (Th1 and Th2) [91]. Recently, IL-4i1 has been reported to play a role in the polarization of macrophages to an M2 phenotype which suppresses T-cell proliferation via a mechanism that involves STAT-6 and STAT-3 phosphorylation and in part through the L-tryptophan and L-arginine depletion [92]. Depletion of IL-4i1 resulted in enhanced B-cell activation through activation of BCR via BCR Syk-Akt-S6 kinase activation pathway [93]. *In vivo* studies have identified CD8 T-cells anti-proliferative role of IL-4i1 in a tumour model. In a spontaneous *in vivo* melanoma model in IL-4i1 knockout mice lead to delayed tumour progression accompanied by an infiltration of Th1 cell and CD 8 T-cell [94]. In a multiple sclerosis model, IL-4i1 showed increased T-cell proliferation in the brain and peripheral tissues. However, in the presence of IL-4i1 T-cell expansion was reduced and recruitment of and survival of oligodendrocytes was increased, thus showing the importance of IL-4i1 in remyelination [95].

Since T effector cell functions play a crucial role in the eradication of pathogens, the T-eff:T-reg balance is critical for immunological homeostasis. Although the primary function is for the maintenance of immune homeostasis, T-reg cells have been associated with immune suppressive activities that block eradication of pathogens by pathogen-specific T-cells thus causing persistence of infection. The accumulation of FoxP3⁺ T-reg cells in lung granulomas and pulmonary lymph nodes of Foxp3-GFP mice following an aerosol infection with Mtb suggested a suppressive capacity for T-regs on Mtb control [96]. Furthermore, mice depleted of T-regs were displayed a one log reduction in Mtb bacterial load. Recently, IL-4i1 has been employed as a biomarker for cancer prognosis in cutaneous melanoma patients. The location of IL-4i1⁺ cells was positively correlated with T-regulatory cells and inversely correlated with the presence of CD8⁺ anti-tumour T-cells supporting the role of IL-4i1 in immune evasion. Molinier-Frenkel et al. [97] showed that single amino-acid induced by either single-nucleotide polymorphisms (SNPs) or acquired mutations may affect enzymatic activity, that could cause alteration in IL-4i1 immunosuppressive capacity. SNP R102G of exon 4 of isoform of IL4i1 gene which is expressed in lymphoid tissues exogenously caused hypomorphic mutant of IL4I1 production in tumour macrophages, N92D SNP expression caused hyperactive IL4I1 production. These data showed that the expression of these SNP may predispose patients to defective anti-tumour T-cell responses, with favourable and unfavourable consequences on patients' prognosis, respectively. The expression of the hyperactive enzyme could protect from the development of an autoimmune disease, while a hypomorphic enzymatic activity may predispose to autoimmunity [97].

Although shown to have antibacterial properties and a well-defined role in tumour pathology, little is known about the role of IL-4i1 on the immunity against pathogenic infections. To determine the function of IL-4i1 on T-cells during Mtb infection *in vitro*, an L-amino acid oxidase non-specific blocker, benzoic acid was used to block the IL-4i1 expression in macrophages *in vitro*. Co-culturing naive T-cells with macrophages stimulated with blocked IL-4i1 expression resulted in increased T-cell proliferation and decreased bacterial burden compared to control cells expressing IL-4i1 [unpublished data]. In light of these findings, it was suggested that the enzyme IL-4i1 which participates in T-reg enrichment and M2 macrophage polarization may apply its immunosuppressive activity on T-cells both by direct inhibition of effector cell proliferation and by indirect immune regulation mediated by FOXP3⁺T-reg cell induction [91] or through the promotion of alternatively activated macrophages in the case of Mtb. Thus targeting IL-4i1 could potentially help dissect its role and mechanism in immunopathology during Mtb infection. Furthermore, while the role of IL-4i1 on immune homeostasis has been studied under

inflammatory conditions and tumour environment, studies on SNPs and mutations of the gene suggest a possible role for IL-4i1 on the development of autoimmunity *in vitro*. However, no studies to date have reported on the role of IL-4i1 on the maintenance of immune homeostasis at steady state *in vivo*.

1.7 Study aim, objectives Overall study aim:

To identify potential novel drug targets for pathogen- and host-directed therapy for tuberculosis.

Pathogen-directed therapy:

Aim

The main of this study was to identify the anti-mycobacterial activity of minor groove binder (MGB) compounds as novel anti-TB drugs and a foundation in the development of a novel inhalable drug formulation for the treatment of tuberculosis.

Objectives

1. To screen a diverse range of S-MGB classes for their anti-mycobacterial tuberculosis activity *in vitro* in culture.
2. Provide lead compounds that will be further evaluated for their intracellular anti-mycobacterial activity and cytotoxicity.
3. Encapsulate lead compounds into NIVs and evaluate for improved efficacy in murine macrophages.
4. Biological profiling of lead compounds *in vivo* in acute Mtb-infected murine models.

Host-directed therapy:

Aim

To determine the functional immune regulatory role of IL-4i1 during steady state and *Mycobacterium tuberculosis* infection through loss of function approach in mice.

Objectives:

1. Characterization of IL-4i1 deficient mice models.
2. To determine the role of IL-4i1 on immune homeostasis at steady state.
3. To determine the role of IL-4i1 during acute *Mycobacterium tuberculosis* infection

Pathogen-directed drug targets for tuberculosis therapy

**Minor groove binders and non-ionic surfactant vesicles
delivery systems as anti-TB therapy**

Chapter 2 Published Manuscript

Evaluation of Minor Groove Binders (MGBs) as novel anti-mycobacterial agents, and the effect of using non-ionic surfactant vesicles as a delivery system to improve their efficacy.

Summary

In this chapter of the thesis, we screened the anti-mycobacterial activity of 172 minor groove binder (MGB) compounds that selectively bind to AT-rich regions of the minor groove of bacterial DNA with the helical structure matching that of DNA in Mtb culture. Of the 172 total compounds screened 17 hits were identified, of which 2, MGB 362 and MGB 364 displayed intracellular mycobactericidal activity against Mtb HN878 at an MIC₅₀ of 4.09 and 4.19 M, respectively, whilst being non-toxic. Encapsulation of MGBs into non-ionic surfactant vesicles (NIVs) demonstrated a 1.6- and 2.1-fold increased intracellular mycobacterial activity, similar to that of rifampicin when compared with MGB alone formulation. The work presented in this chapter was published in the Journal of Antimicrobial Chemotherapy (Hlaka L, Rosslee MJ, Ozturk M, Kumar S, Parihar SP, Brombacher F, Khalaf AI, Carter KC, Scott FJ, Suckling CJ, Guler R. Evaluation of minor groove binders (MGBs) as novel anti-mycobacterial agents and the effect of using non-ionic surfactant vesicles as a delivery system to improve their efficacy. *The Journal of Antimicrobial Chemotherapy*. 2017;72:3334-41). The PhD candidate shared first co-authorship in this publication. She performed all initial H37Rv-GFP optimization drug screening experiments with Dr Santosh Kumar. She performed all the H37Rv-GFP drug screening experiments presented in Figure 2.1 and Table 1.1 with Mr Michael Rosslee. The PhD candidate also performed the intracellular antimycobacterial screening and cell viability experiments in bone-marrow derived macrophages presented in Figure 2.2 with Mr Michael Rosslee and Dr Suraj Parihar. She assisted Mr Rosslee, Dr Ozturk and A/Prof Guler in analyzing the MGB-NIV encapsulation for improved drug efficacy experiments presented in Figure 2.3.

Evaluation of Minor Groove Binders (MGBs) as novel anti-mycobacterial agents, and the effect of using non-ionic surfactant vesicles as a delivery system to improve their efficacy

Lerato Hlaka^{1,2†}, Michael-Jon Rosslee^{1,2†}, Mumin Ozturk^{1,2}, Santosh Kumar^{1,2}, Suraj P. Parihar^{1,2}, Frank Brombacher^{1,2}, Abedawn I. Khalaf³, Katharine C. Carter⁴, Fraser J. Scott⁵, Colin J. Suckling³, Reto Guler^{1,2*}

¹ University of Cape Town, Institute of Infectious Diseases and Molecular Medicine (IDM), Division of Immunology and South African Medical Research Council (SAMRC) Immunology of Infectious Diseases, Faculty of Health Sciences, University of Cape Town, Cape Town 7925, South Africa.

² International Centre for Genetic Engineering and Biotechnology, Cape Town Component, Cape Town 7925, South Africa.

³ WestCHEM Department of Pure and Applied Chemistry, University of Strathclyde, 295 Cathedral Street, Glasgow G1 1XL, United Kingdom.

⁴ Strathclyde Institute of Pharmacy and Biomedical Science, University of Strathclyde, 161 Cathedral Street, Glasgow, G4 ORE, United Kingdom.

⁵ Department of Biological Sciences, University of Huddersfield, Queensgate, Huddersfield HD1 3DH, UK.

*Corresponding author. Tel: +27-21-4066033; Fax: + 27-86-6407594 E-mail: reto.guler@uct.ac.za

†Both authors contributed equally to this work.

Running title: Non-ionic surfactant vesicles to deliver Minor Groove Binders intracellularly for *M. tuberculosis* sterilization

2.1 Abstract

Objectives: The slow development of major advances in drug discovery for the treatment of *Mycobacterium tuberculosis* (Mtb) infection have led to a compelling need for evaluation of more effective drug therapies against tuberculosis. New classes of drugs are constantly being evaluated for anti-mycobacterial activity with currently a very limited number of new drugs approved for TB treatment. Minor Groove Binders (MGBs) have previously revealed promising anti-microbial activity against various infectious agents; however have not yet been screened against Mtb.

Methods: Mycobactericidal activity of 96 MGB compounds against Mtb was determined using H37Rv-GFP microplate assay. MGB hits were screened for their intracellular mycobactericidal efficacy against clinical Beijing Mtb strain HN878 in bone marrow- derived macrophages using standard colony-forming unit counting. Cell viability was assessed by CellTiter-Blue assays. Selected MGB were encapsulated into non-ionic surfactant vesicles (NIVs) for drug delivery system evaluation.

Results: H37Rv-GFP screening yielded a hitlist of 7 compounds at an MIC₉₉ between 0.39 and 1.56 μ M. MGB 362 and MGB 364 displayed intracellular mycobactericidal activity against Mtb HN878 at MIC₅₀ of 4.09 μ M and 4.19 μ M respectively, whilst being non-toxic. Subsequent encapsulation into NIVs demonstrated a 1.6 and 2.1-fold increased intracellular anti-mycobacterial activity, similar to that of rifampicin when compared to MGB alone formulation.

Conclusions: MGBs anti-mycobacterial activities together with non-toxic properties indicate that MGB compounds constitute an important new class of drug/chemical entity, which holds promise in future anti-TB therapy. Furthermore, NIVs ability to better deliver entrapped MGB compounds to an intracellular Mtb infection has provided merit for further preclinical evaluation.

2.2 Introduction

Mycobacterium tuberculosis (Mtb), the causative agent of tuberculosis (TB), has become the top infectious killer worldwide. According to the 2016 World Health Organization (WHO) Global Tuberculosis Report [98], TB killed approximately 1.8 million people in 2015, up from 1.5 million deaths in 2014 [99]. The current six-month treatment regimen for drug-susceptible Mtb, although still effective in most cases, is gradually becoming ineffective due to increasing resistance against the drugs used to treat TB [10]. Several advances have been made in the field of TB drug discovery, spearheaded by global partnerships. For example, the Global Alliance for TB Drug Development currently manages the largest array of novel anti-TB drug compounds and novel regimens for MDR and XDR TB [100]. Other initiatives to eradicate TB include the STOP TB partnership that includes an international working group to develop new TB drugs [9]. Furthermore, several large consortia of pharmaceutical companies (TB Drug Accelerator) and academia (MM4TB) drive the discovery of new TB drugs [101]. Despite the progress in the pipeline for new diagnostics, drugs, regimens, and vaccines, research remains relentlessly underfunded. As a consequence, only a few new drugs have been approved for clinical use, i.e. delamanid, bedaquiline and pretomanid, and only ten new drugs are in advanced phases of clinical trials as of 2016 [102, 103]. With the slow development of major advances in anti-mycobacterial drug discovery and the emergence of multi-drug- and extremely drug-resistant TB, there is an urgent need for the development of more effective therapies and formulations of existing drugs for the treatment of TB [11, 103]. In the area of novel therapeutics discovery, progress has been made in developing new drug classes such as benzothiazinones, which inhibit cell wall arabinan synthesis, and imidazopyridines, which inhibit respiratory chain ATP synthesis [104, 105]. Minor Groove Binder compounds (MGBs) have revealed promising antibacterial properties, but have not yet been investigated for their anti-mycobacterial activity against Mtb *in vitro*.

Derived from the natural product distamycin, MGBs are a class of compounds that selectively bind to the minor groove of bacterial DNA with their helical structure matching that of DNA [106]. Most often, proteins binding to bacterial DNA bind to the major groove, leaving the minor groove exposed and thus, a vacant target for MGBs. Natural forms of MGBs are currently used in clinical treatment of disease. For example, aromatic diamidines, such as pentamidine [107, 108], and berenil [109], known to bind to the minor groove at adenosine-thymine tracts, have been administered clinically against human African trypanosomiasis and *Pneumocystis carinii* pneumonia [110-112]. MGBs display a wide variety of activity profiles against many infectious organisms evaluated, including Gram-positive bacteria [113], *Mycobacterium aurum* [114], chloroquine sensitive and

resistant *Plasmodium falciparum* [36], and *Trypanosoma brucei brucei* [111]. In partnership with MGB-Biopharma, one MGB compound has successfully completed phase I clinical trials for the treatment of *Clostridium difficile* infections [115]. We recently screened a limited number of MGBs for their anti-mycobacterial activity against the laboratory Mtb H37Rv strain with MIC₉₉ reaching 3.1 uM [116]. We have now further extended this work by producing more active MGBs with higher MIC₉₉ values against Mtb H37Rv. In addition, we examined the anti-mycobacterial activity of MGBs against intracellular clinical HN878 Beijing strain of Mtb and evaluated the effect of MGBs exposure on cell viability in macrophages.

Oral drug administration has various limitations such as drug inefficiency resulting from drug insolubility caused by gastric low pH or poor absorbance in the gastrointestinal tract. However, an effective drug delivery system can improve drug retention at the site of infection. Therefore, an ability to deliver the drug to the site of infection may provide a sustained drug concentration enabling increased effectiveness of a drug against its target. In the case of pulmonary TB treatment, oral drug administration leads to high systemic concentrations of the drugs with associated side effects such as liver toxicity and cytotoxicity, amongst others [117]. Ultimately, the drawbacks associated with the oral administration of antibiotics laid the foundation for the development of innovative drug delivery approaches. The use of liposomes as a drug delivery system has been previously reported to reduce microbial drug resistance through faster drug delivery and increasing the antimicrobial drug concentration thereby preventing microbial drug efflux pump activity [118]. Liposome encapsulated drugs kill microbes faster before microbial mutations can develop. For example the incorporation of the antibiotic levofloxacin into liposomes improved the anti-mycobacterial activity to kill Mtb strain resistant to levofloxacin [119]. Other drug delivery systems such as non-ionic surfactant vesicles (NIV) have the ability to encapsulate both hydrophobic and hydrophilic drugs for direct delivery to the site of infection [52]. NIVs are small colloidal particles made of a non-aqueous, non-ionic surfactant bilayer that surrounds a central aqueous compartment. They are thermodynamically stable, easily manufactured and do not require special storage conditions. One of the major advantages of NIVs is that they are able to entrap different types of drug substances and can have their size altered. Their capacity to improve the delivery of small molecules is an important trait that allows for precise targeting of deposition of particles within the respiratory tract. Previous studies have shown NIVs to be a promising inhalable drug delivery system against pulmonary aspergillosis with aerosolized amphotericin B (AMB)-NIV administration reducing fungal lung burden when compared to AMB solution only [54]. More recent studies are showing antibacterial

action of moxiflacin [120] and cefixime [121] and antiviral action of nevirapine [122] in NIV formulations. Although many different drug delivery systems have been utilised to entrap first-line TB drugs, [123] only a few have systematically explored their anti-mycobacterial activity against Mtb and against intracellular Mtb in infected primary macrophages. Thus, we have investigated the use of NIVs as a drug delivery system on the improvement of delivery and efficacy of novel MGB compounds to Mtb-infected macrophages.

2.3 Materials and methods

2.3.1 Minor Groove Binder compounds

MGB compounds were synthesized using distamycin template, a natural product with known infective properties as previously reported [25, 111, 116]. Alterations of the head, tail, side chains and body resulted in a number of diverse compounds with later synthesis driven by acquired screening data (Table S1). MGBs were re-suspended in DMSO to a concentration of 1.25 mM and were stored at -80°C.

2.3.2 Preparation of compounds and non-ionic surfactant vesicles

MGB compounds (Stock: 1.25 mM) and rifampicin (Stock: 20 mM) were diluted to a starting concentration of 50 µM followed by 2-fold dilutions in 7H9 broth medium or DMEM to yield required screening range. Freeze dried NIVs were prepared as previously described [28] and rehydrated in DMEM + 10% FCS (Gibco, Thermofisher Scientific, USA) to a NIV concentration range of 23-5000 µM (empty NIV) and subsequently added to bone marrow-derived macrophages (BMDMs) in order to assess cell viability through CellTiter- Blue (Promega, Wisconsin, USA) assay with fluorescence detection at (544_{ex}/590_{em} nm). Subsequently, drug-NIV solutions were prepared in DMEM + 10% FCS at 2:5 molar ratio (MGB: NIV) at compound two-fold serial dilution range from 1.56 to 12.5 µM (3.91-31.25 µM NIV) to assess cell viability and intracellular anti-mycobacterial activity. Two-fold serial drug dilution was performed as previously reported in other drug screening studies [124].

2.3.3 H37Rv-GFP microplate screening assay

MGB compounds were screened for their anti-mycobacterial activity using 96-well, black clear flat-bottom microplates (Greiner Bio-One, Germany) as previously reported.[125, 126] Single cell suspension of H37Rv-GFP from frozen stock with working concentration of 1x10⁶ cfu/mL, was prepared in Middlebrook 7H9 supplemented with 25 mg/l kanamycin, 10% Middlebrook OADC (v/v) and 0.05% tween 80 (w/v). The H37Rv-GFP Mtb strain was a donation from Ernst lab in New York University School of Medicine, USA. 100 µL of H37Rv-GFP at a concentration of 1x10⁵ cfu/well was added to each experimental well. 100 µL of drug compounds prepared in 7H9 broth supplemented with 25 mg/L kanamycin to generate 0.195-50 µM screening range, was added to well containing H37Rv-GFP for final screening range of 0.0977-25 µM. Wells containing compound only at the highest screening concentration were used to detect autofluorescence of compounds and broth (vehicle control). Fluorescence (485_{ex} /520_{em} nm) was measured at designated time points; days 0, 4, 8, 10 and 12 with BMG Labtech Omega Plate Reader (Germany). The addition of sterile water to the outer wells of each plate served to

minimize the evaporation. Time intervals were selected as previously reported in other drug screening studies [126].

2.3.4 Bone marrow-derived macrophages generation and Mtb infection

BMDMs were generated from 8-12 week old C57BL/6 mice as previously reported [127]. After differentiation, BMDMs were plated into 96-well plates (Nunc, Denmark) at 2×10^5 cells per well. Following overnight adherence, BMDMs were then infected with Mtb HN878 (MOI=5) and cultured at 37°C under 5% CO₂ for 4 hours. BMDMs were washed once with pre-warmed culture media to remove extracellular bacteria or lysed and lysates plated on 7H10 agar plates supplemented with 10% OADC and 0.5% glycerol for cfu counting to determine bacilli uptake. Drug compounds prepared in DMEM media supplemented with 10% FCS at defined concentrations were added to infected BMDMs to determine anti- mycobacterial activity and cell viability using rifampicin no treatment (no-drug) groups as controls. After 5 days of culture, cells were lysed for cfu plating or assessed for cell viability by CellTiter-Blue assay.

2.3.5 Statistical analysis

All data were analysed using R, a student t-test (two-tailed with equal variance) or unless otherwise stated in figure legends. A *p value of less 0.05 was considered significant, with **p < 0.01 and ***p < 0.001

2.4 Results

2.4.1 Minimum inhibitory concentration (MIC₉₉) of MGB compounds against H37Rv-GFP

We screened 96 MGBs for their anti-mycobacterial activity against GFP-labelled H37Rv *Mtb* in liquid broth culture using a 96-well plate assay (Table 1). Relative fluorescence was measured at 0, 4, 8, 10 and 12 days in broth culture of MGBs (serially diluted from 25 μ M to 0.19 μ M) to determine the minimum inhibitory concentration (MIC₉₉) of MGBs required to eradicate 99% of *Mtb* (Figure 2.1). Hit compounds, defined as previously reported [128], were identified as drugs that were active at or below the threshold concentration of 3.12 μ M. A hitlist of 7 compounds were identified with an MIC₉₉ of 1.56 μ M or less (Figure 2.1 and Table 1). Rifampicin, which had an MIC of 0.0977 μ M, was used as the positive control. The selected hit compounds were MGBs 362, 368, 361, 365, 359, 364 and 367 with MIC₉₉ range (0.391-1.56 μ M) and therefore were identified for subsequent intracellular anti-mycobactericidal activity screening.

2.4.2 Intracellular drug activity against clinical *Mtb* and macrophage cell viability

The ability of anti-TB drug compounds to penetrate macrophages and induce mycobactericidal activity, while being non-toxic to the macrophages, is a salient property sought after in TB drug development. Hence, BMDMs were exposed to serial MGB drug concentrations from 1.56 to 12.5 μ M to evaluate their anti-mycobacterial activity against the clinical *Mtb* strain HN878, after 5 days of infection. Compounds were screened for the concentration which eradicated 50% of bacilli (MIC₅₀, Figure 2.2A). Two of the 7 hit compounds identified from screening studies against *Mtb* in Figure 1 had good intracellular mycobacterial killing efficacy against *Mtb*-infected macrophages, with MIC₅₀ values of 4.09 μ M (MGB 362) and 4.19 μ M (MGB 364). Rifampicin, selected as a positive control, had a MIC₅₀ of 1.7 μ M. CellTiter-Blue cell viability assay was performed to assess for macrophage cell viability in MGBs-treated BMDMs after 5 days of exposure (Figure 2.2B). MGB 362 and 364 and rifampicin had no significant effect on macrophage viability at the respective intracellular drug activity MIC₅₀ concentrations (Figure 2.2B). These data suggest that MGB 362 and 364 have an efficient intracellular anti-mycobacterial activity against *Mtb* while being non-toxic to the host cells.

2.4.3 MBGs-NIV encapsulation increased intracellular drug activity against clinical strain of *Mtb*

We next investigated whether encapsulating our hit MGB compounds into NIVs, a drug delivery system that was previously reported to improve drug delivery of amphotericin B

to macrophages,[54] would improve MGBs drug efficacy against the intracellular clinical HN878 Mtb strain. We demonstrated that encapsulating MGBs into NIVs improved the intracellular anti-mycobacterial abilities by 2.1-fold for MGB 362, and 1.6-fold for MGB 364 in Mtb HN878-infected BMDMs, displaying a significant cfu reduction ($P < 0.01$) compared to controls (Figure 2.3A). The anti-mycobacterial killing activity of MGB 362-NIV and MGB 364-NIV were similar to that of rifampicin. MGB 364 displayed a significant decreased cfu counts ($P < 0.033$) when compared to MGB alone. Furthermore, Mtb-infected macrophages were viable following MGB-NIV treatment (Figure 2.3B). Treatment with NIV- alone also had no significant effect on macrophage viability (data not shown). These results demonstrate that NIVs can act as a suitable delivery system by transporting MGB inside macrophages, the target cells for Mtb.

2.5 Discussion

MGB compounds have shown great potential for their use as antibacterial therapeutic agents [25]. However, their activity against Mtb remains unknown. Here, we demonstrated the anti-mycobacterial (MIC_{99}) properties of MGBs against Mtb (H37Rv-GFP) with a reliable screening method that enables the detection of most active compounds,[129] using rifampicin as a positive control (Table 1, Figure. 2.1). All of the active MGB compounds belong to the well- established alkene-linked minor groove binder family discovered at the University of Strathclyde with high killing activities against different pathogens as previously reported [17,19-21, 23, 33]. Since the primary binding sites of all of these MGBs in the DNA minor groove are AT rich regions it is unlikely that target sequence specificity is responsible for the selectivity observed. This is true also for the active compounds against Mtb described here. However, it is more likely that activity and selectivity against a particular pathogen is caused by differential access to cells caused by differing cell wall and cell membrane structures in a way that with the current state of knowledge is idiosyncratic and unpredictable [25]. What can be reliably stated is that the alkene-linked compounds are significantly the most biologically active of the Strathclyde MGB family. In general, MGBs with the most significant antibacterial activity possess a range of different tail groups, all of which are exemplified within the set in our screen. However, all of the most active MGBs identified in this study possess an amidine-containing tail group, which perhaps suggests an important role of tail group pKa for targeting mycobacteria.

Screening of MGB compounds in the context of their cell viability and anti-mycobacterial activity against intracellular clinical Mtb strain HN878 have identified two compounds with promising results, giving a hit rate of 2.1% (2/96) (Figure.2. 2). In most studies the hit rate for hit compounds is in the order of 1%, in-line with previous studies.[130] These findings however warrant *in vivo* testing which aims to allow for better clinical therapeutic translation of the findings. The use of non-ionic surfactant vesicles (NIVs) has been demonstrated repeatedly in literature before and constitutes a prominent focus within current Mtb research in order to combat the infection [52, 131]. NIVs given by nebulisation delivered amphotericin B to the lungs and liver with significantly improved treatment outcome when compared to AMB solution against pulmonary aspergillosis and visceral leishmaniasis [28]. Our investigation of NIVs as a delivery device indeed demonstrate that NIVs can be used to enhance the efficacy of MGB compounds against HN878 in infected BMDMs whilst not increasing the toxicity of the drug to BMDMs. MGB contain hydrophobic head groups (Figure. 2.3) [106] which allows for encapsulation into NIV. Liposomes have previously been reported to encapsulate an alkyl derivative of distamycin A [132] which are naturally occurring backbones for MGB compound synthesis.

NIVs ability to trap the drug within its hydrophilic/-phobic compartment allows the drug to be taken up by phagocytosis by the infected macrophage, thereby transporting the drug to the site of infection. Using NIV drug formulations resulted in higher drug levels compared to similar treatment with drug solution at the site of infection after treatment by the pulmonary or intravenous routes for water soluble [133, 134] and lipid soluble drugs [54]. Studies in dogs treated by the intravenous route with a sodium stibogluconate-dextran (SSG)-NIV formulation increased the elimination half-life and the volume of distribution at steady state compared to SSG-dextran solution [135]. Therefore NIV-MGB formulation can be a feasible pulmonary treatment for Mtb.

In conclusion, this study showed that MGBs constitute an important new class of drug/chemical entity with favourable anti-mycobacterial activity and holds promise in future anti-TB therapy. Furthermore, we demonstrate that NIVs contribute to better delivery of drugs to an intracellular infection and secondly act as a delivery device for entrapped MGB compounds and lastly serve as the initial step into future research of targeted delivery of entrapped drug to Mtb-infected cells.

2.6 Acknowledgements

We thank Ms. Fadwah Booley, Ms. Lorna Gcanga and Mr. George Jacobs for their excellent technical assistance.

2.7 Funding

This work was supported by the Knowledge Exchange Development Fund (KEDF) from the University of Strathclyde to KCC, the International Centre for Genetic Engineering & Biotechnology (ICGEB) Arturo Falaschi PhD Fellowship to MO and SK, the Claude Leon Foundation and CIDRI, Wellcome trust (Grant No. 084323) post-doctoral fellowships to SPP, the South African Medical Research Council (SAMRC) doctoral fellowship to LH, grants from the South African National Research Foundation (NRF) and from the Department of Science and Technology, South African Research Chair Initiative (SARCHi) and South Africa Medical Research Council (SAMRC) to FB, grants from the Department of Science and Technology (DST) / South African National Research Foundation (NRF) Collaborative Postgraduate Training Programme to RG.

2.8 Transparency Declarations

None to declare.

Table 2.1. MIC₉₉ of all screened MGBs against H37Rv-GFP. 7 hits were identified out of 96 MGBs screened. MGBs marked with asterisk symbols were previously screened as reported. [77].

Compound	MIC₉₉	Compound	MIC₉₉	Compound	MIC₉₉	
Rifampicin	0.0977	371	25	235	>25	
Hits	362	0.391	372	25	245	>25
	368	0.391	373	25	246	>25
	361	0.781	374	25	247	>25
	365	0.781	381	25	248	>25
	359	1.56	1	>25	270	>25
	364	1.56	2	>25	271	>25
	367	1.56	9	>25	283	>25
353*	3.12	12	>25	286	>25	
354*	3.12	74*	>25	287	>25	
391	3.12	85	>25	288	>25	
263	6.25	92	>25	289	>25	
343	6.25	114	>25	300	>25	
385	6.25	121	>25	303	>25	
386	6.25	122	>25	304	>25	
351*	12.5	123	>25	305	>25	
352*	12.5	124	>25	306	>25	
376	12.5	131	>25	322	>25	
377	12.5	134	>25	323	>25	

378	12.5	147	>25	324*	>25
379	12.5	154	>25	325	>25
380	12.5	176	>25	329*	>25
383	12.5	185	>25	331*	>25
387	12.5	187	>25	332*	>25
390	12.5	188	>25	333*	>25
282	12.5 - 25	192	>25	334*	>25
4*	25	210	>25	335*	>25
116	25	212	>25	336*	>25
164	25	213	>25	338*	>25
292	25	214	>25	356	>25
317*	25	222	>25	357	>25
330*	25	234	>25	358	>25
337	25				

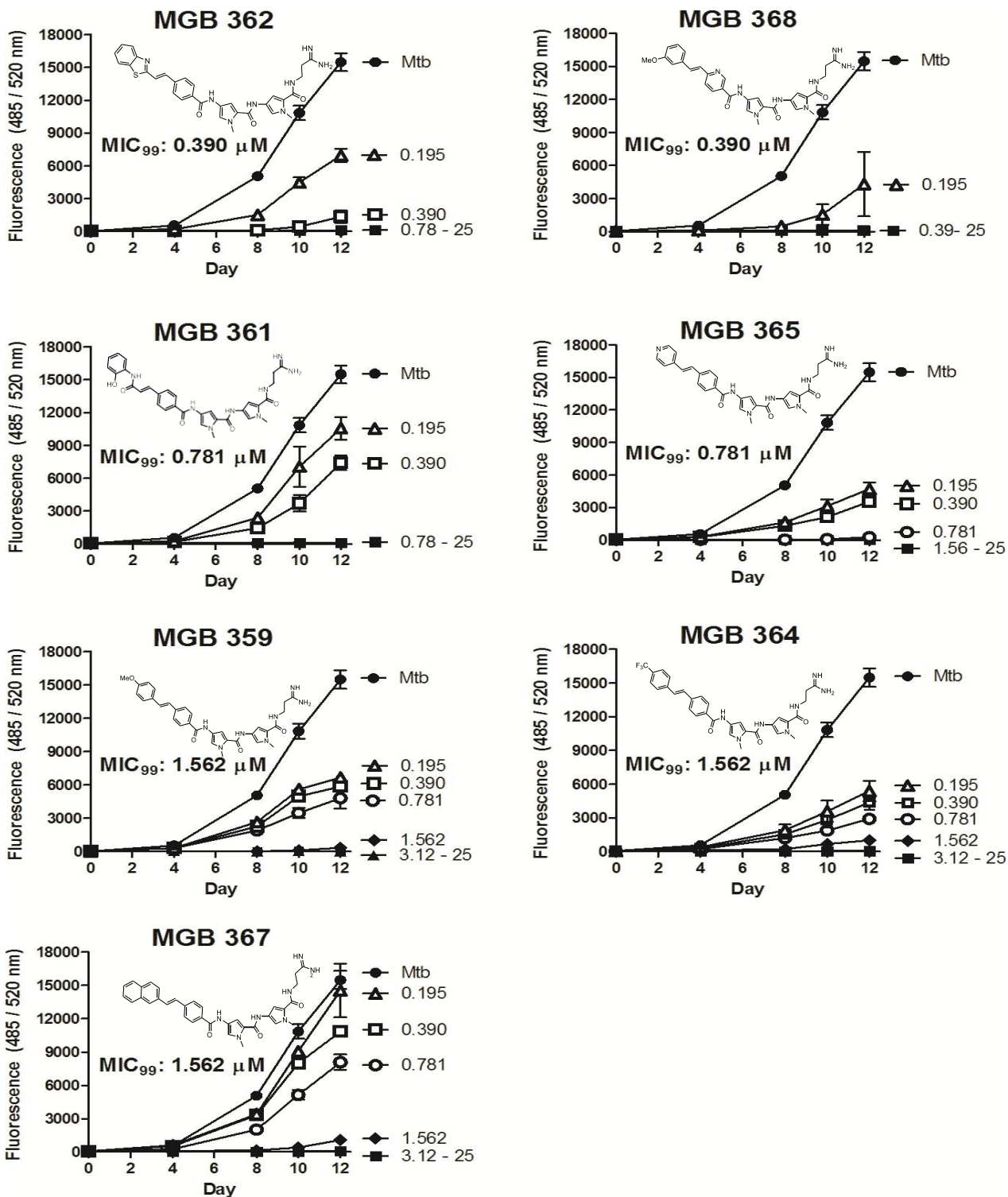


Figure 2.1: Screening of anti-mycobacterial activity of MGB compounds against H37Rv-GFP. Direct antimicrobial activity of MGB compounds at the drug concentration range of 0.195 – 25 μM was tested against H37Rv-GFP (1x10⁵ cfu/well) in 7H9 liquid broth culture using microplate assay. The anti-mycobacterial activity of MGB treatment on H37Rv-GFP was determined at a concentration-dependent manner by measuring fluorescence (485_{ex}/520_{em} nm) on days 0, 4, 8, 10 and 12. Data was corrected for background 7H9 fluorescence. Data show mean ± SEM of duplicates.

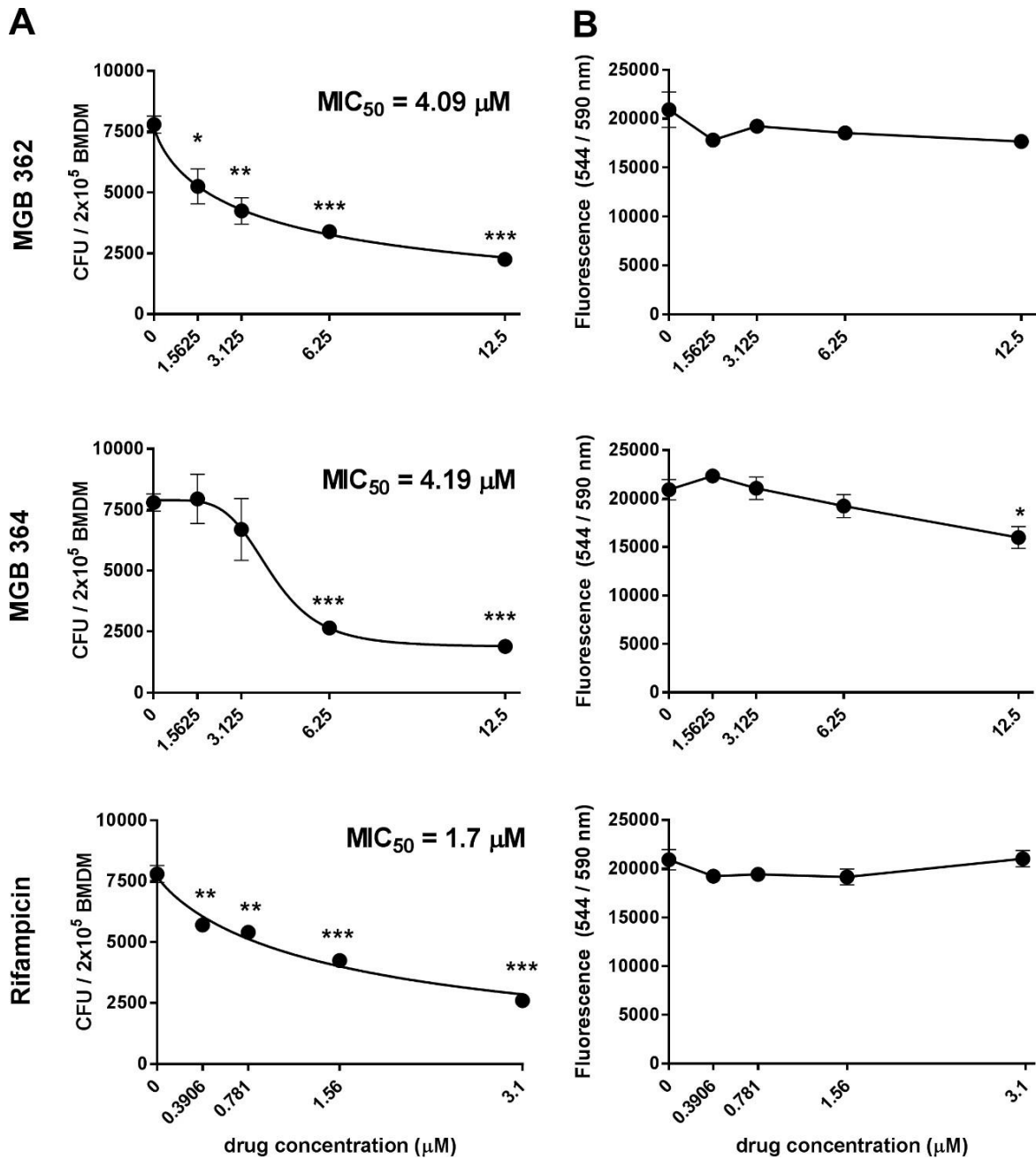


Figure 2.2: MIC₅₀ of MGB compounds in HN878 *Mtb*-infected BMDMs and cell viability. A) The intracellular anti-mycobacterial activities of MGBs (1.5625-12.5 μ M) and rifampicin (0.3906-3.125 μ M) were assessed by counting cfu at the respective concentration at 5 days post *Mtb* HN878 infection. MIC₅₀ values of each drug compound were identified in GraphPad Prism by non-linear regression analysis. B) Macrophage cell viability was determined at 5 days of MGB compound exposure and measured by CellTiter-Blue assay with fluorescence detection at (544_{ex}/590_{em} nm). Data were corrected for background culture medium fluorescence and are shown mean \pm SEM, representative of triplicates. Two-tailed Student's *t*-test, **p* < 0.05, ***p* < 0.01, *** *p* < 0.001 compared to no-drug control.

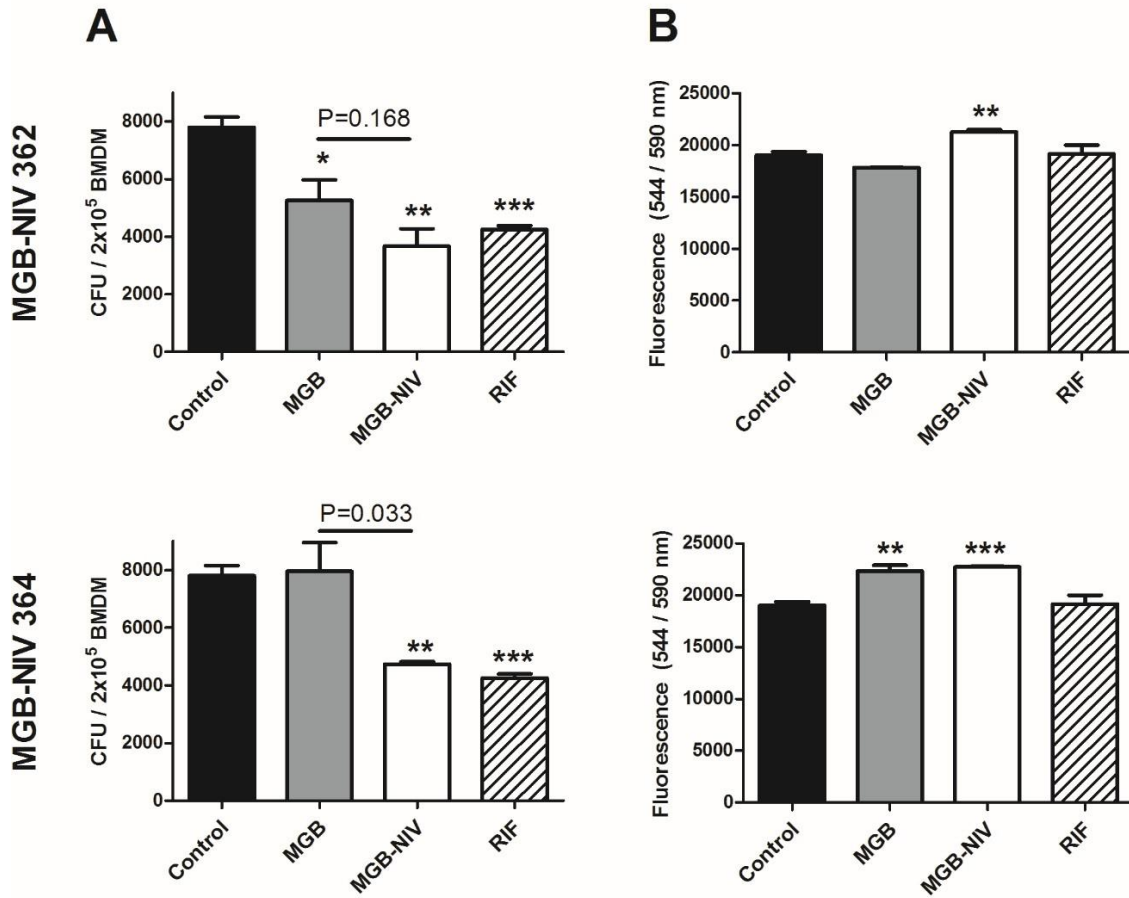


Figure 2.3: MGBs-NIV formulation intracellular mycobacterial activity in HN878 *Mtb*-infected BMDMs and cell viability. A) The intracellular anti-mycobacterial activity of MGBs only, MGBs- NIV formulation and rifampicin was determined in comparison to control (no drug treatment). Cfu was determined at 5 days post *Mtb* HN878 infection. B) Macrophage cell viability was determined at 5 days post *Mtb* HN878 infection and measured by CellTiter-Blue assay with fluorescence detection at (544_{ex}/590_{em} nm). Data were corrected for background culture media fluorescence and are shown as show mean \pm SD, representative of triplicates. Two-tailed Student's *t*-test, *p < 0.05, ** p < 0.01, *** p < 0.001 compared to no-drug control.

Chapter 3 Manuscript in preparation

Evaluation of *in vivo* antimycobacterial activity of MGB and NIV encapsulation via intranasal administration

Summary

In this chapter we assessed the *in vitro* genotoxicity of our lead compound MGB 364 and MGB-NIV 364 in murine bone marrow-derived macrophages infected with clinical Beijing Mtb strain HN878. Detection of γ -H2Ax by flow cytometry was used as a biomarker for DNA double-strand damage. We next investigated the *in vivo* activity of MGB 362, MGB 364 compounds and the use of NIV as an effective delivery system *in vivo*. Here we found that treatment with MGB 364 or MGB-NIV 364 formulation did not cause DNA damage as displayed by low detection of γ -H2Ax compared to H₂O₂ and DMSO treated groups. MGB 364 at low concentrations was effective in killing Mtb *in vivo*. The use of NIVs improved the activity of these compounds. From these studies we could conclude on the potential of MGB 364 as a lead compound against Mtb infection. Interestingly we also observed that intranasal administration of MGB-NIV 364 formulation improved immune responses and pathology during Mtb infection. With this we could conclude on the possibility of an adjunct TB therapy while using NIVs. In this case NIVs would be effective in delivering the drug of interest as well as trigger immune activation necessary for killing of the pathogen. The PhD candidate performed all genotoxicity experiments shown in Figure 3.1. She performed Mtb infections with Dr Mumin Ozturk, treatment experiments by herself; lung homogenates, bacterial burden and lung weight experiments with Dr Mumin Ozturk, Mr Julius Chia and Mr Nathan Kieswetter presented in Figure 3.2. She performed immunohistochemistry in Figures 3.3-3.6; ELISA in Figure 3.7 and flow cytometry experiments in Figure 3.8 by herself.

Evaluation of *in vivo* efficacy of Minor Groove Binders (MGBs) and non-ionic surfactant vesicles (NIVs) encapsulation against *Mycobacterium tuberculosis* via intranasal administration

Lerato Hlaka^{1,2}, Mumin Ozturk^{1,2}, Nathan Kieswetter^{1,2}, Julius Chia^{1,2}, Frank Brombacher^{1,2,3}, Katharine C. Carter⁴, Fraser J. Scott⁵, Colin J. Suckling⁴, Reto Guler^{1,2,3*}

¹ International Centre for Genetic Engineering and Biotechnology, Cape Town Component, Cape Town 7925, South Africa.

² Department of Pathology, University of Cape Town, Institute of Infectious Diseases and Molecular Medicine (IDM), Division of Immunology and South African Medical Research Council (SAMRC) Immunology of Infectious Diseases, Faculty of Health Sciences, University of Cape Town, Cape Town 7925, South Africa

³ Wellcome Centre for Infectious Diseases Research in Africa (CIDRI-Africa), Institute of Infectious Disease and Molecular Medicine (IDM), Faculty of Health Sciences, University of Cape Town, Cape Town 7925, South Africa

⁴ Strathclyde Institute of Pharmacy and Biomedical Science, University of Strathclyde, 161 Cathedral Street, Glasgow, G4 ORE, United Kingdom.

⁵ Department of Biological Sciences, University of Huddersfield, Queensgate, Huddersfield HD1 3DH, UK.

*Corresponding author. Tel: +27-21-4066033; Fax: + 27-86-6407594 E-mail: reto.guler@uct.ac.za

3.1 Abstract

Objectives: Our Strathclyde Minor Groove Binders (S-MGBs) have previously shown promising intracellular anti-mycobacterial activity against Mtb whilst showing modest cytotoxicity to host cells. However, they have not been investigated for *in vivo* efficacy. Furthermore, their ability to potentially cause genotoxicity had not yet been investigated.

Methods: Genotoxicity was assessed in murine bone marrow-derived macrophages infected with clinical Beijing Mtb strain HN878. Expression of γ -H2Ax by flow cytometry was used as a biomarker for DNA double-strand damage. *In vivo* efficacy of MGBs, rifampicin and MGB-NIV formulation against pulmonary Mtb infection was measured in C57BL/6 mice through intranasal administrations once per week for 3 weeks. Four weeks post-infection, lungs and spleens were collected from euthanized mice to determine immunohistopathology, lung inflammatory cell infiltration and bacterial loads using standard colony-forming unit assay.

Results: Treatment with MGB 364 or MGB-NIV 364 formulation did not cause DNA damage as displayed by low detection of γ -H2Ax compared to H₂O₂ and DMSO treated groups. Intranasal administration of 0.5mg/kg MGB 364 or (0.5mg/kg: 30mM) MGB-NIV 364 formulation showed one log reduction in bacterial burden with improved pathology and cytokine production of IL-1 α , IL-17 and IFN- γ when in NIV formulation. However, 10 mg/kg MGB 362 or rifampicin had no effect on bacterial loads.

Conclusions: Our MGB compounds had limited DNA damage to host cells. Intranasal administration of MGB 364 was effective directly at site of infection. Encapsulation of MGBs into NIV improved efficacy through immunomodulatory properties suggesting a potential for intranasal treatment with MGBs as an effective route of administration for pulmonary Mtb infection. Thus, showing a potential for an effective anti-TB drug formulation for TB therapy when using NIVs as a delivery system.

3.2 Introduction

Minor groove binders (MGB)s have shown great potential as antibacterial agents. We previously reported on the anti-mycobacterial properties of various MGBs against *Mycobacterium tuberculosis* (Mtb) [29, 136]. The activity was attributed to specific changes in the structural composition of these compounds in respect to cell wall penetration properties. The inclusion of a thiazole head group in replacement of the pyrrole unit increased lipophilicity and DNA binding which provided the anti-infective activity of first set of MGBs screened [29]. Similar activities of MGB classes containing different head groups was attributed to the similar amidine-containing tail groups which promoted selectivity to the pathogen [136]. We showed that our selected MGB compounds, MGB 362 and MGB 364 had intracellular activity against Mtb. We further showed that encapsulating these MGBs into non-ionic surfactant vesicles improved the intracellular activity of these compounds whilst showing modest mammalian cell toxicity through an approach that measures mitochondrial activity and cellular metabolism [136].

DNA intercalating agents that bind to DNA both covalently and non-covalently have been shown to cause mutagenic shifts especially in bacteriophages and bacterial assays. However, they have shown weak genotoxic and mutagenic activities in mammalian cells [137]. In a study of mutagenicity of N-acyloxy-N-alkoxyamides in *S. typhimurium* TA100, N-acetoxy-N-butoxynaphthamide binding resulted in an increased log *P* value which indicated an increased level of mutagenicity and this was ascribed to DNA intercalating binding rather than hydrophobic binding in the major and minor groove of DNA [138]. The genotoxicity effect of tamoxifen in Chinese hamster V79 cells was a consequence of the formation of covalent adducts with DNA which was attributed to DNA intercalation [139]. Non-covalent bonding which is facilitated by hydrogen bonds and van der Waals forces occurs mainly at the major and minor groove of DNA or through the intercalation of a molecule between base pairs. Minor groove binders such as mitomycins or distamycins are generally non-genotoxic unless covalent bonding of an adjacent molecule or the formation of free radical-dependent DNA double-strand breaks is enabled [140]. Distamycin and diamidine-2-phenylindole (DAPI) were reported to confer chemoprotective activity through the catalytic inhibition of DNA topoisomerase (topo II) which would otherwise facilitate cytotoxicity and the formation of DNA double-strand breaks [141, 142]. Phosphorylation of histone H2Ax occurs during of DNA damage responses (DDR) that are activated due to DNA double-strand breaks [143]. The phosphorylated form γ -H2Ax accumulates at the site of the damage and can be used an indicator of both the number and location of these breaks in the nucleus [143-145]. Here we investigated the ability of

MGB 364 or the encapsulated formulation MGB-NIV 364 to cause genotoxicity using the detection of γ -H2Ax as a biomarker for genotoxic exposure.

Pulmonary administration of TB drug formulations or vaccines by inhalation have shown to be more effective during drug efficacy screening against pulmonary TB. This has shown to increase drug concentration, bioavailability and sustained release pattern at the site of infection [42, 146, 147]. Lipid nanoparticle delivery systems improved lung delivery of poorly soluble molecules like rifampicin [42, 146, 148, 149]. Single dose administration of RIF in freeze-dried liposome formulation in Wister rats via the pulmonary intratracheal or oral routes showed prolonged plasma retention of RIF compared to free drug administered [146]. In the study, RIF was detected from 4 hrs up to 48 hrs when administered in formulation, while free drug was cleared from circulation within 24 hrs [146]. Pharmacokinetic analyses thus showed that RIF in encapsulation with liposome upon pulmonary administration resulted in increased relative bioavailability compared to free drug [146]. To evaluate the chemotherapeutic potential of solid lipid nanoparticles (SLPs) via the respiratory route in guinea pigs, the researchers incorporated three frontline anti-TB drugs (RIF, INH and PZA) in formulation with SLPs [148]. Therapeutic drug concentrations of all three drugs were detected from 45 mins and maintained in the plasma for 5 days and 7 days in lungs, liver and spleen, whereas free drugs were only maintained for 1 or 2 days. Drug bioavailability improved by 8-10 folds in the case of drug-loaded SLPs similarly to Mtb-infected guinea pigs. After 7 weekly (7th day) doses of nebulization treatment of drug-loaded SLPs to infected guinea pigs, no tubercle bacilli were detected in lungs or spleen which was equivalent to 46 daily doses of orally administered drugs to obtain similar therapeutic effect. Furthermore, there was no biochemical hepatotoxicity observed [148]. Pulmonary administration of the second-line TB drug ethionamide when co-encapsulated with its booster BDM41906 into biodegradable polymeric nanoparticles resulted in a 3-log decrease in pulmonary bacterial loads after 6 administrations [150]. Thus, showing the importance of drug delivery systems in the treatment of pulmonary tuberculosis. We therefore tested the *in vivo* efficacy of MGB 362, MGB 364 and MGB-NIV 364 formulation in mice models during pulmonary infection with hypervirulent Mtb strain HN878 via intranasal route of administration using rifampicin as control

3.3 Materials and Methods

3.3.1 Mice

Female wildtype C57BL/6 mice aged between 8-12 weeks old were used. Mice were divided into n=3-6 animals per group for each experiment and kept under pathogen-free conditions in individually ventilated cages at the University of Cape Town Animal Facility unit Biosafety level 2 (BSL-2) or BSL-3 laboratory for Mtb-infected mice. Animal room temperature was maintained at 22-25 °C and 12 hours light/dark cycle. Food pellets and water were made available *ad libitum*.

3.3.2 Ethical statement

All experimental procedures were carried strictly in accordance with the South African National Standard (SANS 10386:2008) and the University of Cape Town's ethical committee guidelines under protocol numbers (015/036 and 015/037). All treatments and infections were performed under intraperitoneal injection (IP) of 10mg/kg xylazine and 100mg/kg ketamine anaesthesia. All euthanasia was performed under halothane to minimize suffering of mice.

3.3.3 Preparation of Minor groove binder compounds and non-ionic surfactant vesicles

Minor groove binder compounds 362 or 364 or 10 mg/kg rifampicin were dissolved in 1x PBS/saline or diluted in DMEM to yield a concentration 10mg/kg (MGB 362) or 0.5mg/kg (MGB 364) per mouse or 10 µM in macrophages. Freeze dried NIVs were prepared as previously described [54] and rehydrated in PBS/saline or DMEM + 10% FCS (Gibco, Thermofisher Scientific, USA) to a final NIV concentration range of 30µM in formulation with MGBs or empty NIV.

3.3.4 Generation of murine bone marrow-derived macrophages and Mtb infection

BMDMs were generated from 8-12 weeks old C57BL/6 mice as described [127]. Following 10 days of differentiation, BMDMs were cultured in triplicates overnight for adherence into 96-well plates (Nunc, Denmark) at 5×10^4 cells per well. Single cell suspension of hypervirulent HN878 *Mycobacterium tuberculosis* (Mtb) from frozen stock was prepared in DMEM media. After 24hr adherence, BMDMs were infected with HN878-*Mtb* at MOI 1:5 CFU per well. At 4hrs post-infection, BMDMs were then washed once with culture media to remove extracellular bacteria or lysed. Lysates were plated on 7H10 agar plates containing 10% OADC and 0.5% glycerol for CFU counting to determine bacilli uptake.

3.3.5 Evaluation of MGB induced genotoxicity

After 24hr post-infection, MGB 364, MGB-NIV 364, rifampicin and toxicity inducing agents, hydrogen peroxide (H₂O₂) and dimethyl sulfoxide (DMSO) were prepared in DMEM media supplemented with 10% fetal calf serum (FCS) at defined concentrations of 10 μ M and added to infected BMDMs. After 4 and 24 post-treatment, cells were harvested and assessed for genotoxicity by flow cytometry by the following antibodies: CD11b (PercCPcy-5.5); mouse/human anti-phospho histone SER-139 H2Ax (H5912) and isotype control (Alexa fluor 488); F/480 (Alexa fluor 647); MHCII-(Alexa fluor 700); polyclonal rabbit anti-histone H2A.X (AB10022), goat anti-rabbit IgG (Alexa fluor 488) secondary antibody. For staining of surface markers, cells were washed in 1x PBS and labelled with respective markers and then washed in FACS buffer (1X PBS with 1% BSA and 0.1% NaN₃). Intranuclear expression of γ H2Ax was detected using BD Pharmingen Transcription Factor Buffer Set (BD Biosciences) according to manufacturer's instruction. Acquisition was conducted using BD LSR Fortessa and data analysis was performed with FlowJo software (Treestar, Ashland, OR, US).

3.3.6 In vivo Mtb infection and intranasal MGB/ MGB-NIV treatment in mice

Mice were infected with HN878-Mtb strain at 100 or 1000 CFU per mouse via intranasal route as described [17]. After 7 days post-infection, mice were anaesthetized with an IP injection of 10mg/kg xylazine and 100mg/kg ketamine and treated once per week for 21 days with 10mg/kg of MGB 362 or 0.5 mg/kg of MGB 364 or 0.5mg/kg: 30mM MGB- NIV 364 formulation. 10mg/kg rifampicin was used as a positive control, while saline and no treatment were used as negative controls. Mice were monitored daily and weighed once weekly and euthanized with halothane when animals lost 20 % of their original body weight or showed any signs of distress such as lack of grooming, coat staring, hunched up posture, open mouth breathing, difficulty in breathing and immobility. At the end of the study, mice were euthanized to assess drug treatment efficacy. Lungs and spleens were isolated to determine bacterial load using CFU assays. Infiltration of inflammatory cells were also determined from single cell suspensions of lung tissues 3 weeks post-treatment by flow cytometry.

3.3.7 Oral MGB treatment in mice

After 7 days following infection with 100 CFU HN878, mice were treated once per week with 10 mg/kg MGB 362 control mice with 10 mg/kg rifampicin or with saline by oral gavage

for 3 weeks. Four weeks post infection, mice were euthanized, lungs and spleens were isolated to determine bacterial loads using CFU assays.

3.3.8 Preparation of tissue homogenates to determine bacterial load

Following sacrifice, lungs and spleens were removed aseptically, weighed, and homogenized in 0.04% Tween-80 in saline solution. Homogenates were diluted into ten-fold serial dilutions and plated onto Middlebrook 7H10 (BD Biosciences, San Jose, CA) agar plates containing 10% OADC and 0.5% glycerol and incubated at 37°C followed by colony counts after 21 days of incubation.

3.3.9 Histopathological and Immunohistochemistry examination

Formalin fixed (4%) Mtb-infected lungs from wild-type littermate controls and IL-4i1^{-/-} mice were stained with hematoxylin and eosin or rabbit anti-mouse iNOS (Abcam) and detection performed using HRP-labelled anti-rabbit and anti-goat, respectively as described [80, 151]. Gelatine-based mounting medium was used to mount the sections. Image acquisition and quantification of alveolar airspaces, iNOS and Arg1 were performed using NIS advanced software on a Nikon (Tokyo, Japan) 90i microscope. Percentage of free alveolar airspaces was defined as the area of ventilated spaces in whole lung sections in relation to the total lung tissue area using the area measurement tool by NIS advanced software on a Nikon 90i microscope and % alveolar spaces calculated using Excel as described [21]. The percentage of iNOS and Arg1 was performed using a blinded quantification method as described [21].

3.3.10 Flow Cytometry

Single cell suspensions from lung tissues were stained for surface markers with the following antibodies: F4/80 (PE-Cy7) from Affymetrix eBiosciences; LY6C (PercCP-Cy5.5); CD11c (V450); MHCII (Alexa Fluor 700); CD103 (PE); CD11c (Alexa Fluor 647); SiglecF (APC-Cy7); CD44 (FITC); NK1.1 (APC-Cy7); CD62L (V450); TCR gamma delta (biotin); CD19 (PercCP-Cy5.5); CD8 (Alexa Fluor 647), Streptavidin (Texas Red), LY6G (FITC) and CD4 (PE) from BD Biosciences in FACS buffer. Acquisition was conducted using BD LSR Fortessa, and data analysis was performed with FlowJo software (Treestar, Ashland, OR, US).

3.3.11 Cytokine responses

Supernatants collected from lung homogenates were used to determine cytokine production using enzyme-linked immunosorbent assay. IL-6, IL-4, IL-12p40, TGF- β and IFN- γ (BD Biosciences); IL-1 α , IL-1 β (R&D Systems, Minneapolis, MN); TNF- α , IL-17, IL-10 (BioLegend) production was measured from the supernatants and data analysed using

SoftMax Pro 6.

3.3.12 Statistical analysis

All data were analysed using Graph-Pad Prism 6.0. Data were calculated as mean \pm SEM. Statistical significance was calculated with one-way ANOVA was used. A * p value of less than 0.05 as considered significant, with ** p < 0.01, *** p < 0.001 and **** p < 0.0001.

3.4 Results

3.4.1 MGB treatment is not genotoxic to murine and human macrophages as determined by Gamma-H2Ax expression

Intranuclear expression of phosphorylated H2Ax was measured to detect drug induced DNA damage in HN878-Mtb infected CD11b⁺F/480⁺MHCII⁺ murine macrophages. Using isotype control as a point of reference, the expression of γ -H2Ax remained significantly low ($p < 0.05$) in MGB 364, MGB-NIV 364 and rifampicin compared to macrophages treated with H₂O₂ at 4-24 hrs post-treatment and DMSO 24 hrs post-treatment (Fig. 3.1). These data suggest that MGB or MGB-NIV compounds do not cause DNA damage to host cells.

3.4.2 MGB-364 reduced bacterial load, NIV encapsulation improved drug efficacy of MGB-364 during acute Mtb infection in mice

Next, we sought to determine the *in vivo* efficacy of MGB compounds by directly targeting the site of infection in mice intranasally infected with HN878-Mtb. We first investigated the *in vivo* efficacy of MGB 364 directed at the site of infection and whether encapsulating MGB 364 into NIVs, a drug delivery system that was previously reported to improve its efficacy in macrophages, would improve MGB 364 efficacy against HN878-Mtb strain *in vivo* [136]. Intranasal treatment with MGB 364 showed a significant one log reduction ($p < 0.01$) in lung bacterial loads 3 weeks post-treatment when compared to no treatment group (Figure 3.2A). However, similar bacterial loads were detected in the spleens, suggesting that MGB 364 was retained and more effective against Mtb directly at the site of infection (Figure 3.2B). We also treated infected mice with MGB-NIV 364 or empty NIV as controls. Intranasal treatment with MGB-NIV 364 showed a significant one log reduction ($p < 0.01$) in lung bacterial loads similarly to that of MGB 364 alone compared to the no treatment group (Figure 3.2A). Surprisingly, empty-NIV treatment had a similar reduction compared to no treatment group, suggesting that NIVs influenced the killing of Mtb *in vivo* (Figure 3.2A). A significant reduction in lung weight index was observed in mice treated with MGB 364, suggesting a reduced inflammation in the lung compared to the no treatment group (Figure 3.2C). To check *in vivo* efficacy of MGB-362, mice were intranasally treated with 10mg/kg of MGB 362 or 10mg/kg rifampicin or saline or left untreated. Bacterial loads were similar across the treatment groups at 3 weeks post-treatment as determined by cfu counts in both lungs and spleens of infected mice (Figure 3.2D and 3.2E). These data suggest that MGB 362 does not reduce Mtb burden *in vivo*. Surprisingly, rifampicin also did not reduce the Mtb burden, suggesting that rifampicin intranasal administration was not effective for Mtb treatment *in vivo* (Figure 3.2D). Similarly, there were no significant differences in lung weight

index across all groups (Figure 3.2F). We next changed the route of administration to oral administration by oral gavage to evaluate the efficacy of MGB 362 *in vivo*. Similarly oral administration of MGB 362 had no effect on bacterial loads and no effect on lung weights across groups were observed, but one log reduction in bacterial burden ($p < 0.05$) was observed with RIF treatment (Figure 3.2. G-I).

3.4.3 Rifampicin improved histopathology of HN878 *Mtb*-infected mice

We next investigated the effect of MGB 364 or MGB-NIV 364 on the histopathology of infected mice through the quantification of lung alveolar airspaces. Treatment with MGB 364 had no effect on the pathology of *Mtb*-infected mice, however treatment with MGB 364-NIV and empty-NIV decreased disease pathology as shown by a significant increase in free alveolar airspaces compared to no treatment group (Figure 3.3A-B). MGB 362 had no effect on the histopathology of infected mice with alveolar spaces similar to the no treatment and saline control groups (Figure 3.4A-B). Surprisingly, although no effect on bacterial loads, intranasal treatment with rifampicin improved the histopathology status of infected lungs as shown by a significant increase ($p < 0.01$) in alveolar airspaces compared to no treatment groups (Figure 3.4A-B). There was no significant difference on tissue iNOS and Arg1 expression in all groups (Figure 3.5A-D; Figure 3.6A-D), suggesting that MGB and MGB-NIV treatment has does not induce iNOS and Arg1 tissue expression in *Mtb*-infected mice.

3.4.4 NIV encapsulation of MGB 364 increased the production of IL-1 α , IL-17 and IFN- γ while MGB 362 reduced IL-1 β , IL-12p40 and IL-10 cytokine production, but increased CD4 T-cell recruitment following *Mtb* infection

We next investigated the effect of MGB 364 and MGB-NIV 364 on immune responses, determined by cytokine production in the lungs. MGB-NIV 364 treatment showed a significant increase ($p < 0.05$) in pro-inflammatory cytokine IL-1 α production, similarly to empty-NIV treatment. Furthermore, IFN- γ and IL-17 were significantly increased ($p < 0.01$ and $p < 0.05$ respectively) in MGB-NIV 364 treated groups, but had no effect on other cytokines measured (Figure 3.7A-B). These data thus suggest that the NIV encapsulation improved effector cytokine production which correlates to improved immunopathology of disease outcome. Interestingly, a significant reduction ($p < 0.01$) in pro-inflammatory IL-1 β , IL-12p40 and regulatory IL-10 cytokines was observed in MGB 362 treated group compared to no treatment group (Figure 3.7C), suggesting that MGB 362 had reduced effect on pro-inflammatory effector responses during *Mtb* infection. Similarly, MGB 364 treatment alone had similar levels of cytokine production when compared to the no treatment group (Figure 3.7A-B). We measured the effects of

MGB 362 and rifampicin on cellular infiltration in the lungs by flow cytometry in Mtb-infected mice. Mice treated with MGB 362 showed significant increase ($p < 0.001$) in CD4⁺ T-cell population compared to control groups. However, rifampicin treatment showed a significant increase in CD11b⁺ MHCII⁺ CD11c^{high} monocyte-derived dendritic cells (mDCs) (Figure 3.8A-B).

3.5 Discussion

We previously reported on the intracellular antimycobacterial properties of MGB 362 and MGB 364 and the use of NIV's to improve their efficacy whilst being non-toxic [136]. The activity of the MGBs was attributed to the amidine-containing tail group and the permeability to different cells types. However, the ability of these compounds to cause DNA damage has not been investigated. Furthermore, the antimycobacterial properties of these compounds *in vivo* remains unknown. Detection of phosphorylated histone H2Ax (γ -H2Ax) in mammalian cells by flow cytometry similarly to foci quantification, is a reliable high-throughput bio-indicative analysis for chemically induced DNA damage [143-145]. Quantification of γ -H2Ax detection by foci formation and flow cytometry in CHO-9 cells treated with 14-well-known genotoxic compounds of which H₂O₂ was amongst them and 10 non-genotoxic compounds, revealed that the induction of γ -H2Ax expression was associated with loss of cell viability in a dose dependent manner. Furthermore, data obtained from foci formation and flow cytometry showed high correlation, suggesting that flow cytometry analysis of γ -H2Ax detection as high-throughput analysis for genotoxicity [143]. Here, observed low detection of γ -H2Ax with both our MGBs and MGB in NIV formulation in mammalian cells in murine macrophages compared to cells treated with 10 μ M genotoxic agent H₂O₂ and DMSO (Figure 3A). These data correlate with our previous studies on cell viability. Macrophages infected with HN878 remained viable following 5 day treatment with MGB 362 and 364 as both free compound and in formulation [136]. We used 10 μ M for treatment as this was shown to be the minimum dose to trigger the onset of γ -H2Ax detection by H₂O₂. These data thus suggest that MGB 362 and MGB 364 are not toxic to mammalian cells. However, additional studies to verify MGB-induced genotoxicity through foci quantification and other methods are in progress.

We next investigated these compounds for their *in vivo* efficacy during Mtb infection. We targeted the site of infection through intranasal administration of MGB compounds and MGB-NIV formulation using rifampicin as a control. Intranasal administration of vaccines or drugs against tuberculosis has been reported to be more effective compared to other routes of administration when doses are exceeding normal clinical doses of most drugs

0.1mg/kg [152]. Rosada et al. 2008 [153] reported that a single intranasal dose of the formulation of DNA-hsp65 complexed with cationic liposomes as delivery system significantly reduced bacterial burden and as effective as four intramuscular administrations. Pandey et al. 2003 [154] showed that single nebulization of rifampicin, pyrazinamide and isoniazid encapsulated in poly (DK-lactide-co-glycolide) nanoparticles was equivalent to 46 daily doses of oral treatment to clear Mtb bacilli in infected guinea pigs. Here, we demonstrated that single weekly administrations of MGB 364 and MGB-NIV 364 at a low concentration (0.5 mg/kg) were effective to reduce bacterial load one log-fold in lungs with no effect on the spleen of mice infected with a high dose of hypervirulent Mtb strain (Figure 3.2A-C). Surprisingly, empty-NIV administration also reduced bacterial load and this was attributed to the previously reported immunomodulatory properties of NIV [156]. Our results showed that the presence of NIVs in the formulation improved histopathology and increased the levels of effector cytokines IL-1 α , IL-17 and IFN- γ , which are all involved in the pathogenesis and clearance of Mtb infection (Figure 3.3; 3.7A). However, MGB 364 treatment did not show any effect on the pathology or immune responses, nor the L-arginine metabolic pathway as shown by iNOS or Arginase 1 expression in lung tissues (Figure 3.5). Although the use of non-ionic surfactant vesicles (NIVs) showed to be reliable delivery system to improve the efficacy of MGBs and deliver to the site of infection, more studies on drug permeability and pharmacokinetics to measure the bioavailability of the compounds and formulation to the site of infection are warranted. On the contrary, 10 mg/kg of MGB 362 and rifampicin had no effect on bacterial load (Figure 3.2D-F). Rifampicin is usually administered orally or intravenously and is fast absorbed after oral administration [155]. It is possible that the intranasal route of administration did not allow absorption of the drug and thus deemed it ineffective against Mtb. Oral administration of MGB 362 similarly not have effect on bacterial burden. Rifampicin showed one log-fold reduction compared to saline group, however, was not statistically significant (Figure 3.2G-I). Furthermore, rifampicin improved pathology due to unclear mechanisms. Although treatment with rifampicin increased the recruitment of monocyte derived dendritic cells which are responsible for the recruitment of other cell types like CD 4 T-cells that are important for the Mtb clearance, treatment with rifampicin did not show any effects on T cell recruitment nor immune cytokine production. Surprisingly, treatment with MGB 362 increased CD4 T cell recruitment (Figure 3.8). However, there was no correlation with the cytokines produced nor bacterial burdens in lung tissues. We observed a reduction in pro-inflammatory cytokines, IL-1 β and IL-12p40 predominantly released by macrophages and dendritic cells in the control of acute Mtb infection together with the reduced levels of regulatory cytokine IL-10 (Figure 3.7C). IL-12p40 is an essential cytokine in the recruitment and activation of CD4 T cells which would mainly release IFN- γ , a key

cytokine responsible for Mtb clearance [156, 157]. However, MGB 362 treatment did not affect the production of IFN- γ nor Mtb clearance as IFN- γ levels and bacterial loads remained similar across groups.

In conclusion, this study showed that our MGB 364 is non-genotoxic to host cells. Furthermore, MGB 364 is an active compound against Mtb directly at the site of infection *in vivo*. The use of NIV improved the efficacy of MGB 364 through mechanisms that induce host protective immune functions. Thus, MGB 364 holds promise as an anti-TB compound. This warrants further mechanistic screening to determine the mode of action of these compounds

3.6 Acknowledgements

We thank the UCT Animal Research Facility for maintaining mice. Mrs. Zarinah Sunday, Ms. Munadia Ansarie, Mr. Marlon Petersen and Mr. George Jacobs for their excellent technical assistance.

3.7 Funding

The work reported herein was made possible through funding by the South African Medical Research Council through its Division of Research Capacity Development under the SAMRC Internship Scholarship Programme from funding received from the South African National Treasury to LH, The LOREAL-UNESCO For Women in Science Sub-Saharan Africa Programme for PhD grant to LH. The content hereof is the sole responsibility of the authors and do not necessarily represent the official views of the SAMRC or the funders. The Knowledge Exchange Development Fund (KEDF) from the University of Strathclyde to KCC, International Centre for Genetic Engineering & Biotechnology (ICGEB) Arturo Falaschi Post-doctoral Fellowship to MO and JC, the National Research Foundation PhD Fellowship to NSK, grants from the South African National Research Foundation (NRF) and from the Department of Science and Technology, South African Research Chair Initiative (SARCHi) and South Africa Medical Research Council (SAMRC) to FB, grants from the Department of Science and Technology (DST) / South African National Research Foundation (NRF) Collaborative Postgraduate Training Programme to RG.

3.8 Transparency Declarations

None to declare

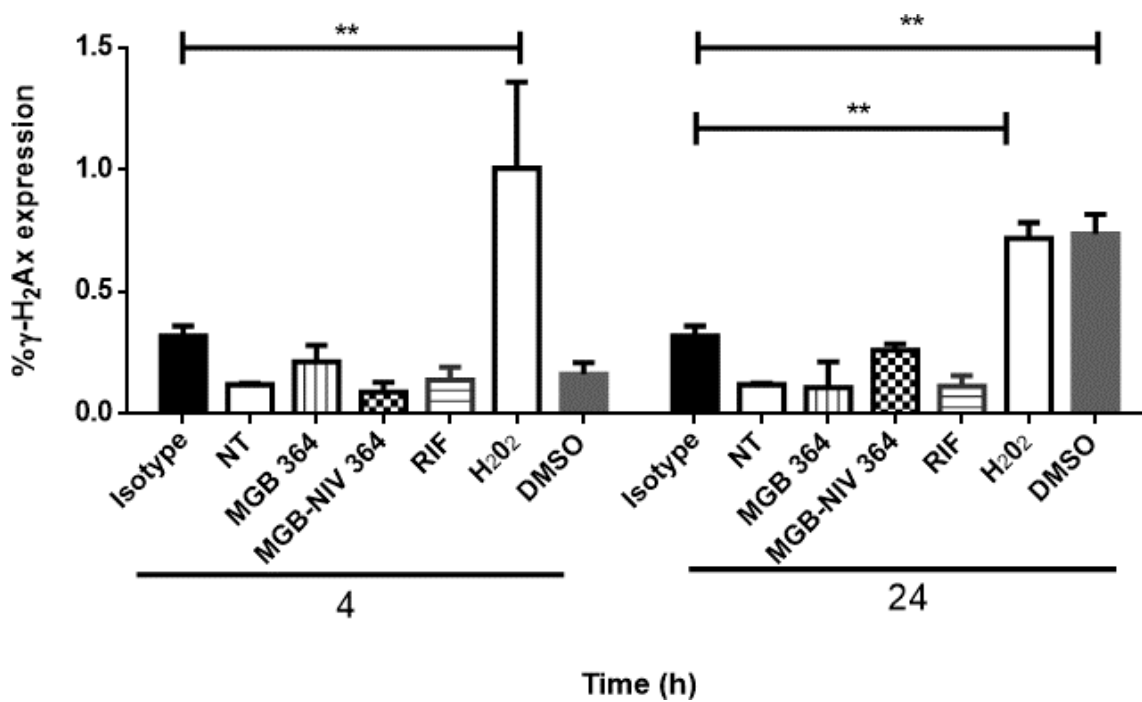


Figure 3.1: No genotoxicity was observed in MGB 364/MGB-NIV 364 treated macrophages. CD11b⁺F4/80⁺MHCII⁺ bone-marrow derived macrophages treated with 10 μ M MGB-364, MGB-NIV 364, H₂O₂, RIF and DMSO. Intracellular detection of γ -H₂Ax expression was measured 4, 24 hrs post-treatment by flow cytometry using isotype control as a measure of detection. Data show mean \pm SEM of triplicates. Two-tailed Student's *t*-test, **P* < 0.05, ***P* < 0.01 compared to isotype control.

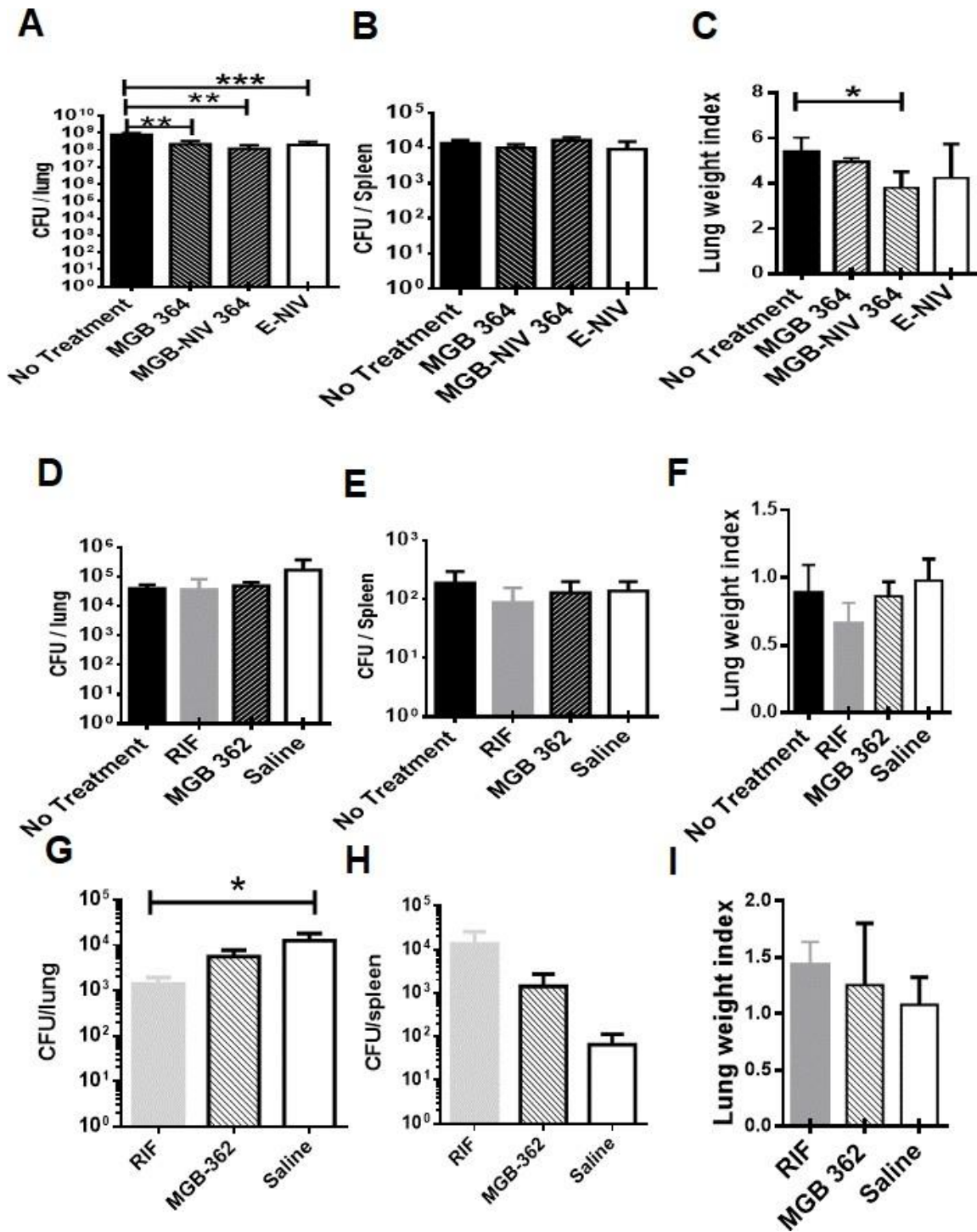


Figure 3.2: MGB-364 and MGB-364 NIV formulation reduced mycobacterial burden in HN878-Mtb infected mice but MGB-362 *in vivo* treatment did not affect mycobacterial load. Mice (n= 3-6 per group) were infected with 100 or 1000 CFU of HN878-Mtb strain via intranasal challenge followed by weekly single intranasal treatment with 0.5 mg/kg of MGB-364; 0.5 mg/kg:30 mM MGB-NIV 364 or 10 mg/kg MGB-362 or 10 mg/kg rifampicin as positive control or left untreated; empty NIV or administered saline as negative controls starting one week post-infection for a duration of 3 weeks. Mice were sacrificed at 4 weeks post-infection (3 weeks post-treatment) and lungs isolated and homogenized for CFU assays. A) Bacterial load measured in lungs B) and spleen of infected mice intranasally treated with MGB-364, MGB-364 NIV or empty NIV. C) Lung weight index of infected mice intranasally treated with MGB-364, MGB-364 NIV or empty NIV. D) Lung and E) spleen bacterial loads of infected mice intranasally treated with MGB-362 or rifampicin. F) Lung weight index of infected mice intranasally treated with MGB-362 or RIF 4 weeks post-infection. G) Bacterial load measured in lungs and H) spleen of infected mice orally treated with MGB-362 or RIF. I) Lung weights of infected mice orally treated with MGB-362 or

RIF. Data show mean \pm SEM of triplicates. One-way ANOVA, * $P < 0.05$, ** $P < 0.01$; compared to no-treatment control.

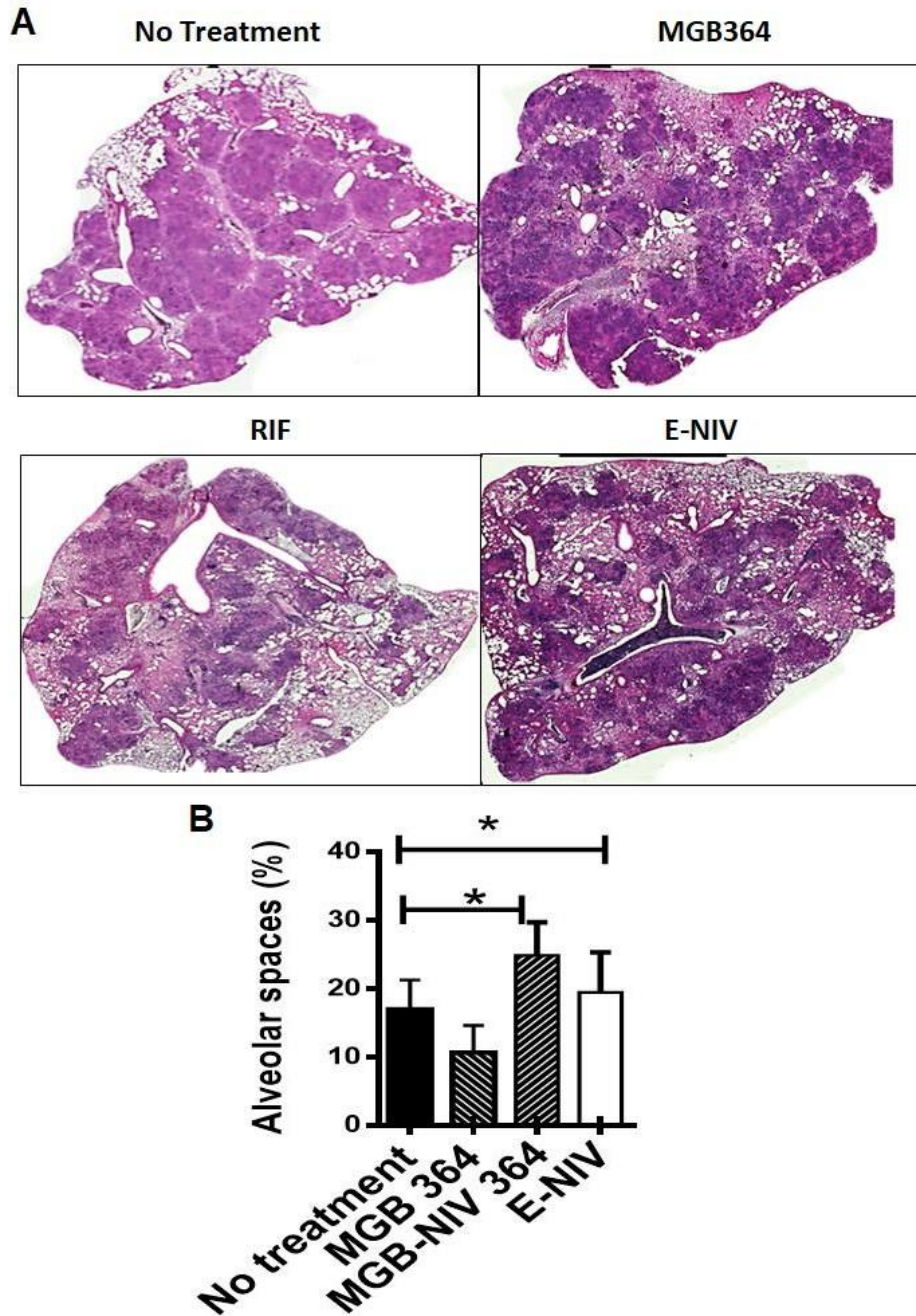


Figure 3.3: NIV encapsulation of MGB-364 improved pulmonary histopathology of HN878-*Mtb* mice. Mice (n= 3-6 per group) were infected with 1000 CFU of HN878-*Mtb* strain via intranasal challenge followed by weekly intranasal treatment with 0.5 mg/kg of MGB-364; MGB-NIV 364 or empty NIV as control or left untreated for 3 weeks. Mice were sacrificed 4 weeks post-infection (3 weeks post-treatment) and lungs isolated and collected in 4% formalin for histopathology analysis. **A)** Representative images of H&E stained sections. **B)** Quantification of alveolar air spaces 4 weeks post- infection. Data show mean \pm SEM of triplicates. One-way ANOVA, * $p < 0.05$, ** $p < 0.01$; *** $p < 0.001$; **** $p < 0.0001$ compared to control.

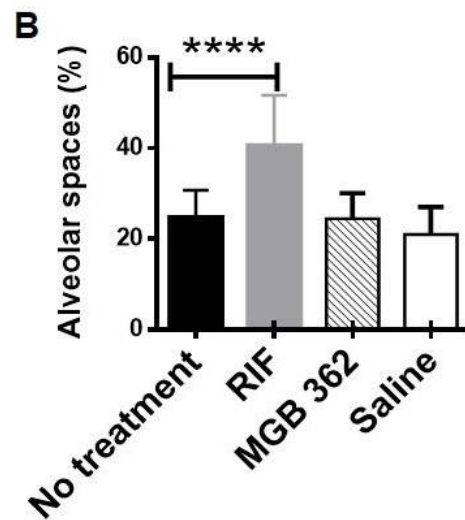
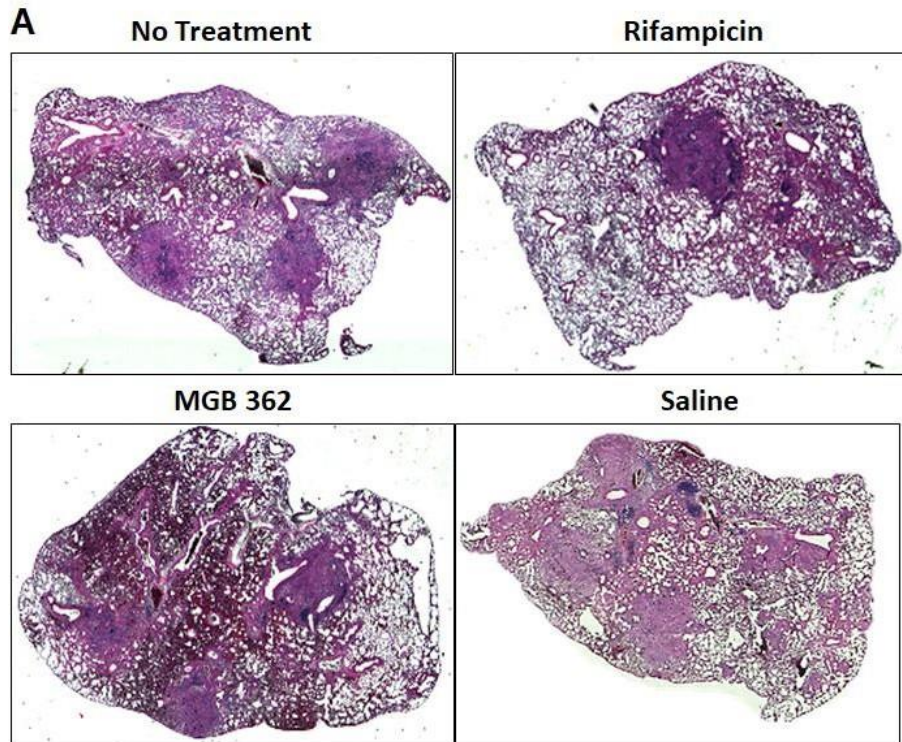


Figure 3.4: MGB-362 had no effect on pulmonary pathology. Mice (n= 3-6 per group) were infected with 100 CFU of HN878-*Mtb* strain via intranasal challenge followed by weekly intranasal treatment with 10 mg/kg of MGB-362 or rifampicin as positive control or left untreated or administered saline as negative control for 3 weeks. Mice were sacrificed 4 weeks post-infection (3 weeks post-treatment) and lungs isolated and collected in 4% formalin for histopathology analysis. **A)** Representative images of H&E stained sections. **B)** Quantification of alveolar airspaces 4 weeks post- infection. Data show mean \pm SEM of triplicates. One-way ANOVA; *p < 0.05, **p < 0.01; ***p < 0.001; ****p < 0.0001 compared to control.

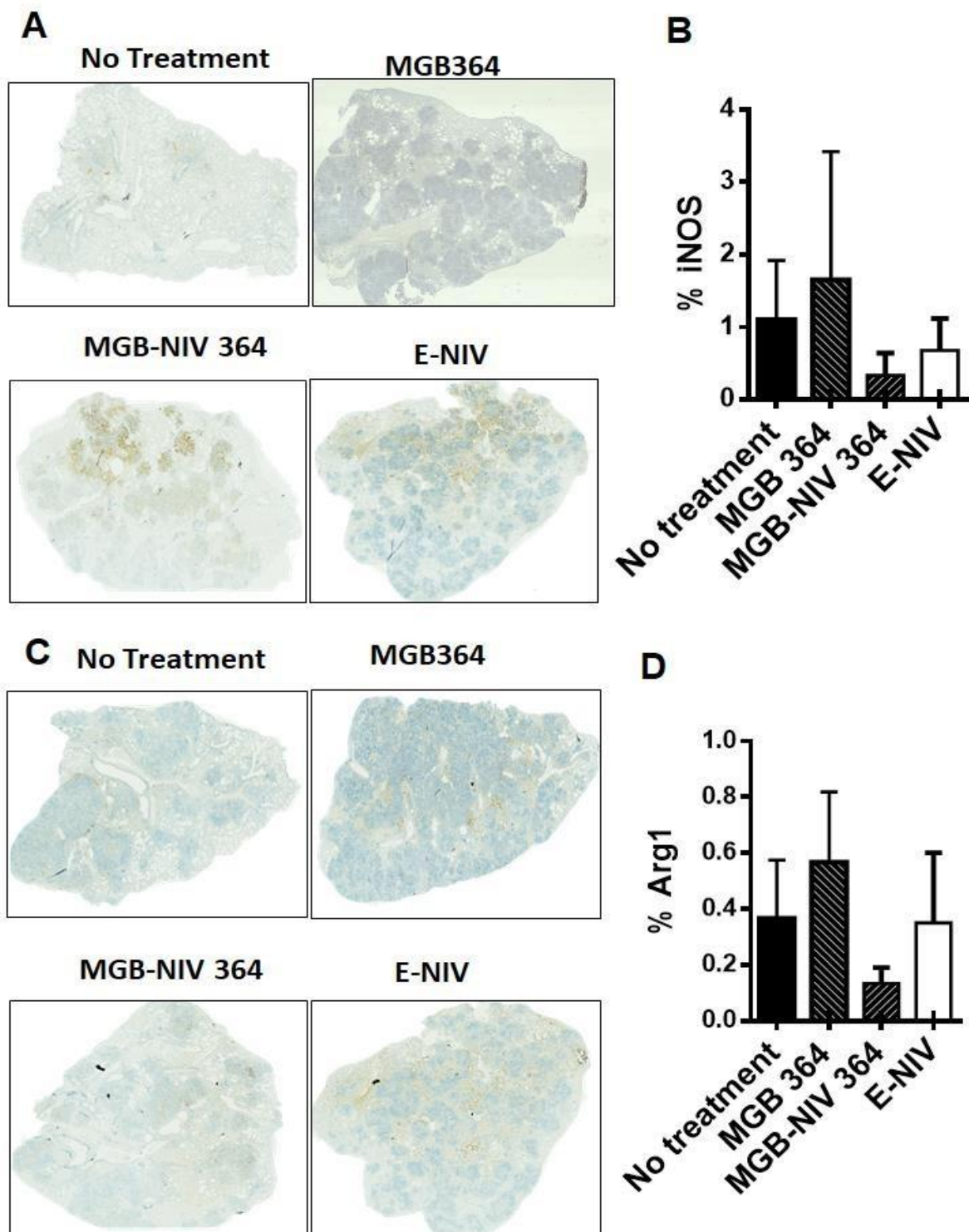


Figure 3.5: MGB-364 and NIV encapsulation had no effect on lung iNOS and Arg1 expression. Mice (n= 3-6 per group) were infected with 1000 CFU of HN878-*Mtb* strain via intranasal challenge followed by weekly intranasal treatment with 0.5 mg/kg of MGB-364; MGB-NIV 364 or empty NIV as control or left untreated for 3 weeks. Mice were sacrificed 4 weeks post-infection (3 weeks post-treatment) and lungs isolated and collected in 4% formalin for histopathology analysis. Representative images of iNOS (A) and Arg1 (C) stained sections are shown. Percentage of lung iNOS (B) and Arg1 (D) positive areas are quantified in the sections of mice 4 weeks post-infection. Data show mean \pm SEM of triplicates. One-way ANOVA, * $p < 0.05$, ** $p < 0.01$; *** $p < 0.001$; **** $p < 0.0001$ compared to control.

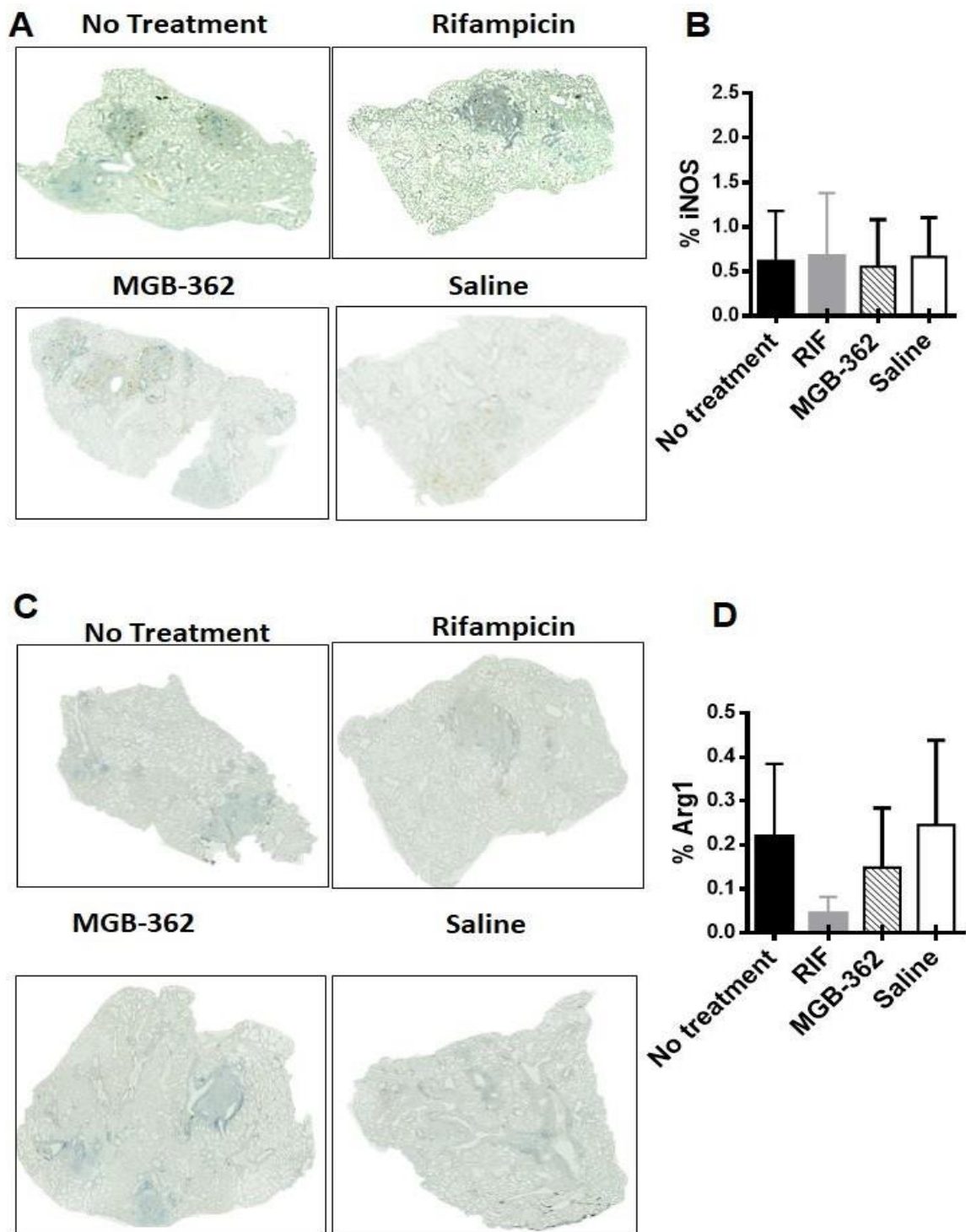


Figure 3.6: MGB 362 had no effect on lung iNOS and Arg1 expression. Mice ($n = 3-6$ per group) were infected with 100 CFU of HN878-*Mtb* strain via intranasal challenge followed by weekly intranasal treatment with 10 mg/kg of MGB 362 or rifampicin as positive control or left untreated or administered saline as negative control for 3 weeks. Mice were sacrificed 4 weeks post-infection (3 weeks post-treatment) and lungs isolated and collected in 4% formalin for histopathology analysis. Representative images of iNOS (**A**) and Arg1 (**C**) stained sections are shown. Percentage of lung iNOS (**B**) and Arg1 (**D**) positive areas are quantified in the sections of mice 4 weeks post-infection. Data show mean \pm SEM of triplicates. One-way ANOVA, * $p < 0.05$, ** $p < 0.01$; *** $p < 0.001$; **** $p < 0.0001$ compared to control.

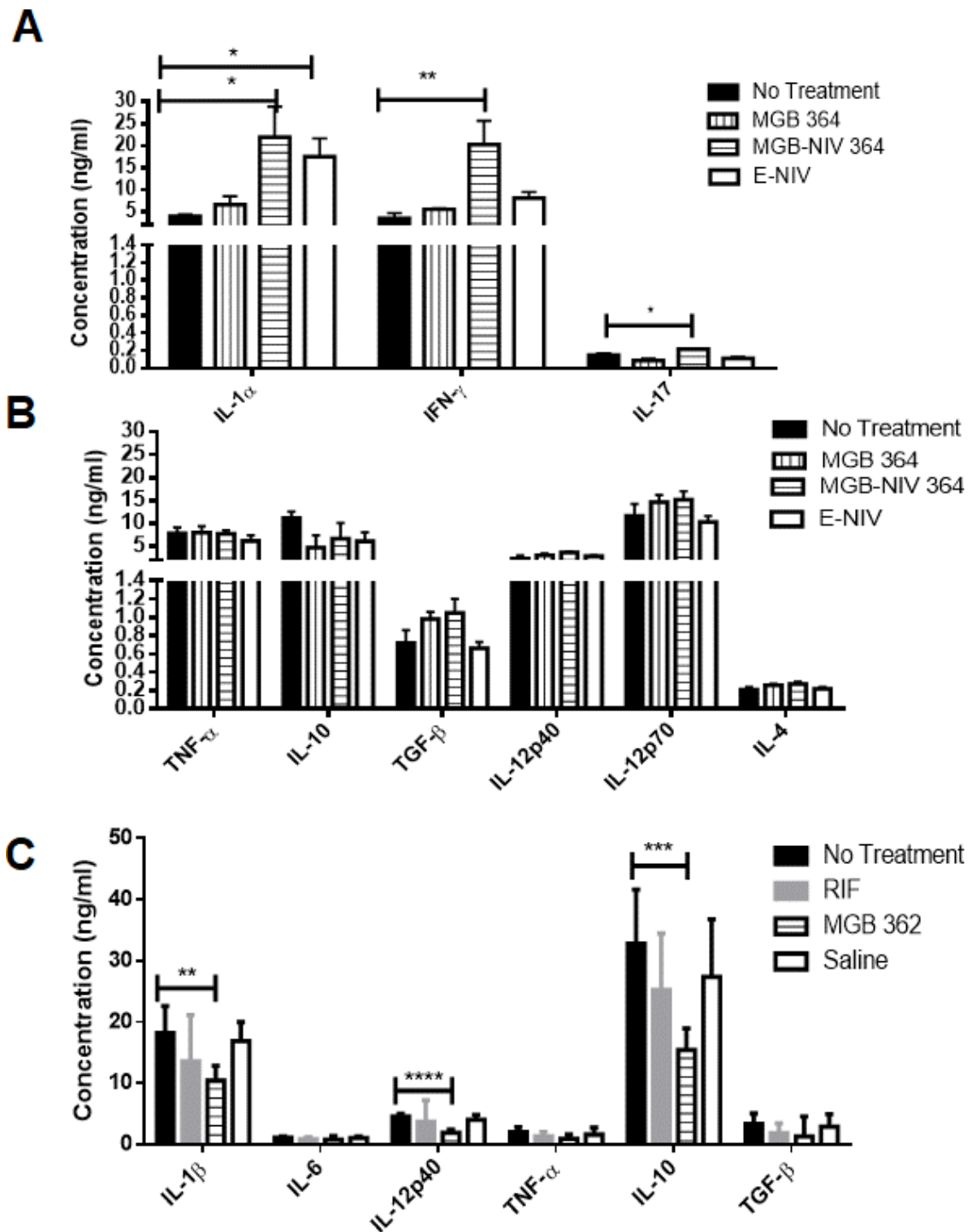


Figure 3.7: Increased pro-inflammatory effector cytokine in lungs of MGB-NIV 364 and reduced pro-inflammatory cytokine responses MGB 362 treated mice following HN878-*Mtb* infection. Supernatants from lung homogenates were collected for cytokine production analysis. **A-B)** Cytokine concentrations of mice treated with MGB-NIV 364. **C)** Cytokine concentrations of mice treated with MGB-362 or rifampicin. Data show mean \pm SEM of triplicates. One-way ANOVA, * $p < 0.05$, ** $p < 0.01$ and *** $p < 0.001$ compared to control.

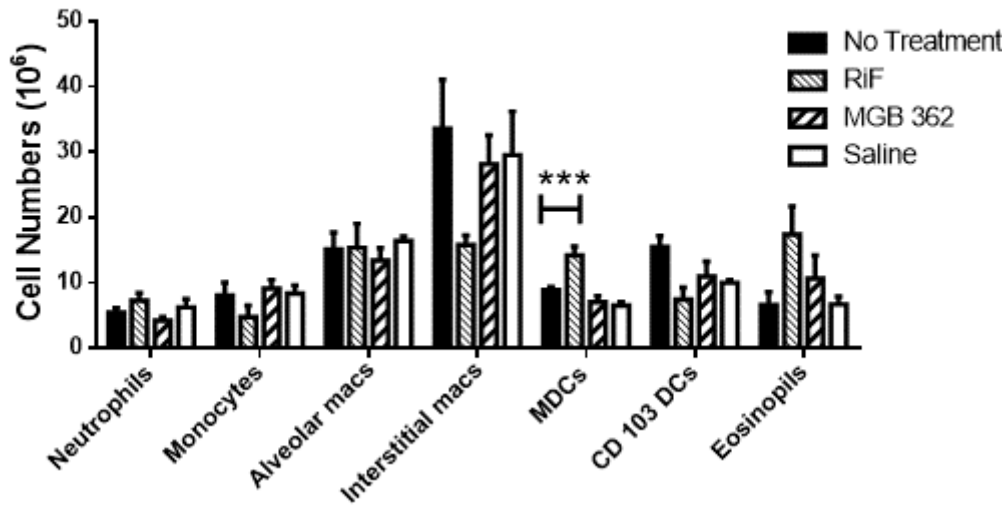
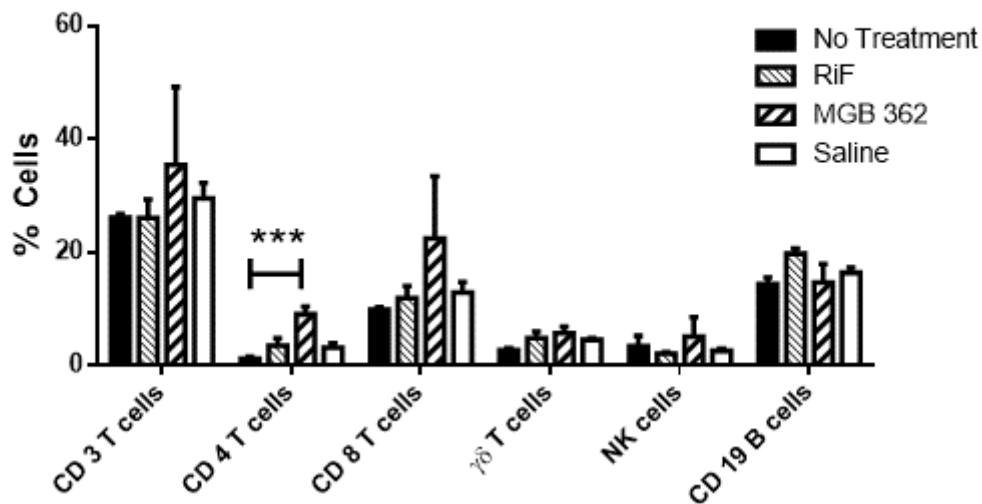
A**B**

Figure 3.8: Increased CD4 T cell recruitment responses in MGB 362 treated mice following HN878-Mtb infection. Mice (n= 3-6 per group) were infected with 100 of HN878-Mtb strain via intranasal challenge followed by weekly intranasal treatment 7 days post-infection with 10 mg/kg MGB 362 or rifampicin as positive control or left untreated or administered saline as negative control with for 3 weeks. Mice were sacrificed 4 weeks post-infection (3 weeks post-treatment) and cellular infiltration analysed from lung cell suspensions by flow cytometry **A**) Percentage of lymphocyte cell populations: (CD3+) T-cells; (CD3+CD4+) T-cells; (CD3+CD8+) T-cells; (CD3+TCRgd+) T-cells; (CD3-CD19+) B-cells; (CD4-NK1.1+) natural killer (NK) cell. **B**) Percentage of myeloid cell populations: (CD11b+Ly6G+) neutrophils; (CD11b+F4/80+Ly6G-) interstitial macrophages; (CD11c+SiglecF+) alveolar macrophages; (CD11b+SiglecF+) eosinophils; (CD11b+MHCII+CD11c+CD103-) mDCs; (CD11b+Ly6C+) monocytes from lung single cells suspensions of mice treated with MGB-362 or rifampicin. Data show mean \pm SEM of triplicates. Two-tailed Student's *t*-test, **p* < 0.05, ***p* < 0.01 compared to control.

Host-directed drug targets for tuberculosis therapy

The role of IL-4i1 on immune homeostasis during steady-state and
Mycobacterium tuberculosis infection

Chapter 4

Manuscript in preparation

IL-4i1 regulates *in vivo* local T-cell activation and proliferation at steady-state

Summary

In this chapter we addressed the role of L-phenylalanine, IL-4i1 on immune homeostasis steady-state *in vivo* using IL-4i1 gene-deficient mice models. IL-4i1 has been reported to promote the generation of Foxp3⁺ regulatory T-cells and inhibit the proliferation of effector and memory T-cells *in vitro*, inhibit B-cell activation and polarize macrophages towards an M2 phenotype, making the enzyme a potential regulator of host immunity *in vivo*. An in-depth characterization of IL-4i1 deficient mice and littermate controls was performed. We first assessed whether gene deletion would not cause any systemic impairment. We showed that IL-4i1 plays a role on activation and proliferation of CD 4 T-cells in spleen and lungs at steady-state *in vivo* and that IL-4i1 is important for immune homeostasis, null mutation or deletion could lead to autoimmunity. The PhD candidate performed all validation PCR, qPCR and flow cytometry experiments to confirm IL-4i1 deletion by herself presented in Figure 4.2. She performed all body and organ weight experiments in Figure 4.3 with Dr Justin Komguep Nono ,Dr Mumin Ozturk and Mr Julius Chia. She performed all flow cytometry experiments in Figure 4.4, 4.5, 4.7 and 4.8 with Dr Justin Komguep Nono, Dr Mumin Ozturk and Mr Julius Chia. She performed immunohistochemistry quantification experiments in Figure 4.6 by herself, validation of the absence morphological differences was performed by pathologist Dr Dhiren Govender. The candidate performed all flow cytometry in 4.9-4.11 by herself, metabolic experiments in 4.12 with Dr Maribanyana Lebeko, and ELISA experiments in Figure 4.13 by herself.

CHAPTER 4

IL-4i1 regulates *in vivo* local T-cell activation and proliferation at steady- state
Lerato Hlaka^{1,2}, Justin Nono-Komgwep^{1,2}, Julius Chia^{1,2}, Mumin Ozturk^{1,2}, Frank
Brombacher^{1,2,3}, Reto Guler^{1,2,3} *

¹ International Centre for Genetic Engineering and Biotechnology, Cape Town
Component, Cape Town 7925, South Africa.

² Department of Pathology, University of Cape Town, Institute of Infectious Diseases and
Molecular Medicine (IDM), Division of Immunology and South African Medical Research
Council (SAMRC) Immunology of Infectious Diseases, Faculty of Health Sciences,
University of Cape Town, Cape Town 7925, South Africa.

³ Wellcome Centre for Infectious Diseases Research in Africa (CIDRI-Africa), Institute of
Infectious Disease and Molecular Medicine (IDM), Faculty of Health Sciences, University
of Cape Town, Cape Town 7925, South Africa.

*Corresponding author. Tel: +27-21-4066033; Fax: + 27-86-6407594 E-mail:
reto.guler@uct.ac.za

4.1 Abstract

Objectives: Amino-acid catabolizing enzymes have gained attention over the past few years on their role of maintaining immune homeostasis mostly through their role on T-cells under inflammatory or autoimmune conditions. IL-4i1, an IL-4 activated gene is a secreted L-amino acid oxidase expressed and secreted by professional antigen presenting cells. The enzyme acts by degrading essential amino acids phenylalanine (Phe) to produce toxic derivatives like phenylpyruvate, hydrogen peroxide and ammonia. Recent studies have reported the ability of the enzyme to promote the generation of Foxp3⁺ regulatory T-cells and inhibit the proliferation of effector and memory T-cells *in vitro* making the enzyme a potential regulator of host immunity *in vivo*. Here we investigated the immunomodulatory role of IL-4i1 in regulating immune homeostasis at steady-state in the absence of inflammation through loss of function mouse.

Methods: To address the relevance of IL-4i1 on immune homeostasis *in vivo*, we generated a BALB/c IL-4i1 deficient mouse model that was backcrossed to BALB/c wild-type mice for nine generations to obtain a congenic background. To eliminate possible flanking gene confounders as a result of mice genetic backgrounds, we used “the reverse F2 strategy”. An in-depth characterization of IL-4i1^{-/-} mice at different generations compared to their littermate controls was performed to assess any physiological, tissue, cellular or immunological defects using qPCR, Immunohistochemistry, Flow cytometry and ELISA. Additionally we investigated the role of IL-4i1 on the metabolic activation of T-cells by assessing their energy phenotypes of IL-4i1^{-/-} compared to WT littermate controls.

Results: We observed a systemic dysregulation at the early generations of breeding marked by an imbalance in the distribution of myeloid and adaptative immune cell distribution in thymus, spleen and lungs as well as an increase in serum IL-12p70, TNF- α and IFN- γ of IL-4i1^{-/-} compared to WT. However this dysregulation stabilized at 9 generations. At 9 generations the true immunological functional role of IL-4i1 at steady state could be elucidated. We observed an increase in the activation and proliferation of T-cells which were marked by increased CD4CD44⁺ effector and CD4CD44Ki67⁺ proliferating T-cells as well as an increase in their metabolic energy status in the spleen, while Foxp3⁺ T-reg cells were reduced in the lungs of IL-4i1^{-/-} compared to WT. Immunohistochemistry analysis of the spleen showed no differences in tissue morphology of spleen, whereas a slight change was observed in the lung with increased alveolar airspace in IL-4i1^{-/-} compared to WT. Additionally, IL-4i1 deficiency promoted the differentiation of CD4 T-cells to effector subsets Th1, Th2 and Th17 subsets.

Conclusions: Collectively and unprecedentedly, our data indicate a critical role of an L-amino acid oxidase, IL-4i1, in the maintenance of local immune homeostasis at steady state, potentially showing an important role in autoimmunity.

4.2 Introduction

Immune homeostasis is governed by mechanisms which maintain a functional and diverse pool of lymphocytes that are would be responsive to foreign pathogens while tolerant to self-antigens [158, 159]. Amongst other cell types, T-cell homeostasis is the most described. The survival of naïve T-cells is mostly governed by contact with self-antigens which categorizes the survival of different repertoire of T-cells. Naïve-antigen T-cell rely on self-antigen contact via T-cell receptor, MHC II interactions and IL-7 while memory T-cells pre-exposed to self-antigen rely mainly on contact with IL-15 independently of MHC-II. Naïve regulatory T-cell survival on the other rely mainly on contact with IL-2 [158-160]. The homeostatic equilibrium is altered as naive T-cells routinely migrate from the thymus into secondary lymphoid tissues and peripheral tissues, differentiate into effector T-cells upon antigen stimulation and form memory T-cells [161]. Some of these peripheral T-cells recirculate in the thymus and affect thymocyte development accounting for 1-5 % of single-positive thymocytes. For example, recirculation by IL-4/STAT6 signaling activated Th2 cells results in decreased numbers of double-positive thymocytes, resulting in overall decrease of thymocytes [162]. The success of adaptive immune responses against pathogens lies primarily on changes in cellular metabolic pathways of these cells which dictate the activation status, survival and function of all immune cells. Amino-acid catabolizing enzymes have gained attention over the past few years on their role of maintaining immune homeostasis mostly through their role on T-cells under inflammatory or autoimmune conditions. One such enzyme, is the L-tryptophan first-rate catabolising enzyme, Indoleamine 2,3-dioxygenase-1 (IDO-1) presented by antigen presenting cells. The depletion of L-tryptophan via the kynurenine pathway, leads to the formation of tryptophan metabolites, including quinolinic and picolinic acid which in-turn inhibits T-cell proliferation [163].

Similarly, the L-phenylalanine oxidase, IL-4i1 has gained insight over the years for its peculiar immunomodulatory role in tumours and inflammatory disease status and has recently been implicated in the development of immune cells. IL-4i1 gained its name due to the early discovery of expression in B-cells. The expression of isoform 1 of the gene previously identified as *Fig-1* was restricted to lymphoid tissues. It was first identified to be expressed in B-cells following *in vitro* stimulation of splenic B cells by the cytokine IL-4 via NFκB and STAT6 signaling [164]. It was later discovered in other antigen presenting cells of myeloid lineage as a secreted enzyme and later identified to be expressed in T-helper 17 cells [89]. The enzyme catabolizes phenylalanine (Phe) into phenylpyruvate and produce toxic derivatives, hydrogen peroxide and ammonia [89]. Its capacity to produce H₂O₂ has been reported inhibit the proliferation and cytokine production of effector T-cells

mostly associated with anti-tumour responses *in vitro*. However, it was recently discovered that IL-4i1 downregulates TCR downstream activation signals irrespective of its enzymatic activity [165]. IL-4i1 has also been reported to promote the generation of Foxp3⁺ regulatory T-cells from naïve CD4⁺ T cells [89, 91]. The expression in Th17 was attributed to its role in the control of cell cycle-progression by limiting the production of IL-2 and through maintaining high levels of Tob1 transcription factor. IL-4i1 has been detected in B-cells of germinal centres [165]. Recently, it has been implicated in the development and activation of B-cells as a negative regulator of the BCR Syk-Akt-S6 kinase activation pathway [93].

In vivo studies have identified anti-proliferative role of IL-4i1 in CD8 T-cells in a tumour model. In a spontaneous *in vivo* melanoma model, IL-4i1 knockout mice showed delayed tumour progression accompanied by an infiltration of Th1 cell and CD 8 T-cells [94]. In a multiple sclerosis model, IL-4i1 knockout mice had increased T-cell proliferation in the brain and peripheral tissues. However; in the presence of IL-4i1, T-cell expansion was reduced and recruitment and survival of oligodendrocytes was increased, thus showing the importance of IL-4i1 in remyelination [95]. Here we investigated the immunomodulatory role of IL-4i1 in regulating immune homeostasis at steady-state in the absence of inflammation through loss of function mouse model which could decipher IL-4i1 as possible role of autoimmune disease.

The generation of knockout mouse by homologous recombination was carried in embryonic stem cells of 129Sv mouse inbred strains. However due to poor breeding quality of these mice, the resulting knockout mouse is usually crossed to wild-type C57BL/6 mice [54, 166]. We generated a BALB/c IL-4i1^{-/-} by backcrossing to BALB/c wild-type mice for nine generations. The importance of backcrossing to at least 10 generations to obtain a congenic background is attributed to the confounding influence of genetic background. In many studies it has been difficult to elucidate whether the underlying effect is of the null mutation or traces of the genetic background, termed the “flanking gene” or “passover gene” [166-168]. The resulting F2 generation would contain a segregation of the null mutation and that of the parental allele [167]. The resulting segregation would not cause serious problems, however could influence behavioural and immunological roles of genes as is the case for IL-10 knockout mice [166]. We characterized our mouse models at different generations of breeding to eliminate the effect of “flanking genes” from genetic background. We observed a systemic dysregulation at the early generations of breeding that stabilized with more backcrossing. At 9 generations the true immunological functional role of IL-4i1 at steady state could be elucidated. We report on the role of IL-4i1 on tissue

localized T-cell activation and proliferative status thus a role in the maintenance of local immune homeostasis at steady state, potentially important role in autoimmunity.

4.3 Materials and Methods

4.3.1 Mice

The mouse strain used for this research project, B6;129S5-*Il4i1^{tm1Lex}*/Mmucd, identification number 011726-UCD, was obtained from the Mutant Mouse Regional Resource Center, a NIH funded strain repository, and was donated to the MMRRC by Lexicon Genetics, Inc. It was then resuscitated. Chimeric mice were bred to C57BL/6J albino mice to generate F1 heterozygous mice which were then inter-crossed to produce wild-type, heterozygous and homozygous mutant progeny. Mice from this progeny were backcrossed 9 generations to wild-type BALB/c mice. All experimental mice were matched for sex and age and used between 8-12 weeks of age. Mice were kept under pathogen-free conditions in individually ventilated cages the University of Cape Town's animal facility unit Biosafety level 2 (BSL-2). Animal room temperature was maintained at 22-25 °C and 12 hours light/dark cycle. Food pellets and water were made available *ad libitum*.

4.3.2 Ethical Statement

All experimental procedures were carried in accordance with the South African National Standard (SANS 10386:2008). The protocol (015/037) was approved by the Ethics Committee, University of Cape Town.

4.3.3 Genotyping and Confirmation of *IL-4i1* deletion

Polymerase chain reaction was used for genotyping of mice. DNA from tail biopsies and splenocytes of naive *IL-4i1^{-/-}* mice and control littermates were isolated for confirmation of *IL-4i1* deletion with the following primer sequences: Neo3a forward 5'-GCAGCGATCGCCTTCTATC-3' and reverse 5'-GTGCTCACTTCCTCTTTGCGACT-3' and wild-type primers: forward 5'-TTGAGACCTTTCTTTCCGAGCAG-3' and reverse 5'-AGGCTAACCTTG-3. Briefly 500µl lysis buffer was added to each sample followed by overnight rotating incubation at 56°C. The samples were then centrifuged at 100rpm for 10mins. Supernatants were replaced with 500µl isopropanol, mixed gently and centrifuged at 1000rpm for 6mins. 1ml of supernatants were removed followed by incubation with 70% ethanol at -20°C for 10mins. Ethanol was then discarded, samples centrifuged at 10000rpm for 2 mins, excess ethanol removed and tubes were left open for ethanol to evaporate. Sample tubes were then heated on heating block for 20 mins for DNA to resuspend. PCR was performed in 50µl reaction mixtures containing 5ul 10x

buffer, 3µl MgCl₂ final concentration 25µM (stock 25mM), 3µl dNTPs (250µM), 2ul DNA, 0.07µl supertherm taq polymerase (1.5 U), 3µl mutant Neo3a forward primer (6.25 µM), 3µl mutant reverse primer (6.25µM); 3µl wild-type forward primer (6.25µM); 3µl reverse primer (6.25µM) and 22.93 of PCR water. The PCR cycle started with initial denaturation step at 94°C for 2 mins followed by 39 cycles of denaturation at 94°C for 20 seconds, annealing at 58°C for 30 seconds, extension at 72°C for 1.30 mins and final extension at 72°C for 5 mins. The PCR product was separated by electrophoresis on ethidium bromide-stained agarose gel, followed by visualization under UV light. The amplicon fragment for wild-type was 325 bp and 187bp for IL-4i1^{-/-}. Confirmation of IL-4i1 deletion from spleen isolated from IL-4i1^{-/-} and tissues from wild-type littermate control was performed by quantitative PCR amplicon 200bp normalised to HPRT 1.

4.3.4 Quantitative tissue expression of IL-4i1

Total RNA was extracted by RNeasy kit from Qiagen and reverse transcribed by Transcriptor First Strand cDNA Synthesis Kit (Roche) according to manufacturer's instructions. Real-time PCR was performed with LightCycler® 480 SYBR Green I Master mix in LightCycler® 480 II (Roche). Quantitative tissue expression analysis of IL-4i1 was normalized against the housekeeping gene Hprt1 with primers forward 5'-GGCCATGAGGCTGGATCTC-3' and reverse 5'-GGCCATGAGGCTGGATCTC-3'. IL-4i1 5'-ATTCCCCAGAGGACATCTACCA-3' and reverse 5' CTGTACCGGAGTCTATCGCTCA-3'.

4.3.5 Flow Cytometry

Single cell suspensions from thymus, spleen and lung tissues were stained for surface markers with the following antibodies: F4/80 (PE-Cy7) from Affymetrix eBiosciences; CD4 (PerCP-Cy 5.5 or PE or FITC); CD11c (V450 or A700 or APC); CD11b (PerCP-Cy 5.5); MHCII (A700); CD103 (PE); SiglecF (APC-Cy7 or APC); CD44 (FITC); CD62L (V450); CD19 (PerCP-Cy5.5); CD8 (V500); LY6G (APC-Cy7); Foxp3 (APC); CD 80 (V450); CD206 (FITC) and Ki67 (PE) from BD Biosciences in FACS buffer (1X PBS with 1% BSA and 0.1% NaN₃). Rabbit polyclonal IL-4i1 antibody and goat anti-rabbit secondary IgG (PE) purchased from Abcam. For surface staining, cells (1x10⁶) were labelled and washed with PBS containing 0.1% BSA (Roche, Switzerland) and 0.1% NaN₃. For intracellular staining, we used the BD Pharmingen Transcription Buffer Set (BD Biosciences) as per manufacturer's instructions to detect Foxp3 and Ki67 expression. Acquisition was conducted using BD LSR Fortessa, and data analysis was performed with FlowJo software (Treestar, Ashland, OR, US).

4.3.6 Cell sorting and ex vivo T-cell differentiation

CD4⁺ T-cells were sorted from spleen single suspension of naïve IL-4i1^{-/-} and wild-type littermate controls using Easy Sep CD4 T-cell negative selection isolation kits (Stemcell) according to manufacturer's instructions. *In vitro* differentiation of CD4⁺ cells into Th1/Th2/Th17 or Foxp3⁺ T-reg cells were induced as previously described by [169]. Cells were then cultured in triplicates per group in flat-bottom 96 well plates coated with 20ug/ml of plate-bound anti-CD3. After 96 hours incubation, cells were re-stimulated with 250ng/ml ionomycin and 50ng/ml phorbol 12-myristate 13-acetate (PMA) and Brefeldin A (BFA) to a final concentration of 80nM to culture medium. Cells were then permeabilized for intracellular and intranuclear immune-staining for detection of transcription factors and hallmark cytokines T-bet, IFN- γ ; Gata-3, IL-4; Ror γ t, IL-17 and Foxp3 for Th-1, Th-2, Th-17 and T-regulatory cells, respectively.

4.3.7 Metabolic activity

To determine the metabolic status of splenic T-cells from IL-4i1 deficient mice, CD3⁺CD4⁺ T-cells of single suspension from spleen of naïve IL-4i1^{-/-} and wild-type littermate controls were sorted using FACS Aria and cultured in RPMI1640 media containing 10% FCS and 0.5% Pen-Strep overnight. Cells were then stimulated with 100U/ml IL-4 or left unstimulated for 24hrs. To measure the energy status of T-cells, we used Agilent Seahorse XF 96 analyzer to measure oxygen consumption rate (OCR) and extracellular acidification rate (ECAR) as an indicator of glycolysis stress as described in [170].

4.3.8 Histology

Formalin fixed (4%) spleen and lungs from wild-type littermate controls and IL-4i1^{-/-} mice were stained with hematoxylin and eosin as described [80, 151]. Gelatine-based mounting medium was used to mount the sections. Image acquisition and quantification of alveolar airspaces were performed using NIS advanced software on a Nikon (Tokyo, Japan) 90i microscope. Percentage of free alveolar airspaces was defined as the area of ventilated spaces in whole lung sections in relation to the total lung tissue area using the area measurement tool by NIS advanced software on a Nikon 90i microscope and % alveolar spaces calculated using Excel as described [21].

4.3.9 The enzyme-linked immunosorbent assay

Blood samples from IL-4i1^{-/-} and wild-type littermate controls were collected by cardiac puncture upon sacrifice. Serum samples were used to determine systemic cytokine production using enzyme-linked immunosorbent assay. IL-12p70, TNF- α , IL-10, IFN- γ and IL-4 (All from BD Biosciences) production was measured from the supernatants and data

analysed using SoftMax Pro 6.

4.3.10 Statistical Analysis

All data were analysed using Graph-Pad Prism 6.0, student t-test (two-tailed with equal variance) was used. A *p value of less 0.05 was considered significant, with **p < 0.01, ***p < 0.001 and ****p < 0.0001

4.4 Results

4.4.1 Generation and genotyping of IL-4i1^{-/-} mice

To understand the functional role of IL-4i1 on immune homeostasis at steady state *in vivo*, IL-4i1 knockout mice were resuscitated from B6;129S5-*Il4i1*^{tm1Lex}/Mmucd, identification number 011726-UCD, obtained from the Mutant Mouse Regional Resource Center, a NIH funded strain repository, and donated by MMRRC by Lexicon Genetics, Inc. Chimeric mice were then mated with C57BL/6 mice to generate heterozygous F1 generation consisting of 50:50% IL-4^{+/-}. F1 generation was inter-crossed to yield 25% IL-4i1^{+/+}; 50% IL-4i1^{+/-} and 25% IL-4i1^{-/-}. The resulting homozygous IL-4i1^{-/-} mice were further backcrossed to BALB/c mouse line for 9 generations to obtain an inbred mouse of IL-4^{-/-} and littermate controls of BALB/c genetic background (Figure. 4.1B). Genomic PCR from tail biopsies from IL-4i1^{-/-} mice confirmed the deleted allele with amplicon of 187bp compared to wild-type allele of 325bp (Figure. 4.2A). Conventional PCR and agarose gel electrophoresis showed IL-4i1 expression in thymus, liver, lung, spleen and heart with no expression in IL-4i1 deletion in spleen (Figure. 4.2B). Expression of IL-4i1 mRNA by qPCR in brain, thymus, heart, lung, liver, mesenteric lymph nodes, spleen, colon and gut showed that colon has the highest IL4i1 mRNA levels with no expression of IL-4i1 in knockout mice (Figure 4.2C). We confirmed the deletion of IL-4i1 protein by flow cytometry in CD3⁺CD4⁺ T-cells, CD3⁺CD8⁺ T-cells, CD19⁺ B-cells, CD11b⁺F4/80⁺ macrophages, CD11b⁺CD11c⁺ dendritic cells of the spleen. The fluorescence levels in IL-4i1^{-/-} were comparable to isotype control as indicated in the histogram plot and the geometric means (Figure. 4.2D-E). Although other cell types express IL-4i1, macrophages and dendritic cells showed the highest expression of IL-4i1 compared to lymphocytes B-cells and T-cells in WT littermate control splenocytes (Figure. 4.2F), suggesting that the myeloid APC's are the key sources of IL-4i1 secretion in murine models at steady state *in vivo* in conformity with previous findings on human IL-4i1 [89].

4.4.2 Phenotypic characterization of IL-4i1^{-/-} mice

To assess whether IL-4i1 deletion probes any phenotypic impairment on the IL-4i1^{-/-} mouse model, we assessed for impairments in body weights, organ development, and cell numbers in WT littermate control and IL-4i1^{-/-} at the different stages of mouse generation (F2, F7 and F9). There were no aberrant alterations in the physiology or development of WT littermate control and IL-4i1^{-/-} mice across all three generations investigated. Body weights and organ weights (liver, lung, heart and spleen) were comparable between WT littermate control and IL-4i1^{-/-} except for the liver at F2

generation (Figure. 4.3A-E). These results suggest an impairment in liver tissue development in the absence of IL-4i1 at F2 IL-4i1^{-/-} progeny. However, this impairment was rescued at later generations. A significant reduction in lung weights of IL-4i1^{-/-} mice when compared to WT controls were observed at F9 generation (Figure.4.3D). These data suggest no major physiological impairments in the absence of IL-4i1 at steady state in IL-4i1^{-/-} mice of congenic BALB/c genetic background.

4.4.3 Functional characterization of IL-4i1 deletion on T-lymphocyte development

To determine whether IL-4i1 deletion would cause impairment on T-cell development at steady state *in vivo*, we compared the frequency of (CD4⁻CD8⁻ Double Negative [DN]; CD4⁺CD8⁺ Double-Positive [DP]; CD4⁺CD8⁻ Single-Positive 4 [SP4] and CD4⁻CD8⁺ Single- Positive 8 [SP8] thymocyte subsets between WT littermate control and IL-4i1^{-/-} mice at F7 and F9 generations. A dysregulation in thymocyte development was observed at F7 generation. A significant increase in DN cells (p<0.001) (Figure. 3.4A), but a significant reduction in DP cells (p<0.001) (Fig. 4B); followed by increased frequencies of SP4 and SP8 (p< 0.001) (Figure. 4.4C-D) in IL-4i1^{-/-} compared to WT littermate control mice. However, this effect was not seen at F9 generation; DN, DP and SP4 percentages were comparable between WT littermate control and IL-4i1^{-/-} mice (Figure. 4.4A-D). It is thus important to note that the major differences observed at F7 between WT and IL-4i1^{-/-} were not observed at F9 generation thus suggesting that IL-4i1 deletion in BALB/c mice does not have an effect on T-cell ontogeny.

4.4.4 IL-4i1 deletion does not alter immune cell distribution but probes T-helper cell activation in secondary lymphoid tissues

To determine whether IL-4i1 deletion would alter immune homeostasis in lymphoid tissues at steady state *in vivo*, we evaluated the overall distribution of immune cells in secondary lymphoid tissue, spleen of WT littermate control and IL-4i1^{-/-}. IL-4i1 deletion did not result in striking changes in spleen morphology (Figure. 4.5A). We observed a slightly imbalanced distribution of the lymphocyte compartment in spleens of IL-4i1^{-/-} at earlier generations. CD19⁺ B-lymphocyte distribution was significantly increased (p<0.05) in IL-4i1^{-/-} compared to WT at F7 generations (Figure. 4.5B). There were no differences in distribution at F9 generation in these subsets. CD3⁺ total T-cells and CD3⁺CD4⁺ T-helper subset distributions were not affected by IL-4i1 deletion in spleens of IL-4i1^{-/-} compared to WT littermate controls across all generations (Figure. 5C-D). However, percentages of CD3⁺CD8⁺ cytotoxic T-lymphocyte subset was significantly reduced F2 generation but increased in IL-4i1^{-/-} compared to WT at F7 generation (p<0.01). However,

these differences were not seen at F9 generation (Figure. 5D). IL-4i1 has previously been reported to suppress effector T-cell activation, proliferation and facilitate the development of regulatory T-cells through mechanisms that involve the inhibition TCR downstream signaling events that induce activation and proliferation *in vitro* [89, 91, 165]. Next, we sought to evaluate the role of IL-4i1 deletion on the activation status of T-helper and cytotoxic T-cell subsets and immune tolerance at steady state *in vivo*. CD62L and CD44 markers were used to differentiate effector and naïve T cell subsets. Differential expressions of CD62L and CD44 in both T-helper and cytotoxic T-cell compartment at early generation (F2 and F7) were observed but were comparable between WT littermate control and IL-4i1^{-/-} at F9 generation (Figure. 4.5F-H; J-L). However, consistent with the earlier generations, slight increase in effector CD4⁺ T-helper cells was observed, suggesting that absence of IL-4i1 may probe activation of CD4⁺ T-helper cells. No differences in Foxp3⁺ regulatory T-cells were observed between WT littermate controls and IL-4i1^{-/-} mice and within the myeloid cell compartment across all generations (Figure. 4.5 I, M-N). MHCII expression was decreased in IL-4i1^{-/-} when compared to WT littermate controls at earlier generation (F7) in myeloid cells as shown by the geometric mean fluorescence of MHCII (Figure. 4.5O), thus suggesting that MHCII expression was not affected by IL-4i1 deletion at F9 generation.

4.4.5 IL-4i1 deletion reduces frequency of Foxp3⁺ T-regulatory cells in lungs *in vivo*

To evaluate the effects of IL-4i1 deletion on lung immune homeostasis at steady state *in vivo*, we evaluated the overall morphology in lungs of WT littermate control and IL-4i1^{-/-}. IL-4i1^{-/-} deletion improved alveolar spaces compared to WT littermate controls and IL-4i1^{-/-} lung tissues as shown by H&E sections and percentage alveolar airspaces (Figure. 4.6A-B). IL-4i1 deficiency resulted in significantly increased alveolar airspaces, thus suggesting that IL-4i1 deficiency slightly changes lung morphology at naïve state (Figure. 5.6B). However, similarly to secondary lymphoid tissues, a dysregulated distribution of lymphocyte compartment in lungs of IL-4i1^{-/-} at earlier generations was observed. CD19⁺ B-lymphocyte distribution was significantly reduced in IL-4i1^{-/-} compared to WT littermate controls at F7 generations (Figure. 4.7A). Distribution of CD3⁺CD8⁺ lymphocyte subset was significantly reduced ($p < 0.01$) across all generations. A reduction CD3⁺ total T-cells was observed at earlier and later generations, whereas CD3⁺CD4⁺ T-helper subset distributions stabilized at F9 generation in lungs of IL-4i1^{-/-} compared to WT (Figure. 4.7B-D). Next, we sought to evaluate the role of IL-4i1 deletion on the activation status of T-helper and cytotoxic T-cell subsets. Again, differential expression of CD62L and CD44 expression in both T-helper and cytotoxic T-cell

compartment at early generation (F2 and F7) were observed but were comparable between WT littermate control and IL-4i1^{-/-} at F9 generation (Figure. 4.7E-G; I-K). Interestingly a reduction in Foxp3⁺ regulatory T-cell population measured at F9 generation was observed (Figure. 4.7H). No differences were observed in the myeloid cell compartment across all generations (Figure. 4A-C). Similarly, MHCII expression was decreased in myeloid cells at F9 generation; however similar levels of MHCII expression in lungs of IL-4i1^{-/-} mice and WT mice were detected (Figure 4.8D). Notably, the activation of T- cells because of IL-4i1 depletion is independent of MHC II expression to T-cell interaction at steady state *in vivo*. Overall, our findings were indicative of systemic stabilization in IL-4i1^{-/-} mice of congenic genetic background.

4.4.6 IL-4i1 deletion promotes proliferation of effector T-helper cells and reduces proliferation of Foxp3⁺ regulatory T-cells

Next we sought to evaluate whether the observed activation status of CD4⁺ T-helper cells as marked by the increased expression of CD44⁺ is related to the proliferative status in spleen at F9 generation. We observed a significantly higher ($p < 0.05$) expression of proliferative marker Ki67 on CD4⁺CD44⁺ effector T-cell (Fig. 4.9A), but a significantly reduced ($p < 0.01$) expression of Ki67 in Foxp3⁺ regulatory T-cells (Figure. 4.9B) in IL-4i1^{-/-} mice compared to littermate controls. Comparable overall expression of Ki67 was observed for both CD4⁺ T- helper and CD8⁺ cytotoxic T-cells between WT littermate controls and IL-4i1^{-/-} mice (Figure. 4.9C- D). Contrary to the observed distribution of Foxp3⁺ regulatory T-cells in the lungs, these cells expressed higher levels of Ki67 in IL-4i1^{-/-} compared to their WT counterparts (Figure. 4.10A). No significant differences were observed in Ki67 expression of effector CD44⁺ effector T-cells and the overall CD4⁺ T-helper and CD 8⁺ cytotoxic T-cells of IL-4i1^{-/-} compared to WT littermate controls (Figure. 4.10B-D).

4.4.7 IL-4i1 deletion promotes effector T-helper cells differentiation

IL-4i1 has previously been reported to play a role in the differentiation of Th cells to different subsets. Analysis of T-cell differentiation from conventional splenic naïve CD4⁺ (GFP⁻ CD25⁺CD62L⁺) cells from Foxp3-EGFP transgenic mice cultured with IL-4i1 expressing or HEK control cells and naïve CD4⁺ cells from PBMC cultured with THP1 or THP1-IL-4i1, showed that IL-4i1 stimulates the generation of FoxP3⁺ regulatory (T-regs) from mouse and human T cells through the ablation of mTORC1 kinase signaling pathways in activated CD4⁺ T cells while limiting the differentiation of T effector (Th1 and Th2) cells [91]. Here we validated the role of IL-4i1 on naïve CD4⁺ T-cell polarization through loss of function using splenocytes from IL-4i1^{-/-} mice and WT littermate controls.

Isolated CD4⁺ T-cells were stimulated with polarizing cytokines for each subset. For Th1 subset, cells were stimulated with IL-2, IL-12 and anti-IL-4; Th2 with IL-2, IL-4, anti-IL-12 and anti-IFN- γ ; Th17 with IL-2, TGF- β , IL-6, anti-IL-4, anti-IFN- γ and anti-IL-12; while for T-reg IL-2 and TGF- β were used. The differentiated CD4⁺ subsets were characterized by the expression of transcription factors, T-bet, Gata-3, ROR γ t and Foxp3. The deletion of IL-4i1 promoted differentiation into T-effector subsets showing significant increase ($p < 0.05$) in Th17 ROR γ t expression and an increasing trend in GATA-3 and T-bet expressions compared to WT CD 4⁺ T-cells (Figure. 11A). Functional validation of these subsets was confirmed by significant increase in IL-4 and IFN- γ production for Th-2 and Th-1 cells respectively in IL-4i1 deficient mice compared to WT mice (Figure. 4.11B).

4.4.8 IL-4i1 deletion activates metabolic state of *ex-vivo* T-helper cells

To confirm the role of IL-4i1 deletion on the activation status of CD4 T-cells, we evaluated the metabolic status of CD4 T-helper cells isolated from the spleens of IL-4i1^{-/-} and WT littermate controls and stimulated with 100U/ml of rIL-4. We measured oxygen consumption rate (OCR) as a measure of oxidative phosphorylation and extracellular acidification rate (ECAR) as an indicator of glycolytic flux. Mammalian cells usually generate energy through oxidative phosphorylation via the mitochondria or through glycolysis (non-mitochondrial). Activation of T-cells drives cells into a glycolytic state compared to B lymphocytes which use a balance between oxidative phosphorylation and glycolysis [170, 171]. The energy map of OCR and ECAR categorizes both stimulated and unstimulated IL-4i1^{-/-} T-cells at high energy and glycolytic status compared to the WT littermate controls with OCR and ECAR values of 120-180 pmol/min and 5.5-7mpH/min, respectively (Figure. 4.12 A-C). These data are in conformity with the proliferation and effector phenotype of CD4 T-helper cells observed in the spleen of IL-4i1^{-/-} mice compared to WT littermate controls.

4.4.9 Characterization of IL-4i1 deletion on systemic cytokine production

Next we sought to evaluate whether IL-4i1 deletion would have an effect on systemic cytokine production following T-cell activation. Similarly, a dysregulation in serum cytokines produced was observed at F2 and F7 generations. Increased levels of IL-12p70 were observed in IL-4i1^{-/-} compared to WT littermate controls at F2 generation in the absence of IL4i1, but comparable levels were observed at F7 and F9 generations (Figure. 4.13A). Significantly increased levels of TNF- α , IFN- γ and IL-4 were observed at F7 generation, but were all similar levels at baseline for F9 generation (Figure. 4.13 B-E). These data suggest distinction between events occurring in the local tissue environment and blood circulation.

4.5 Discussion

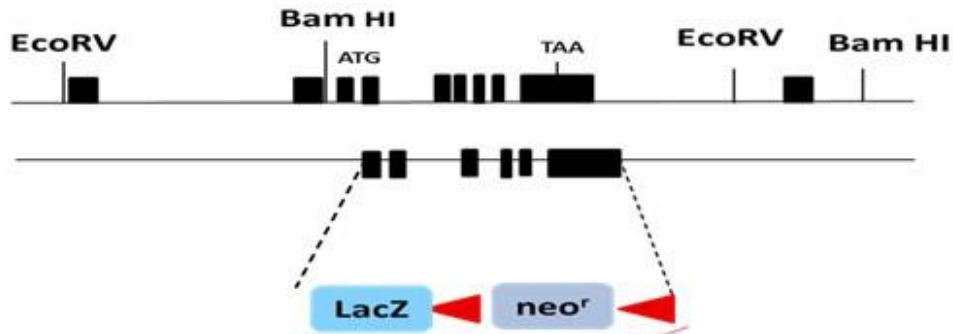
In this study we evaluate the role of IL-4i1 in the maintenance of immune homeostasis at steady state *in vivo*. We identified the expression of IL-4i1 in various tissues of the body thus illustrating an importance of the enzyme in systemic immune regulation. To address this, we resuscitated and IL-4i1 knockout mice of 1B6;129S5-*Il4i1*^{tm1Lex}/Mmucd, background, chimeric mice were then crossed with C57BL/6 mice and backcrossed nine generations to obtain IL-4i1^{-/-} and WT littermate controls of BALB/c congenic background (Figure 4.1). Deletion was confirmed on genomic, mRNA and protein levels from cell types and tissues of the knockout and wild-type littermate control mice (Figure 4.2). In our study, the knockout mouse of interest originates from three different backgrounds and thus backcrossing to many generations was essential to eliminate possible confounders. Wolfer et al. addressed possible strategies to deal with flanking genes [167]. One possible method was “the reverse F2 strategy. Here we employed a similar method where we characterize the resulting IL-4i1 knockout and wild-type littermate controls across different generations (F2, F7 and F9). We observed no impairment in the physiological and morphological appearance of the knockout and wild-type littermate control mice across different generations (Figure 4.3). However, a systemic immune imbalance was apparent at earlier generations as illustrated by the dysregulation in cellular compartments of myeloid and lymphocyte lineages in various tissues (Figure 4.4, 4.5, 4.7, 4.8). Furthermore, we notice elevated levels of systemic cytokine production IL-12p70, TNF- α and IFN- γ at baseline (Figure 4.13). However, this dysregulation was balanced at F9 generation. No major differences were observed in cell type distributions between IL-4i1^{-/-} mice and wild-type littermate controls in primary, secondary lymphoid organs and peripheral tissues. However, the differences observed at F9 generation that were consistent with previous findings at F2 generation, these were attributed to the null mutation rather than the mouse genetic background. Consistent with previous findings, we first identified that the expression of IL-4i1 was greater in myeloid APCs compared to other cells types. In line with previous studies on the immunomodulatory functions of IL-4i1 on T-cell adaptive immune responses in inflammatory conditions and cancer [86, 94, 95], we identified the role of IL-4i1 in T-cell activation and proliferation in secondary and peripheral tissues at steady state *in vivo*. Deletion of IL-4i1 resulted in elevated frequencies of proliferative CD4 effector T-cells and reduced distribution of proliferative Foxp3 T-regulatory cells in the spleen at F9 generation (Figure 4.9). Although the distribution of Foxp3 T-reg cells was reduced in the lung, its proliferative status was elevated as indicated by Ki67 expression (Figure 4.10), thus indicating a tissue specific role of IL-4i1 in regulating immune homeostasis.

Previous studies reported on the *in vitro* effect of IL-4i1 secreted by myeloid APCs on the downregulation of TCR ζ -chain via its enzymatic activity and H₂O₂ production thus inhibiting T-cell proliferation. In our study, MHC II expression in APCs was not affected at F9 generation thus suggesting that the activation of T-cells at earlier generation was inversely proportional to the maturity of antigen presenting cells at steady state in secondary lymphoid tissues and that the TCR ζ -chain previously reported to be downregulated by IL-4i1 [89] works independently of MHCII. Aubatin et al. [165] reported that IL-4i1 was secreted at immune synapse and inhibited TCR downstream signaling events independently of its enzymatic activity. Cousin et al. [91] reported on the role of IL-4i1 on the development of Foxp3 T-cells. IL-4i1 promoted the generation and proliferation of T-reg cells via the inhibition of mTORC1 signaling. In light with these findings, we showed that IL-4i1 deletion in reverse promotes the differentiation of CD 4 effector subset, enhanced for Th1 and Th17 subset (Figure 4.12). Previous *in vivo* studies have identified an anti-proliferative role of IL-4i1 on CD8 tumour cells. Psachoulia et al. 2016 [95] showed that IL-4i1 reduced T-cell expansion and supports oligodendrocytes survival and remyelination during multiple sclerosis *in vivo*. Interestingly, in that study they used the original F2 generation of the mouse model we used. Due to the possibilities of the “flanking gene” effects, it again raises the question whether their result was a question of the IL-4i1 mutation or whether genetic background had an influence on the results obtained, this remains unclear. To further illustrate the role of IL-4i1 on T-cell activation, we measured the metabolic energy status of T cells stimulated with IL-4. Here we show the importance of IL-4i1 on the regulating and maintaining of balanced adaptive immune-checkpoint at steady-state *in vivo*. Naïve T-cells when activated undergo a proliferative chain reactions inducing a metabolic remodeling of these cell types governed by anaerobic glycolysis and oxidative phosphorylation [171-173]. Although oxidative phosphorylation plays the major role in the energy status due to the production of ATP, glycolysis is able to generate metabolic intermediates important for cell growth and proliferation [172-174]. Upon activation T-cells move from a quiescent resting state to an almost complete glycolytic energy state [173, 175]. In the absence of IL-4i1, we observed an energy shift that maps cells in the higher energetic zone where mitochondrial activation occurs marked by oxidative phosphorylation as well as a higher glycolytic state compared to WT littermate counterparts when stimulated with IL-4 in naïve T-cells *in vitro*. These data thus confirm the role of IL-4i1 in the activation and proliferation of T-cells by controlling metabolic cues that drive cell activation. We noticed that the systemic cytokine production was not affected by IL-4i1 deletion at F9 generation irrespective of tissue T-cell activation and proliferation.

4.6 Conclusion

Here, we described the importance of IL-4i1 in regulating immune homeostasis at steady state *in vivo* using loss of function mouse models. We showed the importance of characterizing gene modified mice at different generations of breeding to extract the function of the null mutation from the mouse genetic background. IL-4i1 deletion introduced a systemic dysregulation at early generations, but the effect was stabilized with a pure congenic mouse. We could thus decipher the important role of IL-4i1 in maintaining localised T-cell activation and proliferation through the control of metabolic cues that drive T-cell activation status and function. Although we showed an important role of IL-4i1 in modulating and maintaining immune homeostasis at steady state *in vivo*, more mechanistic studies on the role of IL-4i1 on localised tissue T-cell activity at steady are warranted. Our results highlight the importance of IL-4i1 in the maintenance of immune homeostasis and that the absence of this gene could cause autoimmunity.

A



B

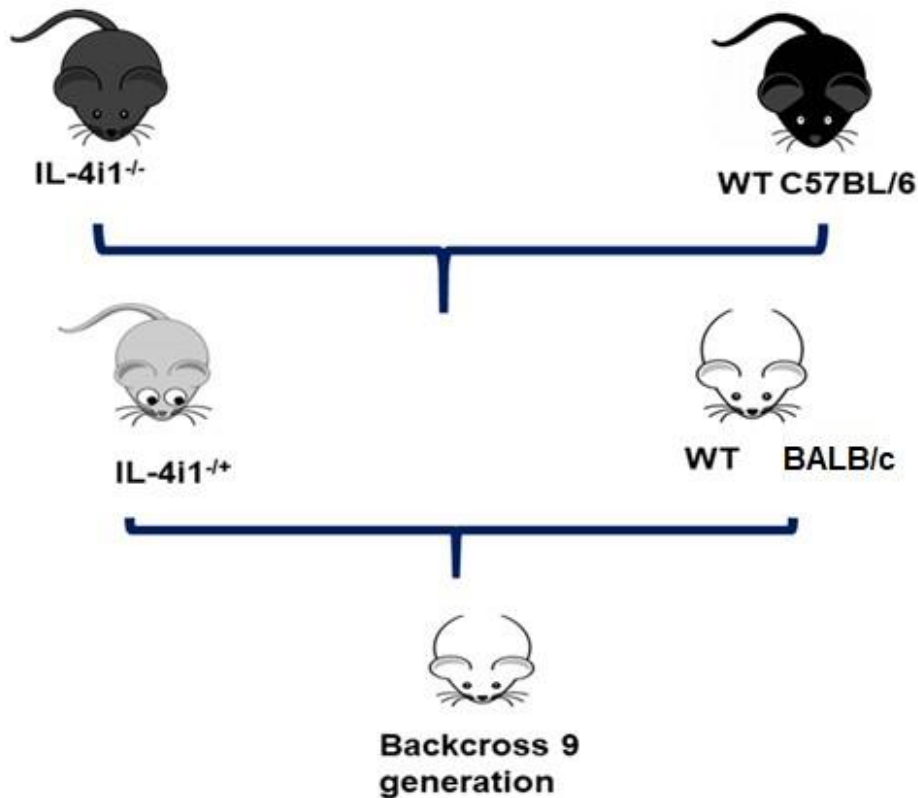


Figure 4.1: Generation of IL-4i1 deficient mice: A) Targeting strategy for IL-4i1 genomic locus, targeting construct and targeted allele, targeting coding exons 1-7. **B)** IL-4i1 knockout mice were generated in 129s/SvEvBrd embryonic stem cells through homologous recombination through and then mated with C57BL/6 mice. The resulting heterozygous IL-4i1^{+/-} mice were backcrossed 9 generations to wild-type BALB/c mice.

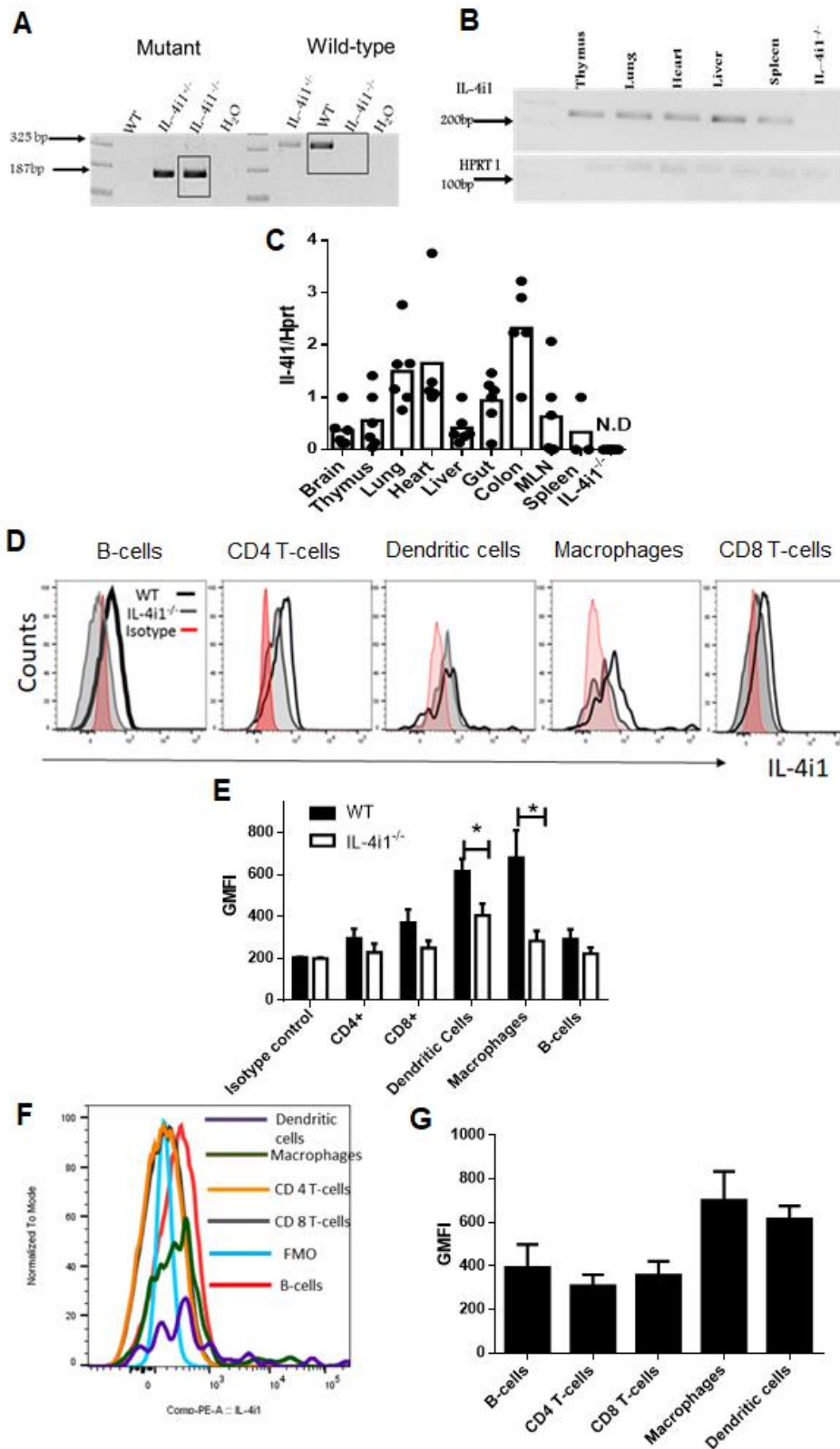


Figure 4.2: Genotyping of IL-4i1 deficient mice: **A**) Deletion of IL-4i1 was confirmed from splenocytes of wild-type and IL-4i1 knockout mice. The amplicon fragment for wild-type is 325 bp and 187bp for IL-4i1^{-/-}. **B**) Agarose gel image of IL-4i1 expression from thymus, heart, lung, liver wild-type mice, confirming deletion in IL-4i1^{-/-} samples. **C**) Quantitative PCR analysis of IL-4i1 expression was analysed from different tissues (brain, thymus, heart, lung, liver, mesenteric lymph nodes, spleen, colon and gut) of wild-type BALB/c mice as well as spleen of IL-4i1^{-/-} mice,

Il4i1 levels were normalised to Hprt1. **D)** Confirmation of IL-4i1 deletion by flow cytometry from different cell types (CD3⁺CD4⁺ T-cells, CD3⁺CD8⁺ T-cells, CD19⁺ B-cells, CD11b⁺F4/80⁺ Macrophages, CD11b⁺CD11c⁺ Dendritic cells) isolated from spleen of IL-4i1^{-/-} (grey) and wild-type littermate control mice (black), red line represents isotype control. **E)** Geometric mean fluorescence intensity of IL-4i1 in different cell types of spleens from IL-4i1^{-/-} and wild-type littermate control mice. **F)** Cell-type expression of IL-4i1 by flow cytometry in spleens of wild-type littermate controls, (CD11b⁺CD11c⁺ Dendritic cells, CD11b⁺F4/80⁺ macrophages, CD3⁺CD4⁺ T-cells, CD3⁺CD8⁺ T-cells, CD19⁺ B-cells). **G)** Geometric mean fluorescence intensity of IL-4i1 in different cell types. Data are representatives of two independent experiments with at least n= 4-6 mice per group. Data are shown as mean ± SEM. Student t-test analysis *p<0.05 was used to determine significance.

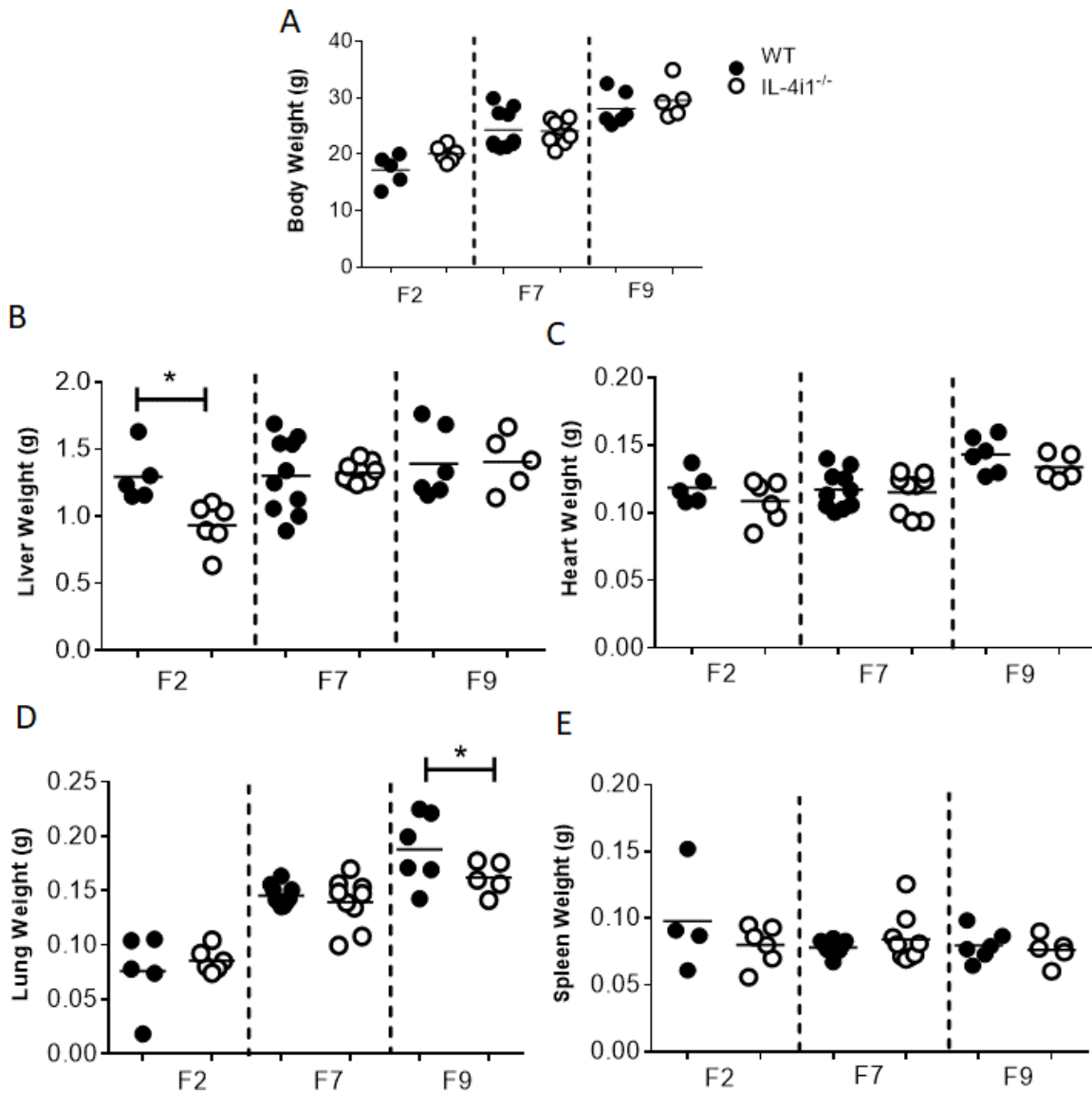


Figure 4.3: Phenotypic characterization of IL-4i1 deficient mice across F2, F7 and F9 generations following backcrossing: **A)** Body weights of WT littermate control (filled) and IL-4i1 knockout mice (empty) in a BALB/c genetic background. **B-E)** Liver, heart, lung and spleen weights. Data are representative of two independent experiments with at least n= 5-10 mice per group. Student *t-test* analysis * $p < 0.05$ was used to determine significance.

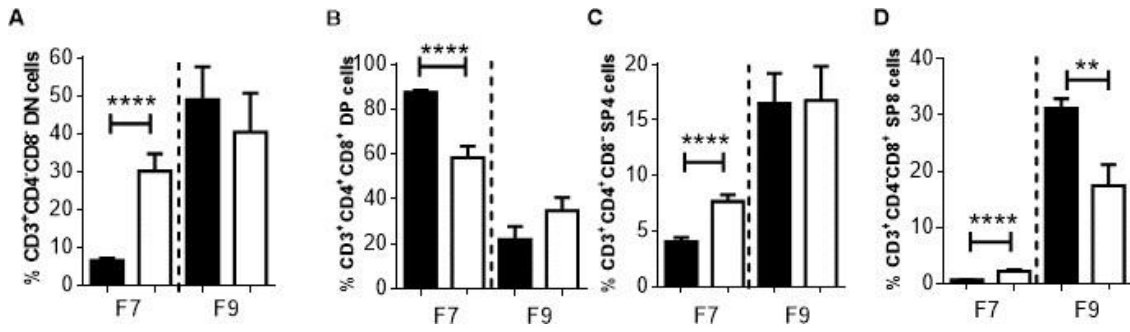


Figure 4.4: Functional characterization of IL-4i1 deletion on T-cell ontogeny across F2, F7 and F9 generations of IL-4i1 deficient mice. A) Flow cytometry analysis of percentage CD3⁺CD4⁺CD8⁻ double-negative (DN); **B)** CD3⁺CD4⁺CD8⁺ double-negative (DP); **C)** CD3⁺CD4⁺CD8⁻ single-positive 4 (SP4) and **D)** CD3⁺CD4⁺CD8⁺ single-positive 8 (SP8) thymic T-cells. Data are representative of two independent experiments with at least n= 5-10 mice per group. Student *t*-test analysis ** $p < 0.01$, **** $p < 0.0001$ was used to determine significance.

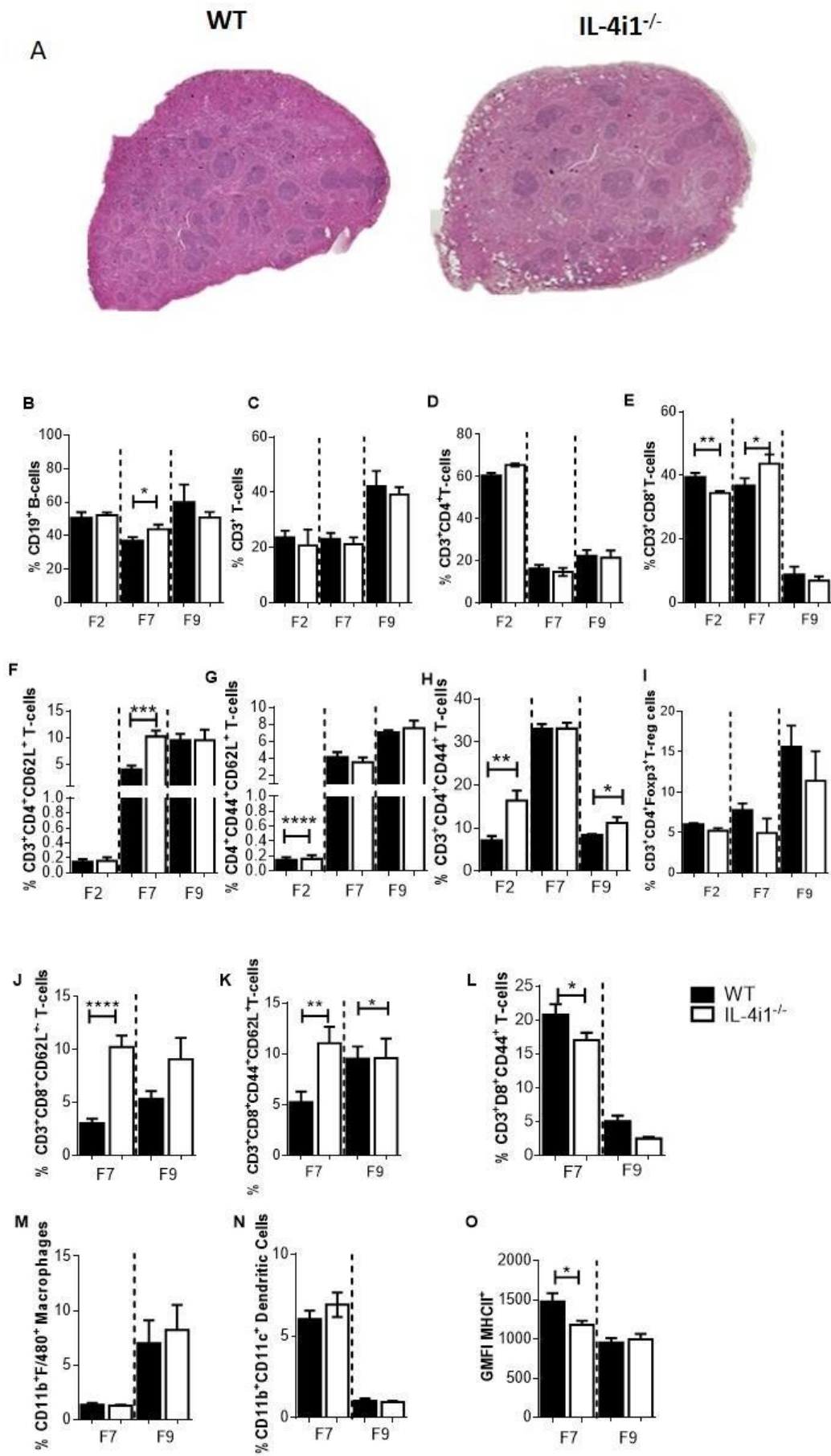


Figure 4.5: IL-4i1 deficiency promotes T-cell activation in naïve spleen. **A)** Representative section of H&E stained section (400x) of spleen tissue at F7 generation. Percentages of **B)** CD19⁺ B-cells. **C)** CD3⁺ T-cells, **D)** CD3⁺CD4⁺ T-helper cells, **E)** CD3⁺CD8⁺ cytotoxic T-cells, **F)** CD4⁺CD62L⁺CD44⁻ T-helper cells, **G)** CD4⁺CD44⁺CD62L⁺ central memory T-helper cells, **H)** CD4⁺CD44⁺CD62L⁻ Effector T-helper cells, **I)** CD3⁺CD4⁺Foxp3⁺ T-regulatory cells, **J)** CD4⁺CD62L⁺CD44⁻ Cytotoxic T-cells, **G)** CD4⁺CD44⁺CD62L⁺ central memory cytotoxic T-cells, **H)** CD4⁺CD44⁺CD62L⁻ Effector Cytotoxic T-cells, **M)** CD11b⁺Ly6G⁻F4/80⁺ macrophages, **N)** CD11b⁺CD11c⁺F4/80⁻Siglec F⁻ dendritic cells and **O)** Geometric mean fluorescence of MHCII in macrophages are shown. Data are presentative of two independent experiments with at least n= 5-10 mice per group. Student *t*-test analysis *p<0.05, **p< 0.01, ***p< 0.001, ****p< 0.0001 was used to determine significance.

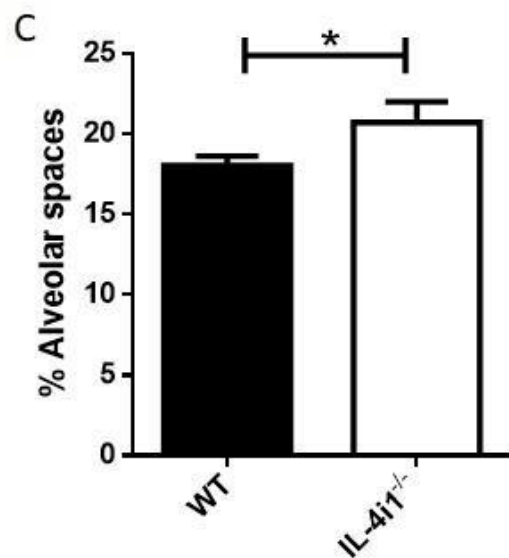
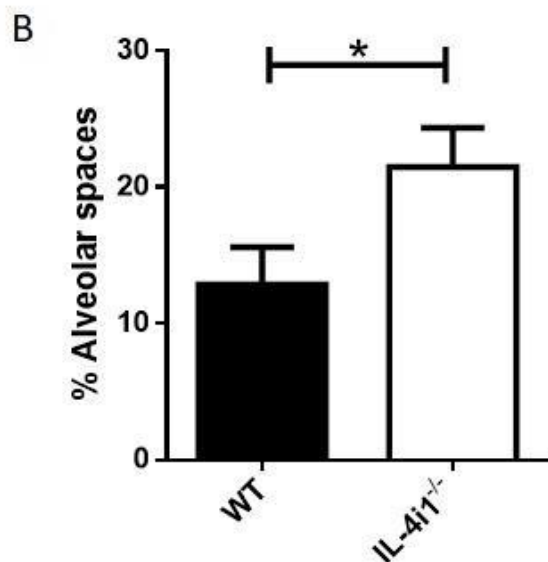
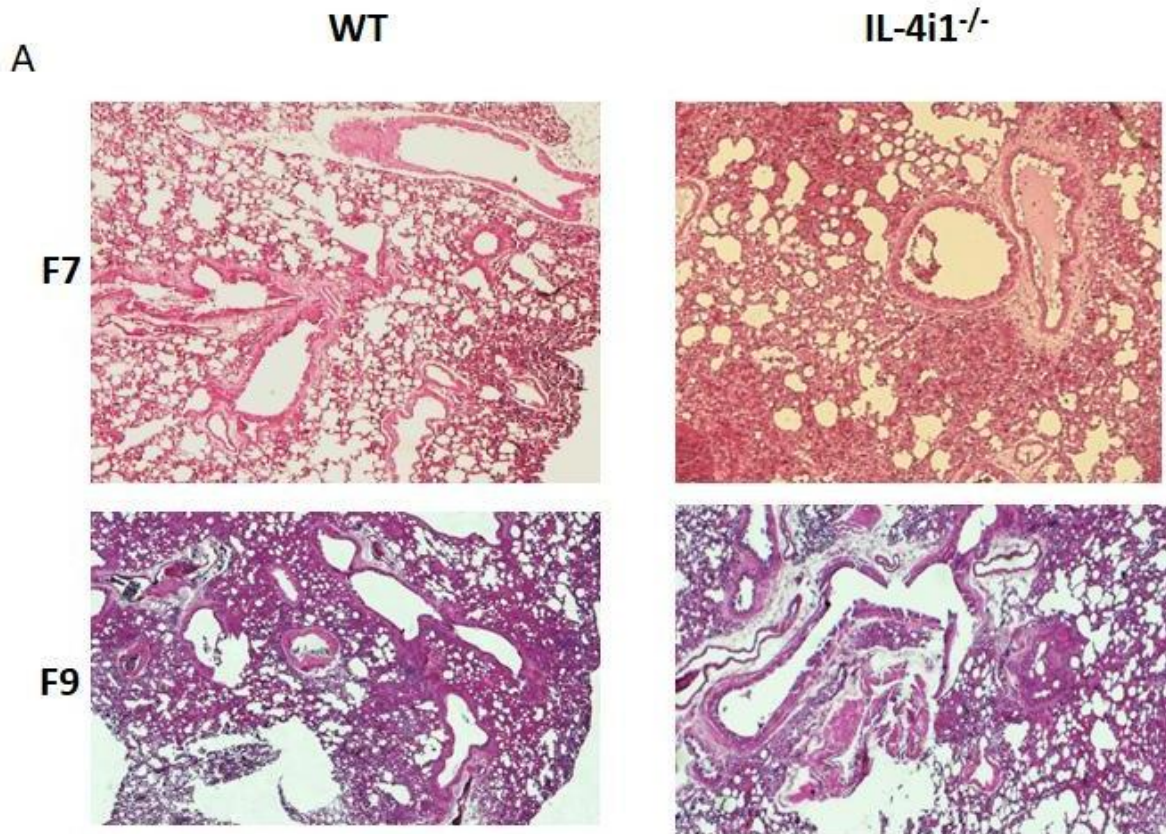


Figure 4.6: IL-4i1 deficiency improves naïve lung pathology at steady state. Lung sections were isolated from naïve IL-4i1^{-/-} and WT littermate controls at F7 and F9 generations. A) Representative section of H&E stained section (20) of lung tissue at F7 and F9 generation. Quantification of alveolar airspaces in B) F7 and C) F9 generation. Data are representative of two independent experiments with at least n=3-4 mice per group. Student *t*-test analysis *p<0.05 was used to determine statistical significance.

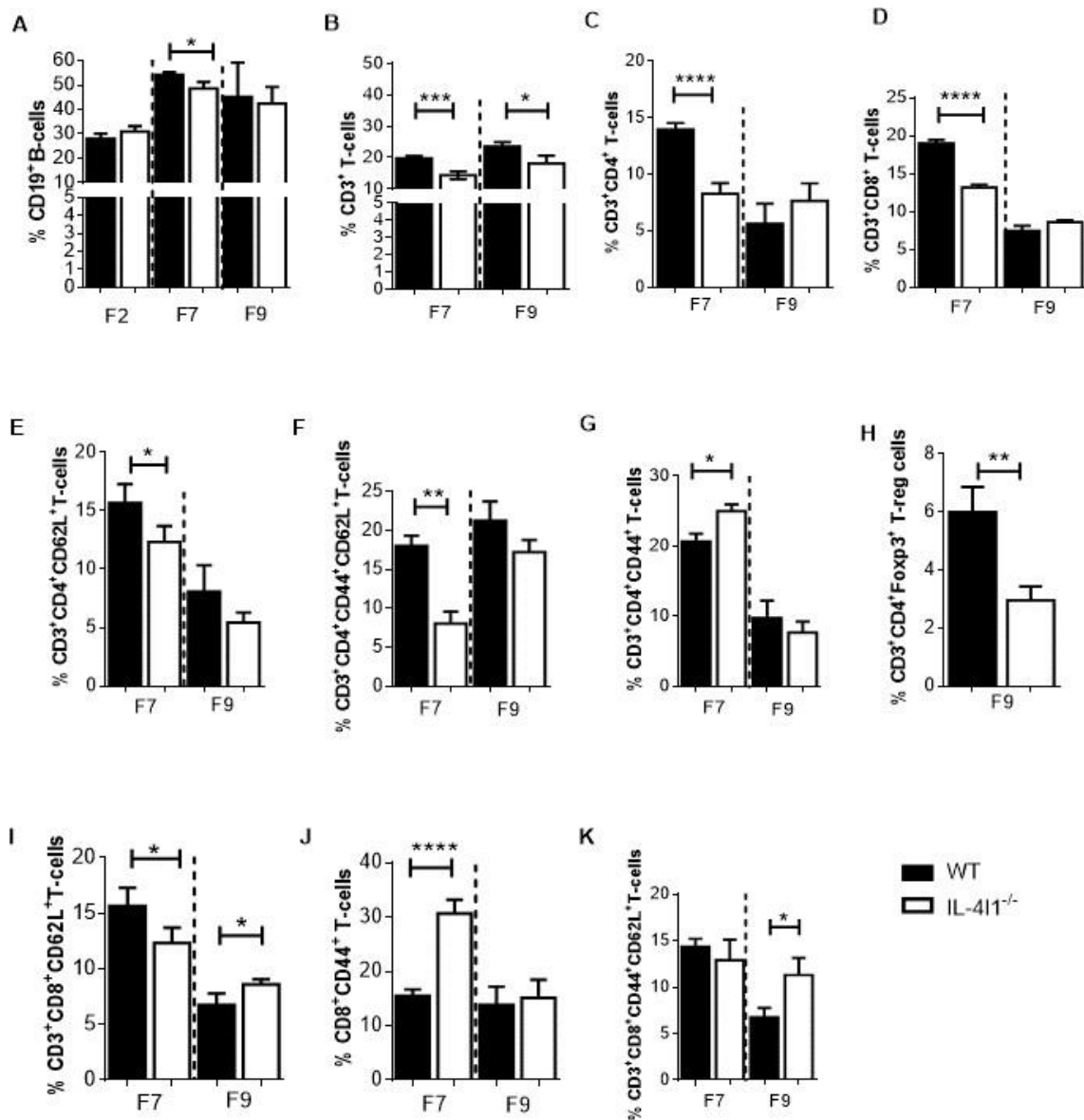


Figure 4.7: IL-4i1 deficiency reduces frequency of total T-cell population; Foxp3+ regulatory T-helper cells at F9 generation in lungs. Percentages of **A)** CD19⁺ B-cells, **B)** CD3⁺ T-cells, **C)** CD3⁺CD4⁺ T-helper cells, **D)** CD3⁺CD8⁺ cytotoxic T-cells, **E)** CD4⁺CD62L⁺CD44⁻ T-helper cells, **F)** CD4⁺CD44⁺CD62L⁺ central memory T-helper cells, **G)** CD4⁺CD44⁺CD62L⁻ Effector T-helper cells, **H)** CD3⁺CD4⁺Foxp3⁺ T-regulatory cells, **I)** CD4⁺CD62L⁺CD44⁻ Cytotoxic T-cells. **J)** CD4⁺CD44⁺CD62L⁺ central memory Cytotoxic T-cells, **K)** CD4⁺CD44⁺CD62L⁻ Effector Cytotoxic T-cells are shown. Data are representative of two independent experiments with at least n= 5-10 mice per group. Student *t*-test analysis **p*<0.05, ***p*< 0.01, ****p*< 0.0001 was used to determine statistical significance.

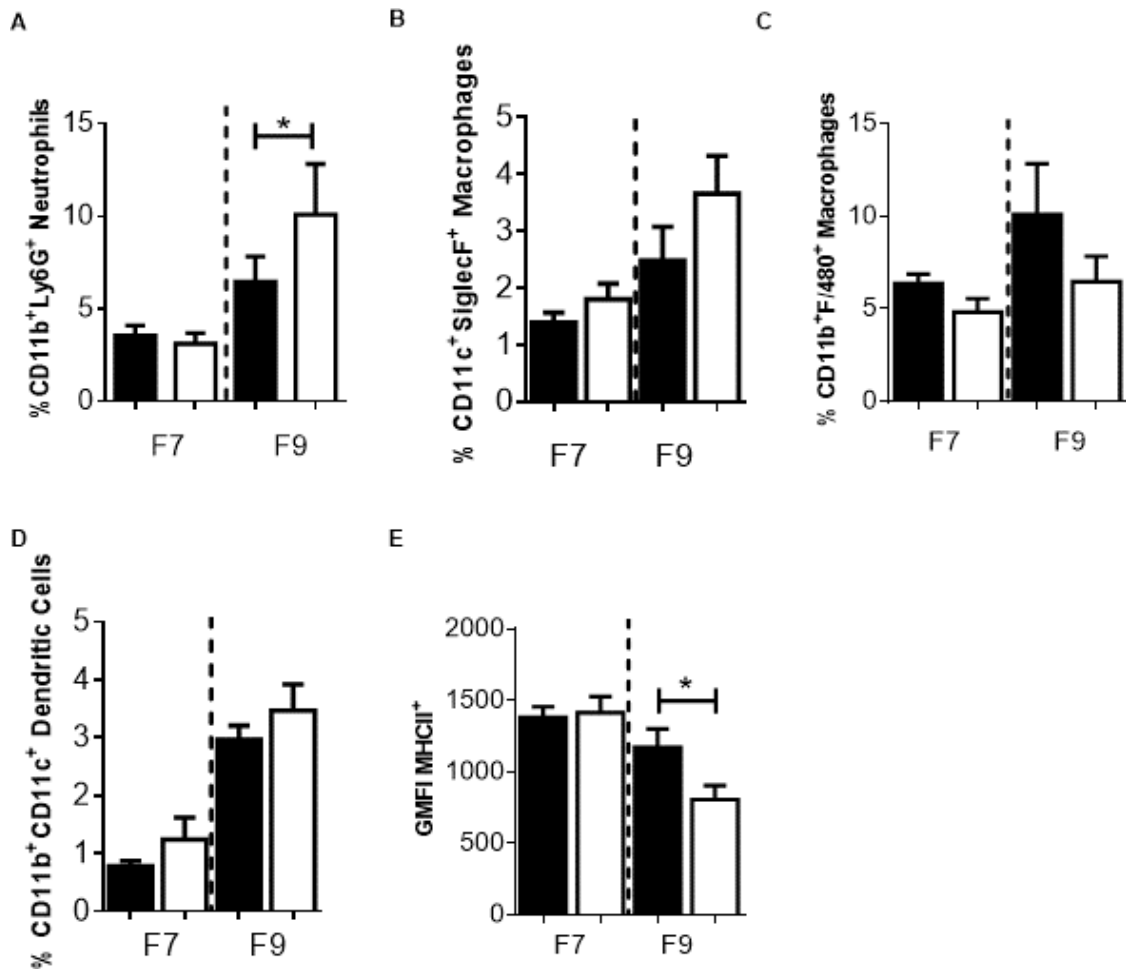


Figure 4.8: IL-4i1 deletion did affect lung myeloid cell compartment but the expression of MHC II from antigen presenting cells Percentages of **A)** CD11b⁺Ly6G⁺F4/80⁺ macrophages, **B)** CD11b⁺CD11c⁺F4/80⁺SiglecF⁻ dendritic cells, **C)** CD11b⁺CD11c⁺F4/80⁺SiglecF⁺ alveolar macrophages, and **D)** Geometric mean fluorescence of MHCII in macrophages cells are shown. Data are representative of two independent experiments with at least n= 5-10 mice per group. Student *t*-test analysis *p<0.05 was used to determine significance.

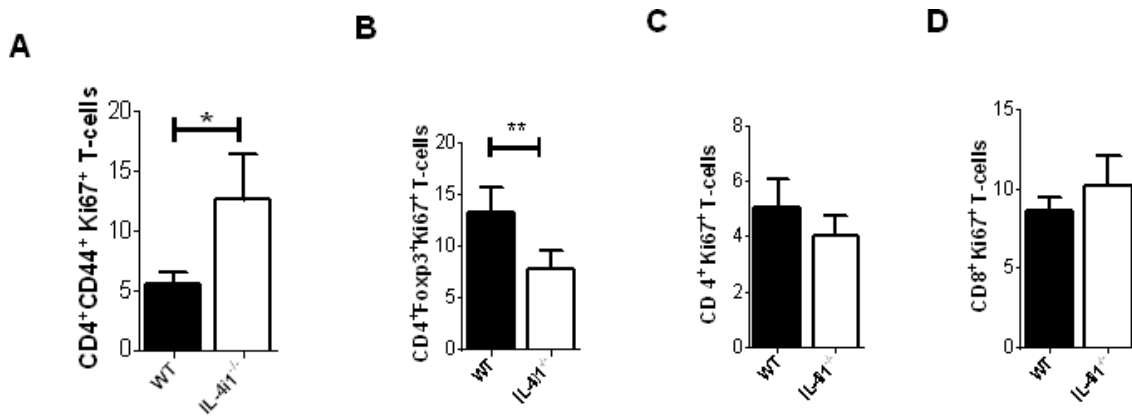


Figure 4.9: IL-4i1 deficiency promotes *in vivo* proliferation of activated T-helper cells but reduces proliferation of Foxp3⁺ regulatory T cells in spleens. Frequency **A)** of Ki67 expressing CD44⁺T-helper cells, **B)** Ki67 expressing Foxp3⁺ T-helper cells, **C)** Ki67 expressing CD4⁺ T-helper cells, **D)** Ki67 expressing Cytotoxic T-cells are shown. Data are representative of two independent experiments with at least n= 5-10 mice per group. Student *t*-test analysis *p<0.05, **p< 0.01 was used to determine statistical significance.

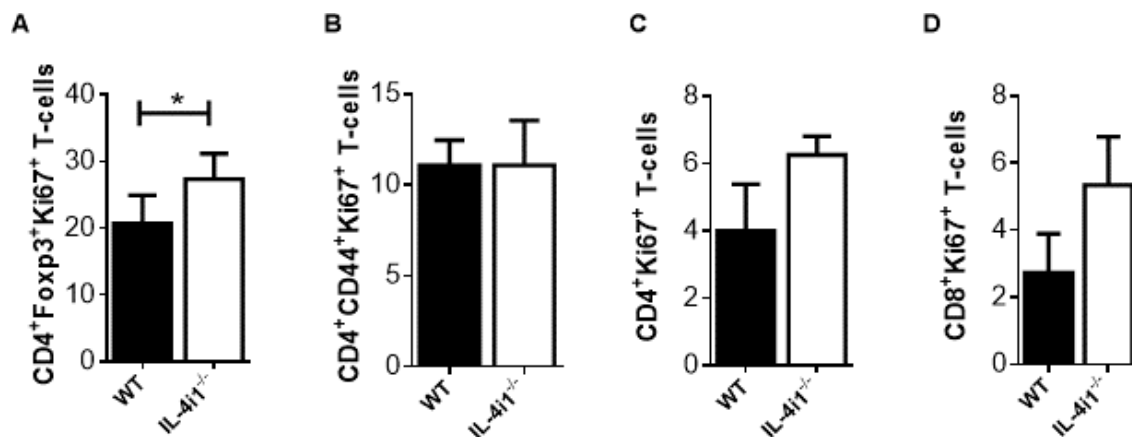


Figure 4.10: IL-4i1 deficiency promotes *in vivo* proliferation of Foxp3⁺ regulatory in lungs of WT littermate control and IL-4i1^{-/-} mice. Frequency of **A)** Ki67 expressing Foxp3⁺ T-helper cells, **B)** Ki67 expressing CD44⁺T-helper cells **C)** Ki67 expressing CD4⁺ T-helper cells **D)** Ki67 expressing cytotoxic T-cells are shown. Data are representative of two independent experiments with at least n= 5-10 mice per group. Student *t*-test analysis **p< 0.01 was used to determine significance

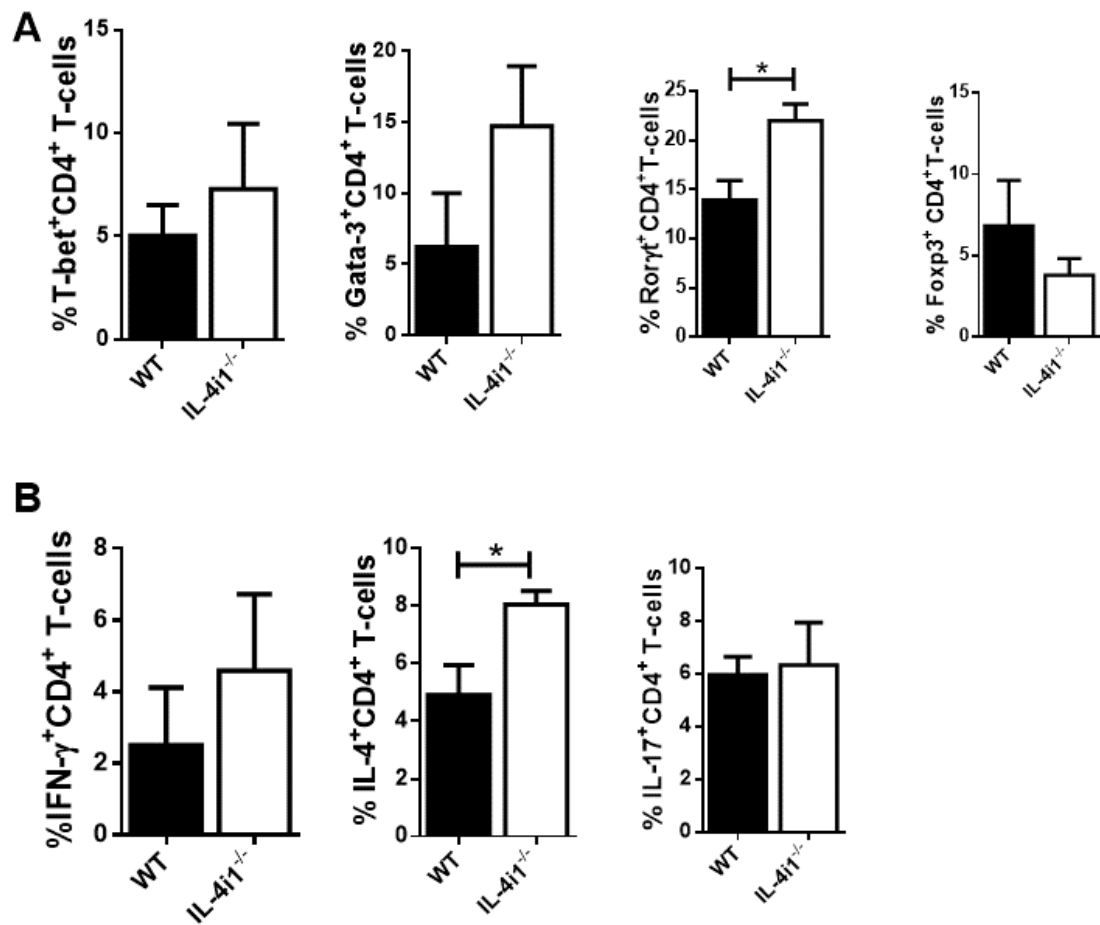


Figure 4.11: IL-4i1 deficiency promotes differentiation of effector CD4⁺ T-cells. A) Frequencies of transcription factor expressing T-helper cells; T-bet CD4⁺ T-cells, Gata-3 CD4⁺ T-cells, Roryt CD4⁺ T-cells, Foxp3⁺ expressing CD4⁺ T-cells respectively are shown. **B)** Frequencies of cytokine producing T-helper cells are presented. Data are representative of two independent experiments with triplicates per experiment. Student *t-test* analysis **p* < 0.05 was used to determine significance.

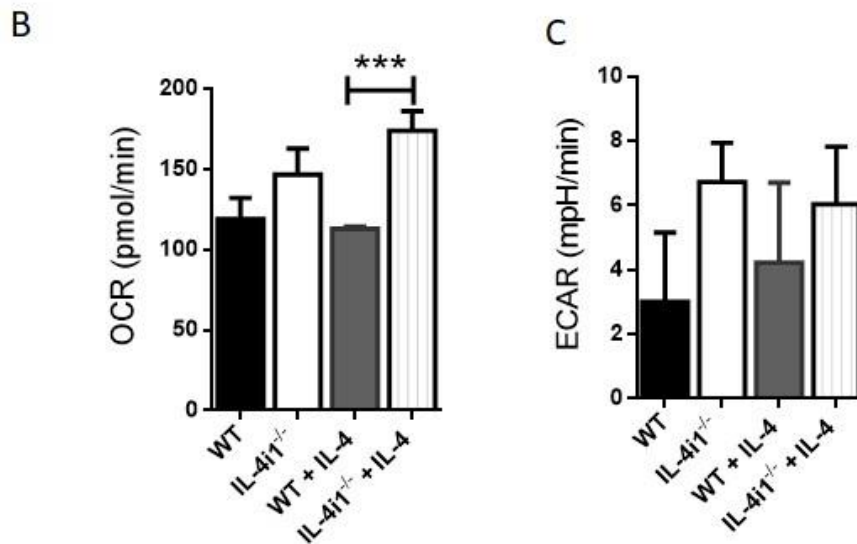
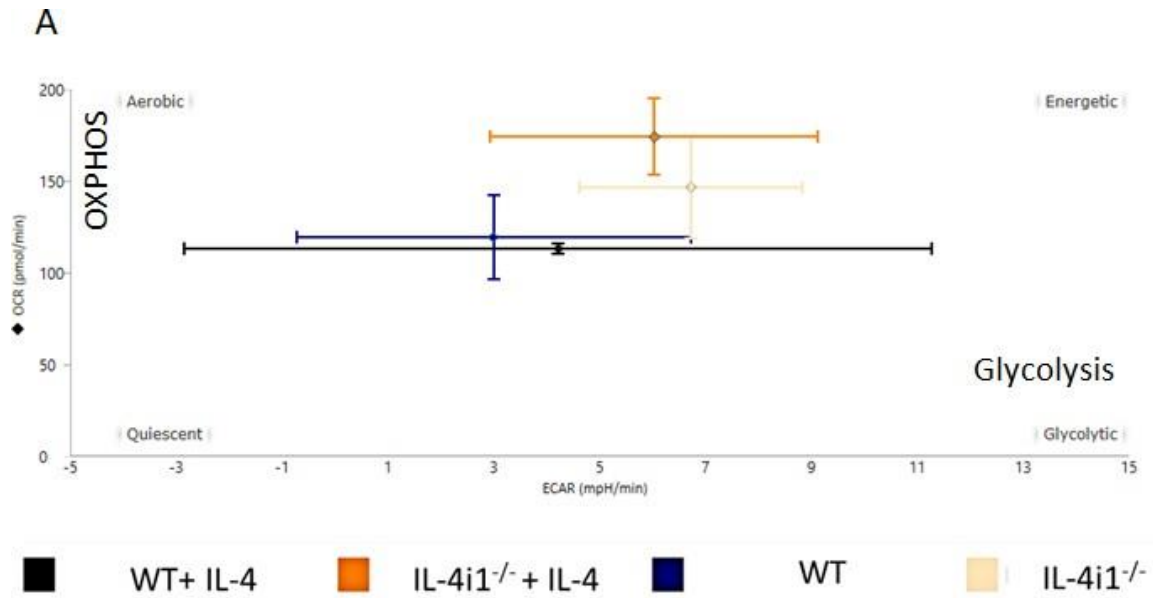


Figure 4.12: IL-4i1 deficiency increases ex-vivo metabolic energy status of T-helper cells. **A-B)** Extracellular acidification and oxygen consumption rates of 5×10^5 T-helper cells stimulated with 100U/ml IL-4 or left unstimulated isolated from spleens of WT littermate control and IL-4i1^{-/-} mice. Data is from one experiment with triplicates per group. Student *t*-test analysis *** $p < 0.001$ was used to determine significance.

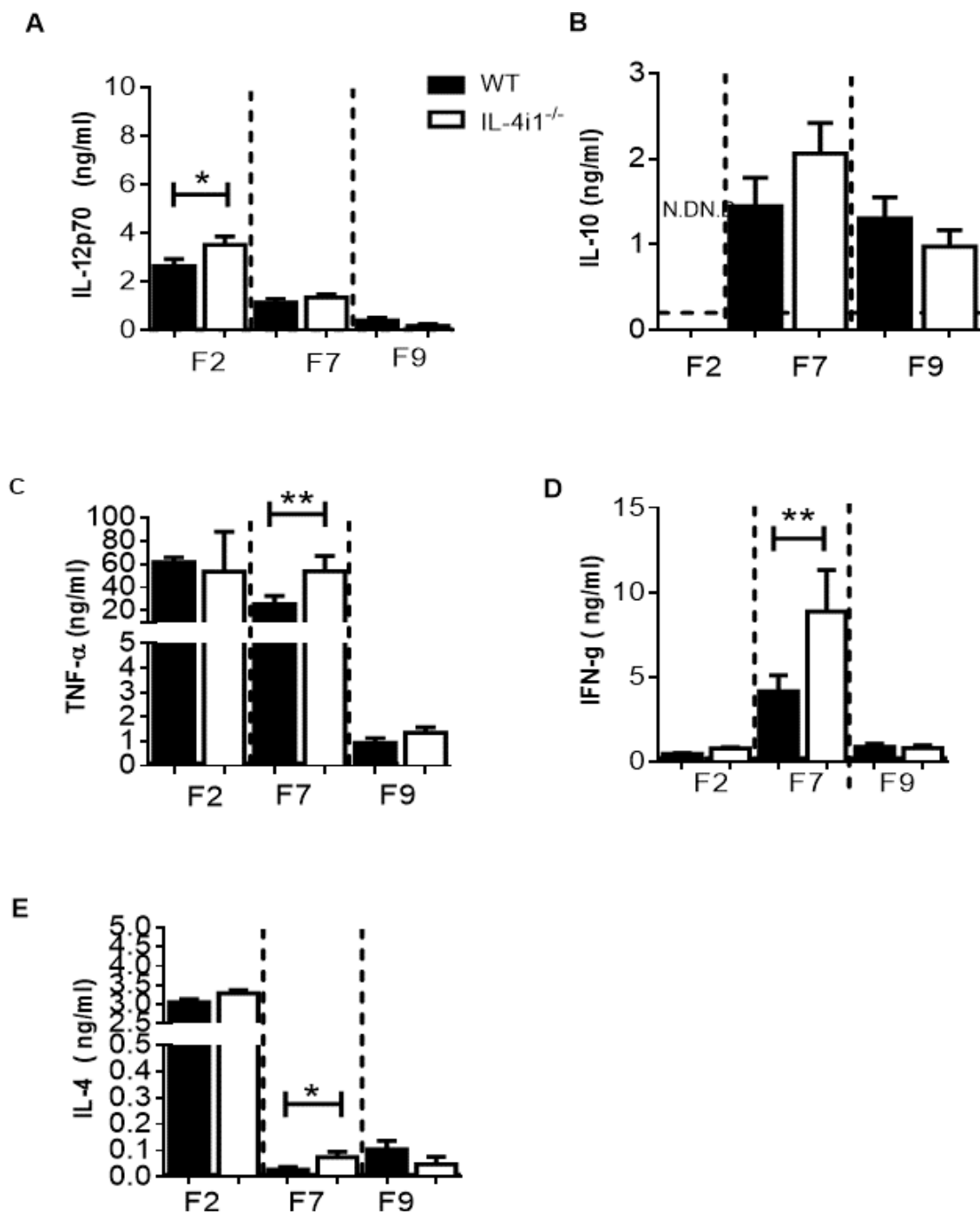


Figure 4.13: IL-4i1 deficiency increased serum IFN- γ and TNF- α production at F7 but not at F9 generations. Serum levels of **A)** IL-12p70, **B)** IL-10, **C)** TNF- α , **D)** IFN- γ , **E)** IL-4 in WT and IL-4i1 deficient mice. Data are representative of two independent experiments with at least n= 5-10 mice per group. Student *t*-test analysis *p<0.05, **p< 0.01 was used to determine significance. N.D= not detectable.

4.7 Summary

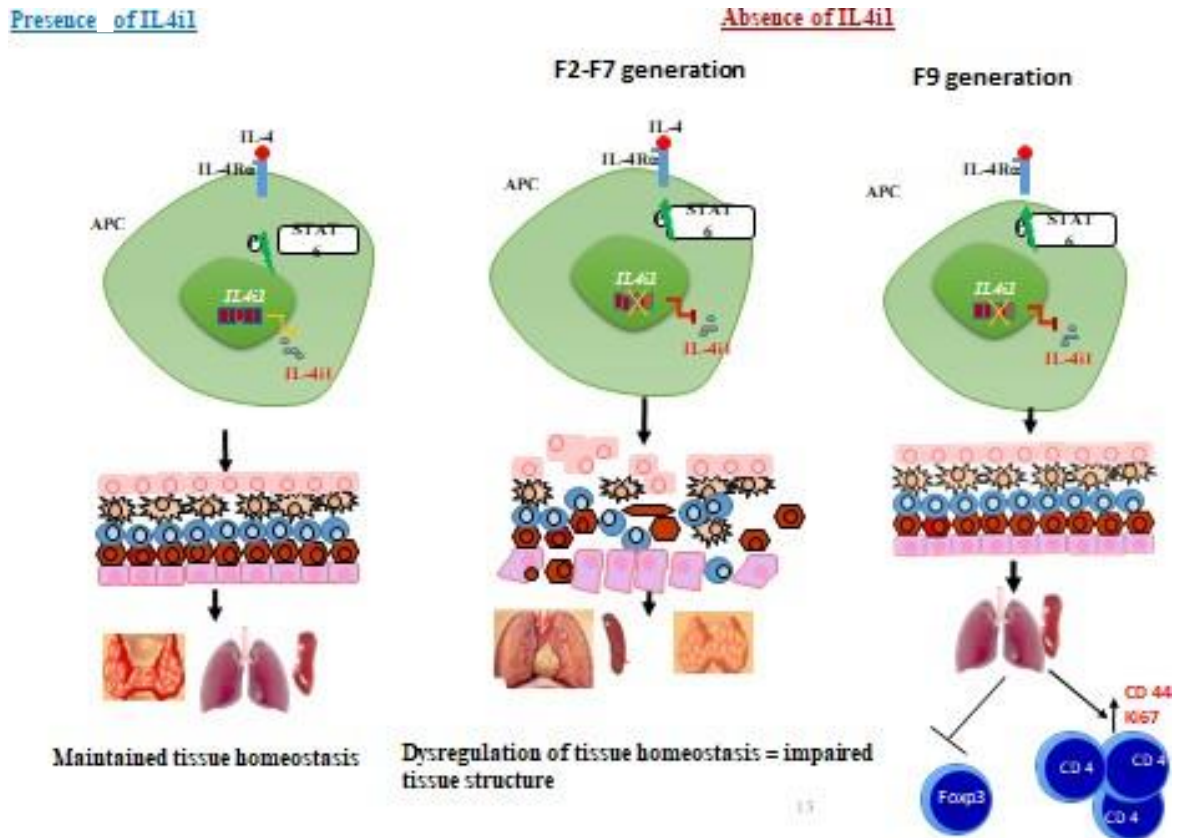


Figure 10: Graphical representation of the role of IL-4i1 on immune homeostasis at steady state *in vivo*.

4.8 Acknowledgements

We thank the UCT Research Animal Facility for maintaining mice, Munadia Ansari for genotyping mice, Zarinah Sunday, Faried Abbass, Marlon Peterson, for their valuable technical assistance. We are grateful to Lizette Fick, for her excellent histology services.

4.9 Funding

The work reported herein was made possible through funding by the South African Medical Research Council through its Division of Research Capacity Development under the SAMRC Internship Scholarship Programme from funding received from the South African National Treasury to LH. The content hereof is the sole responsibility of the authors and do not necessarily represent the official views of the SAMRC or the funders.

ICGEB, Cape Town Component with Arturo Falaschi fellowships to MO and JEC. Claude Leon Foundation fellowship to JKN; Sydney Brenner Fellowship from the Academy of Science of South Africa to JKN as well as support by the South African National Research Foundation (NRF) Research Chair initiative (SARChi) to FB and NRF Competitive Program for Unrated Researchers (CSUR) and DST/NRF postgraduate training program to RG. The funders had no role in study design, data collection and analysis, decision to publish, or preparation of the manuscript.

4.10 Transparency Declarations

None to declare

Chapter 5

Manuscript in preparation

IL-4i1 regulates macrophage mediated immune responses during acute *Mycobacterium tuberculosis* infection

Summary

In this chapter we addressed possible targets of host-directed therapy for tuberculosis. Using CAGE analysis, we selected candidate genes in polarized macrophages that might be used by Mtb to subvert immune responses. Here we selected IL-4i1, a candidate gene which was highly upregulated in M2 macrophages. This gene codes for an L-amino acid oxidase and was selected based on its T-cell immunoregulatory properties. We hypothesized that the enzyme secreted by macrophages, upon release would limit T-cell responses that are responsible for Mtb killing. We used gene deficient mouse models to address the functional role of IL-4i1 on infectious immunity during Mtb infection. We showed that IL-4i1 deletion rendered mice resistant to both lab H37Rv and HN878 hypervirulent Mtb strains and that the role of IL-4i1 on Mtb infection is at early infection and is associated with macrophage responses not T-cells. We showed that IL-4i1 deletion promoted the recruitment of the “M1-like” which was accompanied by reduced bacterial burden and increased pro-inflammatory chemokine, IFN- γ and NO production macrophage phenotype. Thus showing an important immunoregulatory role for IL-4i1 during Mtb infection and that IL4i1 might be a potential immunomodulatory target for host-directed therapy for tuberculosis. The PhD candidate performed all validation qPCR experiments in Figure 5.1 by herself. She performed bacterial burden, lung homogenates and lung weight experiments in Figures 5.2 and 5.5 with Dr Mumin Ozturk and Mr Julius Chia. The candidate performed all flow cytometry experiments in Figure 5.2, 5.3, 5.4 and 5.6; Immunohistochemistry in Figure 5.2 and 5.5 and ELISA experiments in Figure 5.4 and 5.7 by herself.

Chapter 5

IL-4i1 regulates macrophage mediated immune responses during acute *Mycobacterium tuberculosis* infection

Lerato Hlaka^{1,2}, Mumin Ozturk^{1,2}, Julius Chia^{1,2}, Frank Brombacher^{1,2,3}, Reto Guler^{1,2,3}*

¹ International Centre for Genetic Engineering and Biotechnology, Cape Town Component, Cape Town 7925, South Africa.

² Department of Pathology, University of Cape Town, Institute of Infectious Diseases and Molecular Medicine (IDM), Division of Immunology and South African Medical Research Council (SAMRC) Immunology of Infectious Diseases, Faculty of Health Sciences, University of Cape Town, Cape Town 7925, South Africa.

³ Wellcome Centre for Infectious Diseases Research in Africa (CIDRI-Africa), Institute of Infectious Disease and Molecular Medicine (IDM), Faculty of Health Sciences, University of Cape Town, Cape Town 7925, South Africa.

*Corresponding author.

Tel: +27-21-4066033; Fax: + 27-86-6407594

E-mail: reto.guler@uct.ac.za

5.1 Abstract

Objectives: *Mycobacterium tuberculosis* (Mtb) resides in lung macrophages upon infection. Macrophages can be polarized into distinct classically M1(IFN- γ) or alternatively M2) activated phenotype depending on the activation stimuli upon infection which then engages different responses relative to disease control and progression. Mtb has been reported to manipulate the transcriptional profile of the M2(IL-4 or IL-4/IL-13) macrophage for immune evasion strategies to promote its survival. The L-phenylalanine oxidase, IL-4i1 implicated in various tumours and other inflammatory disorders has recently been reported to drive macrophage polarization towards an alternatively activated M2 phenotype. In our genome-wide transcriptional analysis of IFN- γ activated M1 macrophages, and IL-4 and IL-4/IL-13 activated M2 macrophages that were then infected with Mtb, high IL-4i1 transcripts were induced in M2 (IL-4 or IL-4/IL-13) and M2 (IL-4 or IL-4/IL-13) infected macrophages. Other studies have reported the expression of IL-4i1 in TB lesions of patients with pulmonary tuberculosis and those with tuberculosis meningitis (TBM) co-infected with HIV when as well as in lungs of mice following aerogenic *Mycobacterium tuberculosis* (Mtb) infection. However, the role of IL-4i1 in host immunity to Mtb infection has not been investigated to date.

Methods and Results: Here we investigated the role of IL-4i1 during Mtb infection. High mRNA expression of IL-4i1 was observed in M2 (IL-4 or IL-4/IL-13) macrophages infected with Mtb. In order to uncover a possible role of IL-4i1 in tuberculosis *in vivo*, we generated an IL-4i1-deficient mouse BALB/c strain and infected with Mtb H37Rv or hyper-virulent HN878 Mtb strain and littermates control. IL-4i1 deficient mice were highly resistant to tuberculosis compared to littermate controls at 12 and 21 days post-infection. IL-4i1^{-/-} had increased IFN- γ and nitric oxide (NO) killing effector functions, leading to decreased bacteria in the lung with highly increased host protective chemokines CCL-5, CXCL-1 CXCL-5 as well as high recruitment of “M1-like” macrophages compared to littermate controls.

Conclusions: Taken together, our findings suggested that at early infection, transient expression of IL-4i1 regulates macrophage-mediated immunity. These data provide an indication of an immune regulatory role of IL-4i1 during Mtb infection. In conclusion, inactivation of IL-4i1 might be a potential immunomodulatory target for tuberculosis host-directed therapy.

5.2 Introduction

Classically activated macrophages characterized by the release of nitric oxide are essential for Mtb killing. Upon Mtb infection, recognition of PAMPS by PRR leads the release of NO via the MyD88-dependent signalling. Mice deficient of NOS-2 had increased arginase production and developed increased bacterial burden due to the absence of NO production [71, 78]. However, Mtb has found subverting strategies to this hostile environment. One mechanism is the induction of an M2-like environment. Recently, it was reported that Mtb induces arginase (Arg-1) production which competes with NOS2 for L-arginine substrate [80]. Macrophage polarization is important in the outcome of granuloma formation. The infiltration of M1 or M2 macrophages determines the type of granuloma that forms. Necrotic granulomas were associated with M1-like macrophages that are characterized by short NFκB signalling intervals in non-human primates [176]. Increased expression of CD206 mannose receptor associated with “M2-like” macrophages in lungs was associated with caseating granulomas in TB patients. Genome-wide transcriptional analysis of IFN-γ activated M1 macrophages and IL-4 or IL-4/IL-13-activated M2 macrophages infected with HN878 Mtb revealed IL-4i1 as one of the candidate genes upregulated in M2 (IL-4 or IL-4/IL-13) macrophages suggesting a role for IL-4i1 during Mtb infection. The most characterized role of IL-4i1 is its immunomodulatory properties during inflammatory conditions which are mostly associated with its enzymatic activity [89]. Its major role is in limiting T-and B-cell activation and proliferation [90, 91, 93, 94]. Recently, IL-4i1 was reported to promote macrophage polarization towards an M2 phenotype via STAT-6/STAT-1 phosphorylation and partly through the depletion of L-tryptophan and L-arginine which in-turn limited T-cell proliferation. However, the role of IL-4i1 in infectious immunity has not been investigated to date [92]. To determine the functional role of IL-4i1 during Mtb infection, we used gene knockout mouse models. We postulated that IL-4i1 expression by M2 (IL-4 or IL-4/IL-13) macrophages would in-turn limit proliferation and activation of pro-inflammatory T-cells that are responsible for Mtb killing. Here we report on the role of IL-4i1 in regulating macrophage mediated immune responses at early acute Mtb infection.

5.3 Materials and Methods

5.3.1 Mice

IL-4i1 deficient mice (IL-4i1^{-/-}), wild-type control littermates (IL4^{+/+}) or wildtype BALB/c mice were used for this study. All experimental mice were matched for sex and age and used between 8-12 weeks of age. Mice were kept under pathogen-free conditions in individually ventilated cages at the University of Cape Town's animal facility unit Biosafety level 2 (BSL-2) or BSL-3. Animal room temperature was maintained at 22-25 °C and 12 hours light/dark cycle. Food pellets and water were made available *ad libitum*.

5.3.2 Ethical Statement

All experimental procedures were carried in accordance with the South African National Standard (SANS 10386:2008). The protocol (015/037) was approved by the Ethics Committee, University of Cape Town.

5.3.3 Generation of BMDMs, MDMs, Mtb infection and quantitative expression of IL-4i1 in macrophages

BMDMs were generated from 8-12 weeks old BALB/c mice as described [127]. Following 10 days of differentiation, BMDMs were cultured in triplicates overnight for adherence into 96-well plates (Nunc, Denmark) at 5×10^4 cells per well. Monocyte-derived macrophages (MDMs) were isolated from human peripheral nuclear cells (PBMCs) generated blood samples obtained from healthy donors. At 24hrs post adherence, BMDMs were stimulated with 100U/ml recombinant IFN- γ or 100U/ml IL-4 or IL-4/IL-13. Single cell suspension of hypervirulent HN878 *Mycobacterium tuberculosis* (Mtb) from frozen stock was prepared in DMEM media. After 24hr of stimulation or 24hrs post adherence for MDMs cells were infected with HN878-Mtb at MOI 1:5 CFU per well. Cells were then washed once with culture media to remove extracellular bacteria or lysed. Lysates were plated on 7H10 agar plates containing 10% OADC and 0.5% glycerol for CFU counting to determine bacilli uptake. At 2, 6, 12 and 24 hours post-stimulation, or 4hr, 12hr, 24hrs or 48hrs post-infection, cells were lysed with 1 ml of Qiazol and total RNA will be extracted by RNAeasy kit from Qiagen from which cDNA was synthesized using the Transcriptor First Strand cDNA Synthesis Kit (Roche) according to manufacturer's instructions. Real-time PCR was performed with LightCycler® 480 SYBR Green I Master mix in LightCycler® 480 II (Roche). A time-course quantitative expression analysis of IL-4i1 normalized against the housekeeping gene Hprt with primers, IL-4i1 forward 5' ATCCCCAGAGGACATCTACCA and reverse 5' CTGTACCGGAGTCTATCGCTCA.

5.3.4 *In vivo* Mtb infection and quantitative tissue expression of IL-4i1

Mice were infected with hypervirulent HN878 or H37Rv laboratory Mtb strains at 100 per mouse via intranasal route as described in [17]. Quantitative real-time RT-PCR of total murine RNA extracted by RNAeasy kit from Qiagen was reverse transcribed by Transcriptor First Strand cDNA Synthesis Kit (Roche) according to manufacturer's instructions. Real-time PCR was performed with LightCycler® 480 SYBR Green I Master mix in LightCycler® 480 II (Roche). Quantitative tissue expression analysis of IL-4i1 was normalized against the housekeeping gene Hprt1 with primers , IL-4i1 forward 5' ATTCCCCAGAGGACATCTACCA and reverse 5' CTGTACCGGAGTCTATCGCTCA.

5.3.5 Flow Cytometry

Single cell suspensions from infected lung tissues were stained for surface markers with the following antibodies: F4/80 (PE-cy7) from Affymetrix eBiosciences; CD4 (PercCP-cy 5.5 or PE or FITC); CD11c (V450 or A700 or APC); CD11b (PercCP-cy 5.5); MHCII (A700); CD103 (PE); SiglecF (APC-cy7 or APC); CD44 (FITC); CD62L (V450); CD19 (PercCP-cy5.5); CD8 (V500); LY6G (APC-cy7); Foxp3 (APC); CD 80 (V450); CD206 (FITC) and Ki67 (PE) from BD Biosciences in FACS buffer. Rabbit polyclonal IL-4i1 antibody was purchased from Abcam and goat anti-rabbit secondary IgG (PE) purchased from (Abcam). For surface staining, cells (1×10^6) were labelled and washed with PBS containing 0.1% BSA (Rosche, Switzerland) and 0.1% NaN₃. For intracellular staining, we used the BD Pharmingen Transcription Buffer Set (BD Biosciences) as per manufacturer's instructions to detect Foxp3 and Ki67 expression. Acquisition was conducted using BD LSR Fortessa (BD Biosciences Immunocytometry systems), and data analysis was performed with FlowJo software (Treestar, Ashland, OR, US).

5.3.6 Histology

Formalin fixed (4%) Mtb-infected lungs from wild-type littermate controls and IL-4i1-/- mice were stained with hematoxylin and eosin or rabbit anti-mouse iNOS (Abcam) and detection performed using HRP-labelled anti-rabbit and anti-goat, respectively as described [80, 151]. Gelatine-based mounting medium was used to mount the sections. Image acquisition and quantification of alveolar airspaces, iNOS and Arg1 were performed using NIS advanced software on a Nikon (Tokyo, Japan) 90i microscope. Percentage of free alveolar airspaces was defines as the area of ventilated spaces in whole lung sections in relation to the total lung tissue area using the area measurement tool by NIS advanced software on a Nikon 90i microscope and % alveolar spaces calculated using Excel as described [21]. The percentage of iNOS and Arg1 was performed using a blinded quantification method as described [21].

5.3.7 The enzyme-linked immunosorbent assay

Blood samples from IL-4i1^{-/-} and wild-type littermate controls were collected by cardiac puncture upon sacrifice. Serum samples were used to determine systemic cytokine and chemokine production using enzyme-linked immunosorbent assay. IL-1 β , IL-12p40, IL-12p70, TNF- α , IL-2, IL-10, IFN- γ , IL-4, CCL-2, CCL-3, CXCL-1, CXCL-2, CXCL-5 and CCL-5 (All from BD Biosciences) production was measured from the supernatants and data analysed using SoftMax Pro 6.

5.3.8 Statistical Analysis

All data were analysed using Graph-Pad Prism 6.0, student *t*-test (two-tailed with equal variance) was used. A **p* value of less 0.05 was considered significant, with ***p* < 0.01, ****p* < 0.001 and *****p* < 0.0001.

5.4 Results

5.4.1 Identification of IL-4i1 expression during *Mtb* infection.

To confirm CAGE identified expression of IL-4i1 in macrophages. Bone marrow-derived macrophages from WT BALB/c mice were subjected to polarization to classically (M1) or alternatively activated (M2) macrophages following stimulation with IFN- γ and IL-4; IL-4/IL-13 respectively. Subsequent to stimulation, mice were infected with HN878 *Mtb* strain. Time-course mRNA expression of IL-4i1 was determined by qPCR. Early transient expression of IL-4i1 was observed at 6 hrs post-stimulation in IL-4 stimulated alternative activated macrophages. Infection with *Mtb* induced IL-4i1 at 12 hrs post- infection (Figure 5.1A). Time-course expression of IL-4i1 was measured in human monocyte-derived macrophages from healthy donors following HN878 *Mtb* infection. IL-4i1 expression was maintained at 1.5-2 fold higher throughout 48hrs study when compared to 0hrs (Figure 5.1B). *In vivo* expression of IL-4i1 was determined in lungs of BALB/c mice intranasally infected with HN878 *Mtb* strain. *Mtb* infection showed a trend towards increased expression at 21 days post-infection (Figure 5.1C). Different types of human TB granulomas showed differential levels of IL-4i1 expression (Figure 5.1D). Previously, granulomas biopsies from TB patients have shown high expression of IL-4i1 in areas enriched with myeloid antigen presenting cells, macrophage and dendritic cells. Taken together, these data suggest a role for IL-4i1 during *Mtb* infection. However, a role of IL-4i1 in infectious immunity has not been investigated to date. We thus sort to investigate the role on immune regulation during *Mtb* infection using IL-4i1 gene-deficient mouse model.

5.4.2 IL-4i1 deletion reduces bacterial burden and histopathology during acute H37Rv infection.

Control littermate (WT) and IL-4i1 deficient mice (IL-4i1^{-/-}) were infected intranasally with 100 H37Rv *Mtb* strain and bacterial burden measured by colony forming units were measured at 21 days post-infection. Bacterial burdens were significantly reduced in lungs of IL-4i1^{-/-} mice compared to WT ($p < 0.01$) (Figure 5.2A). Lung weights were not affected (Fig 2B). Total lung cell numbers showed a trend of reduction (Figure 5.2C). Frequency of total and total number of infiltrating CD3⁺ T-cells was not affected (Figure 5.2D and E). Histopathology analysis showed significantly reduced granulomas ($p < 0.05$) (Figure 5.2F and H) and significantly less iNOS expression in infected lungs (Figure 5.2G and I). These data suggest that the reduced histopathology is a result of the reduced bacterial burden, further suggesting that IL-4i1 deletion promotes resistance to infection.

5.4.3 IL-4i1 deletion does not influence adaptive immune responses, but reduces inflammatory macrophage recruitments and increases NO production.

The major characterized role of IL-4i1 is in the activation and proliferation of T-cells and recently of B-cell activation. To determine cellular infiltration in the lungs, we determined different adaptive cell populations by flow cytometry in the lungs 21 days-infection with H37Rv infection. There were no differences in B and T-cells and the different subsets nor their proliferative status between WT and IL-4i1^{-/-} (Figure 5.3A-F). IL-4i1 deletion significantly reduced interstitial macrophage recruitment compared to WT ($p < 0.05$) (Figure 5.4A-B). Pro-inflammatory cytokine production measured from lung supernatants showed a trend towards reduction (Figure 5.4C). The cytokine IL-12 produced by both macrophages and dendritic cells responsible for the activation of Th1 pro-inflammatory responses was reduced in IL-4i1^{-/-} compared to WT mice (Figure 5.4C). The reduction correlated with the reduction in interstitial macrophages as dendritic cell population was not affected. Interestingly, a significant increase in nitric oxide production was observed at 21 days post-infection in IL-4i1^{-/-} compared to WT mice (Figure 5.4D). Similarly to cytokine production, we observed a significant reduction in pro-inflammatory chemokines CXCL-1 ($p < 0.001$) and CXCL-2 ($p < 0.05$) responsible for neutrophils and monocytes (Figure 5.4E) in IL-4i1^{-/-} compared to WT mice. These data suggest a regulatory role of IL-4i1 in macrophage responses during Mtb infection which contribute to the reduced CFU burden as a result of IL-4i1 deficiency.

5.4.4 IL-4i1 deletion renders resistance to HN878 Mtb infection by promoting the recruitment of “M1-like” restrictive macrophages as early as 12 days post-infection.

To determine the role of IL-4i1 on macrophage mediated immune responses, we intranasally infected mice with 100 CFU hypervirulent strain previously used in CAGE macrophage atlas experiments. Mice were sacrificed at 12 days post-infection, a time-point where only innate immunity takes place and 21 days post-infection after adaptive immunity is established during Mtb infection. IL-4i1 deletion significantly reduced bacterial burden at 12 and 21 days post-infection (Figure 5.5A) while lung weights were not affected ($p < 0.05$) (Figure 5.5B). These data suggest a regulatory role of IL-4i1 in macrophage responses during Mtb infection which contribute to the reduced CFU burden as a result of IL-4i1 deficiency with no differences in lung weight (Figure 5.5A-B). Histopathology H&E analysis showed no differences in alveolar airspaces between WT and IL-4i1^{-/-} at 12 post-infection (Figure 5C-D). Contrary to H&E and iNOS reduced histopathology observed in IL-4i1^{-/-} during H37Rv infection 21 days post-infection, no differences were observed in mice infected with HN878 while iNOS expression was significantly ($p < 0.05$) increased at 21 days post-infection (Figure 5.5E-H). Previously, IL-4i1 has been reported to promote macrophage polarization towards M2 phenotype *in vitro* via STAT-6 phosphorylation and partly through its role in arginine depletion towards arginase production. To determine the role of IL-4i1 on macrophage polarization *in vivo*, different populations of myeloid cells were determined by flow cytometry in lungs of WT and IL-4i1^{-/-} infected with 100 CFU HN878. There were no differences in myeloid cell populations between WT and IL-4i1^{-/-} mice (Figure 6A-B). We next determined the number of “M1-like” restrictive and “M2-like” permissive macrophages infiltrating the lung. There were no differences in MHCII⁺ CD206⁺ M2-like permissive alveolar macrophages, MHCII⁺CD80⁺ M1-like alveolar macrophages. GMFI expressions of CD 206⁺ and CD 80⁺ in alveolar macrophages were not affected in IL-4i1^{-/-} compared to WT (Figure 6C-E). Interestingly, percentages and total cell numbers of M2-like CD 206⁺ interstitial macrophages were reduced in IL-4i1^{-/-} compared to WT mice, while and the opposite effect was observed for M1-like CD80⁺ interstitial macrophages (Figure 6F-G). No differences were observed in GMFI expressions of CD 206⁺ and CD 80⁺ in interstitial macrophages between WT and IL-4i1^{-/-} mice (Fig H-I). Lung production of pro-inflammatory cytokines (IL-1 β , IL-6, TGF- β) showed an increase towards increased levels while pro-inflammatory chemokines (CCL-2, CCL-3, CXCL-1, CXCL-2, CXCL-5, CCL-5) were enriched by IL-4i1^{-/-} deletion. Taken together, these data suggest that IL-4i1 deletion leads to increased pro-inflammatory macrophage immune responses that are characterized by “M1-like” phenotype that promote NO production leading to reduced

bacterial burden at early Mtb infection.

5.5 Discussion

Our mRNA expression data in infected M2 (IL-4 or IL-4/IL-13) BMDMs, MDM and acute Mtb infection in mice showed an early transient expression of IL-4i1 (Figure 1 5.1A-B) suggesting that Mtb may induce the expression of IL-4i1 for protection from pro-inflammatory macrophage killing suggesting an immune regulatory role during Mtb infection. Granuloma expression of IL-4i1 in TB patients substantiates this claim. Immunohistochemistry of lung biopsies from TB infected patients previously showed that the expression of IL-4i1 was restricted to areas that were macrophage and dendritic cells enriched [86]. To determine the role of IL-4i1 on immune responses during Mtb, we used gene deficient mice models. IL-4i1 deficiency rendered mice resistant to H37Rv and HN878 Mtb infection at 21 days post-infection as denoted by reduced bacterial burden and reduced histopathology with less infiltrating inflammatory T-cells (Figure 5.2). These data suggested that immunohistopathology was associated with the reduced bacterial burden. Surprisingly, T-cell mediated immune responses had no influence of the infection outcome (Figure 5.3). Interestingly, we observed reduced infiltration of CD11b⁺ F/480⁺ interstitial macrophages in the lungs at 21 days post-infection, but increased lung NO production (Figure 5.4), suggesting that IL-4i1 had a role on macrophage mediated immune responses during acute infection. To determine the role of IL-4i1 on macrophage mediated responses, we infected mice with HN878 for 12 days, a time-point where only the innate immunity was established. Bacterial burden was reduced as early 12 days post-infection in IL-4i1 deficient mice (Figure 5.5). We observed an increase in “M1-like” MHCII⁺ CD80⁺ restrictive macrophages in IL-4i1^{-/-} compared to MHCII⁺CD 206⁺ permissive macrophages (Figure 5.6) which in-turn promoted an increase pro-inflammatory cytokines and chemokines (Figure 5.7), suggesting that IL-4i1 regulates macrophage mediated responses. These findings are in line with Psachoulia et al. [95] findings on remyelination. Immunohistochemistry of the brain revealed that CD 11b⁺ infiltrating cells were iNOS enriched in the absence of IL-4i1. Furthermore, Monin et al. [177] showed that *S. mansoni* induced arginase reduced tupe-1 infiltration F/480⁺ cells in lungs of different mouse models. “M1-like” and “M2-like” macrophages distinct metabolic statuses. Mtb strives permissive macrophages which are characterized by fatty acid oxidation while restrictive macrophages are highly glycolytic [178]. It is possible that Mtb induces IL-4i1 early upon infection to promote the infiltration of M2-like permissive macrophages for its protection. It is

important to note that these cell numbers are very low to suggest that this is solely the mechanism by which IL-4i1 regulated immune responses during Mtb infection. However, these data may suggest a contributing mechanism. Furthermore, these data are indicative of the differential possible role of IL-4i1 within the context of the same infectious model. At early infection, transient expression of IL-4i1 regulates macrophage-mediated immunity while at chronic phase may be involved in T-cell mediated immunity. These provide an indication of a possible immunoregulatory role for IL-4i1 during Mtb infection making it a possible immunomodulatory target for host-directed therapy for tuberculosis.

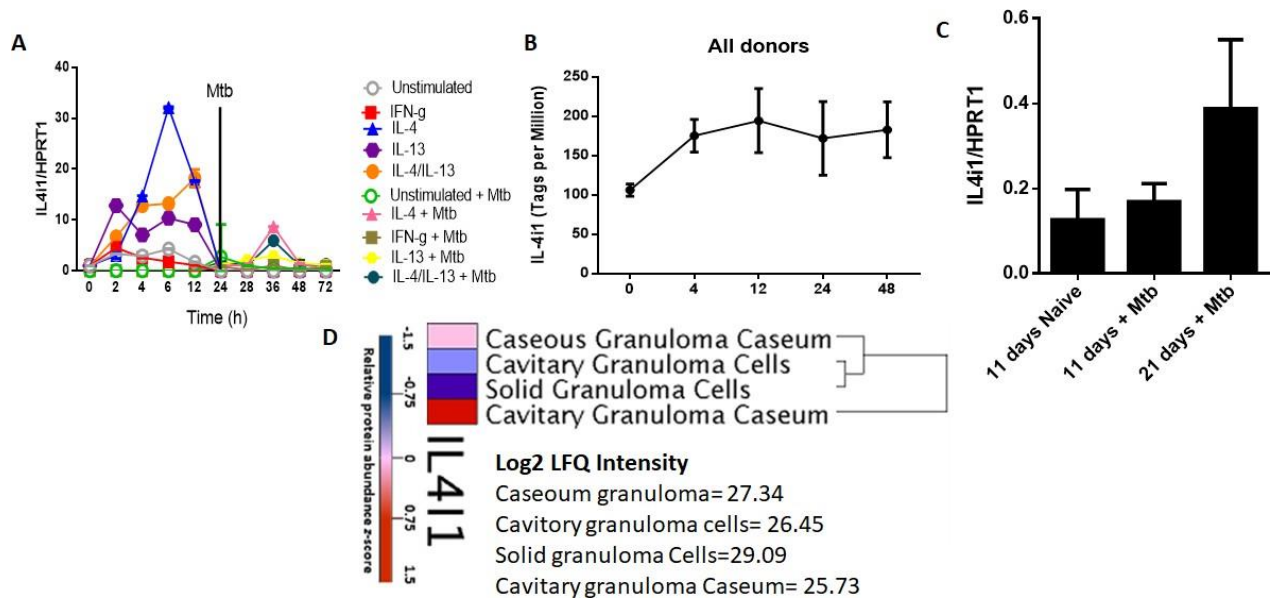


Figure 5.1: mRNA expression of IL-4i1 during *Mycobacterium tuberculosis* infection: A) Bone marrow-derived macrophages were infected with HN878 Mtb strain following macrophages polarization to IFN- γ (classically activated, M1) or IL-4 or IL-4/IL-13 (alternatively activated, M2) macrophages. Time-course expression of IL-4i1 was determined by qPCR normalized to HPRT1. **B)** Time-course IL-4i1 expression from human monocyte-derived macrophages infected with HN878 Mtb. **C)** IL-4i1 expression from lung tissues of BALB/c mice intranasally infected with HN878 at 11 and 21 days post-infection relative expression in naïve mice (n=3). **D)** Hit-map of IL-4i1 expression TB granulomas.

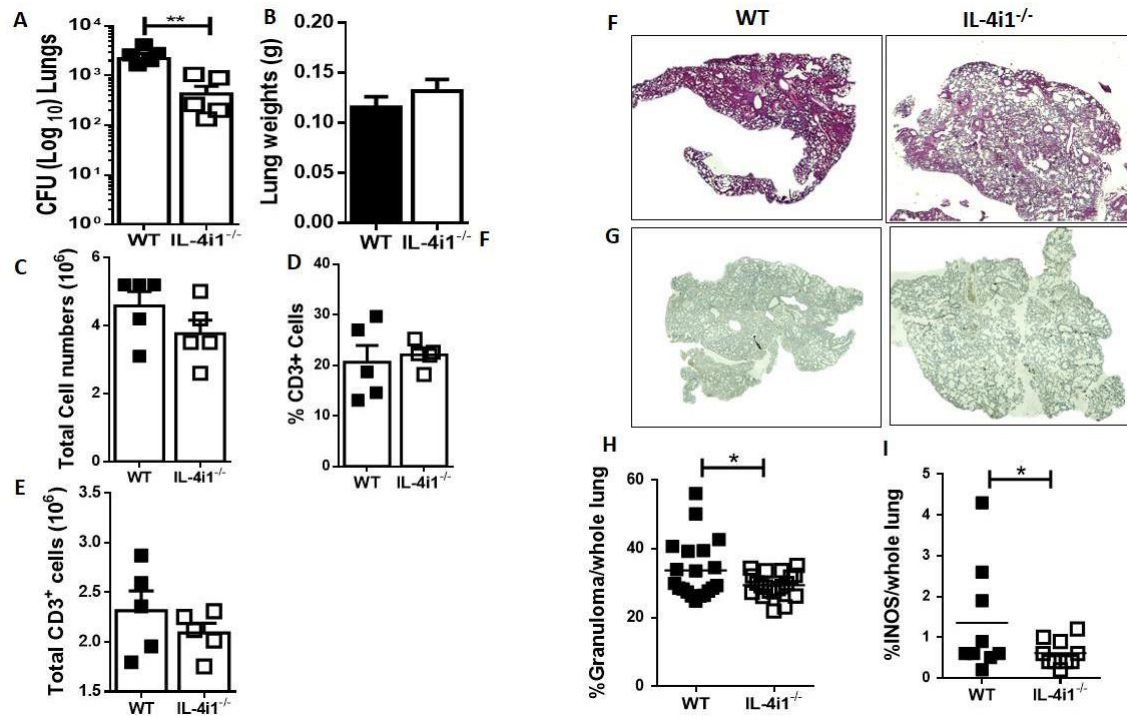


Figure 5.2: IL-4i1 deficient mice were resistant to H37Rv Mtb infection with reduced pathology and cellular infiltration. Control littermate (WT) and IL-4i1 deficient mice (IL-4i1^{-/-}) (n=5) were infected intranasally with 100 H37Rv Mtb strain. Mice were sacrificed 21 days post-infection. **A)** Bacterial burden in lungs of infected mice. **B)** Lung weights of infected mice. **C)** Total cell numbers from single cell suspensions of infected lung tissues. **D)** Percentage and **E)** Total cell CD3⁺ T-cells infiltrating the infected lung tissues measured by flow cytometry. **F)** Representative histopathology sections (×20) at 21 days post infection for H&E sections. **G)** Representative iNOS sections (×20) at 21 days post infection. **H)** Lung granulomas were quantified by measuring area of solid tissue vs ventilated airspaces from 4 deep cuts H&E lung sections per mice (30μm apart) at 3 weeks post- infection. **I)** iNOS staining per lung section was quantified from 1–2 deep cut lung sections per mice at 3 weeks p.i. (30μm apart). Data are representatives of 3 independent experiments. Error bars show mean±SEM. Student's *t*-test *P<0.05; **P<0.01 was used to determine significance.

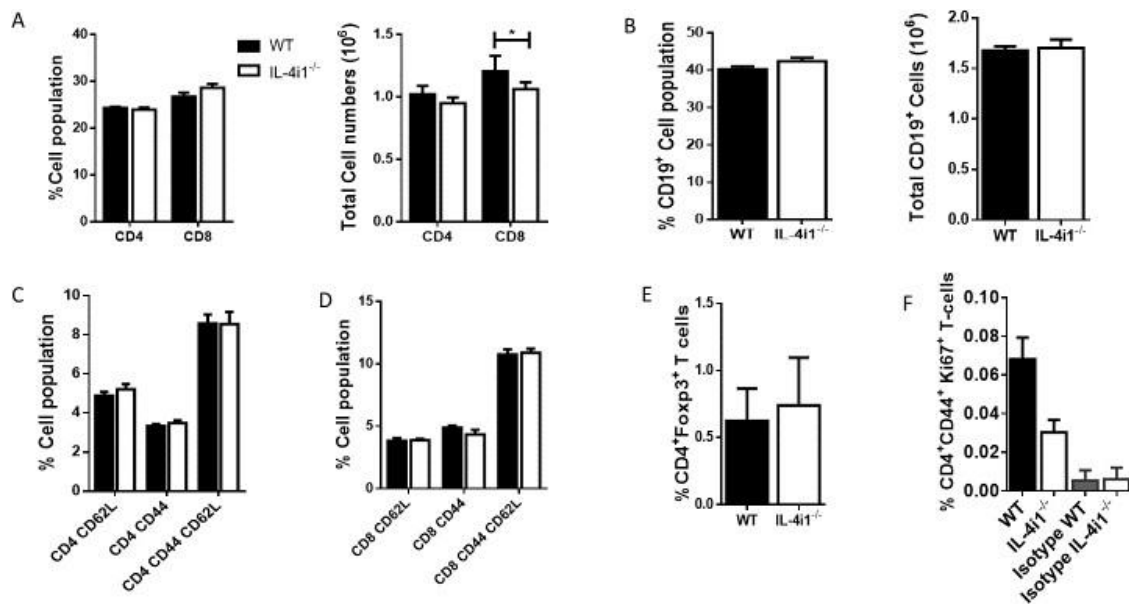


Figure 5.3: IL-4i1 deletion did not influence adaptive immune responses at 3 weeks post H37Rv-Mtb infection. Control littermate (WT) and IL-4i1 deficient mice (IL-4i1^{-/-}) (n=5) were infected with 100 H37Rv Mtb strain. Mice were sacrificed 21 days post-infection to determine adaptive immune responses to infection. **A)** Percentage and total cell numbers of CD3⁺CD4⁺ T-cells and CD3⁺CD8⁺ T-cells in lungs of infected mice. **B)** Percentage and total cell numbers of CD19⁺ B-cells in lungs of infected mice. **C)** Percentage and of CD4⁺ CD62L⁺ naïve T-cells; CD4⁺CD44⁺CD62L⁺ central memory T-cells; CD4⁺CD44⁺ effector T-cells. **D)** Percentage and of CD8⁺CD62L⁺ naïve T-cells; CD8⁺CD44⁺CD62L⁺ central memory T-cells; CD8⁺CD44⁺ effector T-cells measured by flow cytometry. **E)** Percentage CD 4⁺ regulatory T-cells. **F)** Percentage of proliferating Ki67⁺ CD4⁺CD44⁺ effector T-cells. Data are representatives of 3 independent experiments. Error bars show mean±SEM. Student's *t-test* *P<0.05 was used to determine significance.

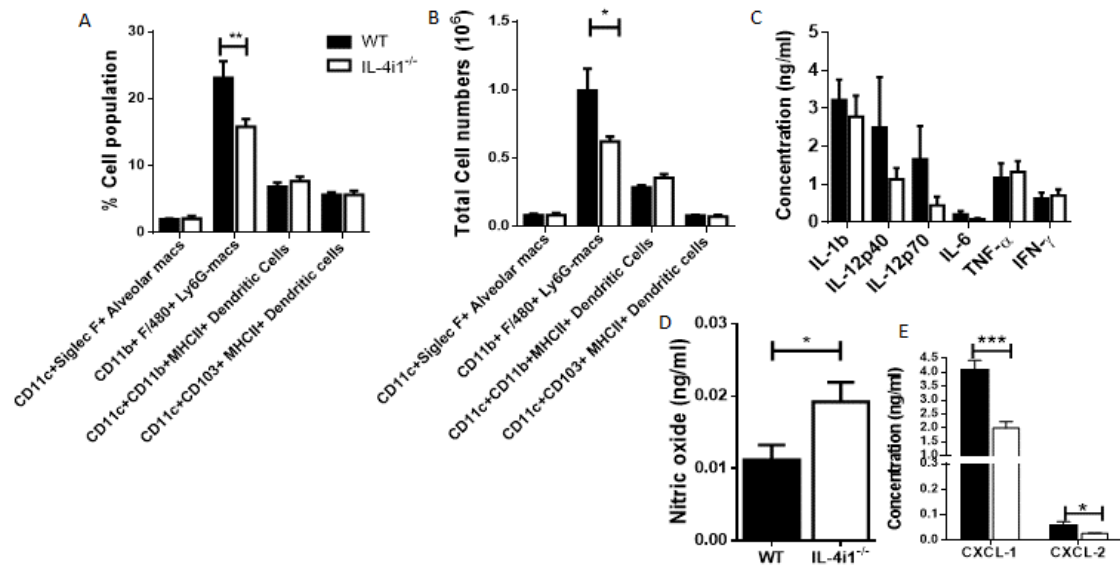


Figure 5.4: IL-4i1 deletion reduces interstitial macrophage recruitment in infected lungs but increases nitric oxide production in H37Rv-Mtb infected lungs. Control littermate (WT) and IL-4i1 deficient mice (IL-4i1^{-/-}) (n=5) were infected with 100 H37Rv Mtb strain. Mice were sacrificed 21 days post- infection to determine innate immune responses to infection. **A)** Percentage myeloid cell populations (CD11c⁺SiglecF⁺ Alveolar macrophages; CD11b⁺F/40⁺ Interstitial macrophages; CD11b⁺CD11c⁺MHCII⁺ Dendritic cells; CD11c⁺CD103⁺MHCII⁺ Migratory dendritic cells) in infected lungs. **B)** Total cell numbers of myeloid cell population (CD11c⁺Siglec F⁺ Alveolar macrophages; CD11b⁺F/40⁺Interstitial macrophages; CD11b⁺CD11c⁺MHCII Dendritic cells; CD11c⁺CD103⁺MHCII⁺ Migratory dendritic cells) in infected lungs. **C)** Lung cytokine production determined from lung homogenates. **D)** Nitric oxide production from infected lung homogenates. **E)** Lung chemokine production determined from lung homogenates. Data are representatives of 3 independent experiments. Error bars show mean±SEM. Student's *t*-test *P<0.05; **P<0.01; P< 0.001) as used to determine significance.

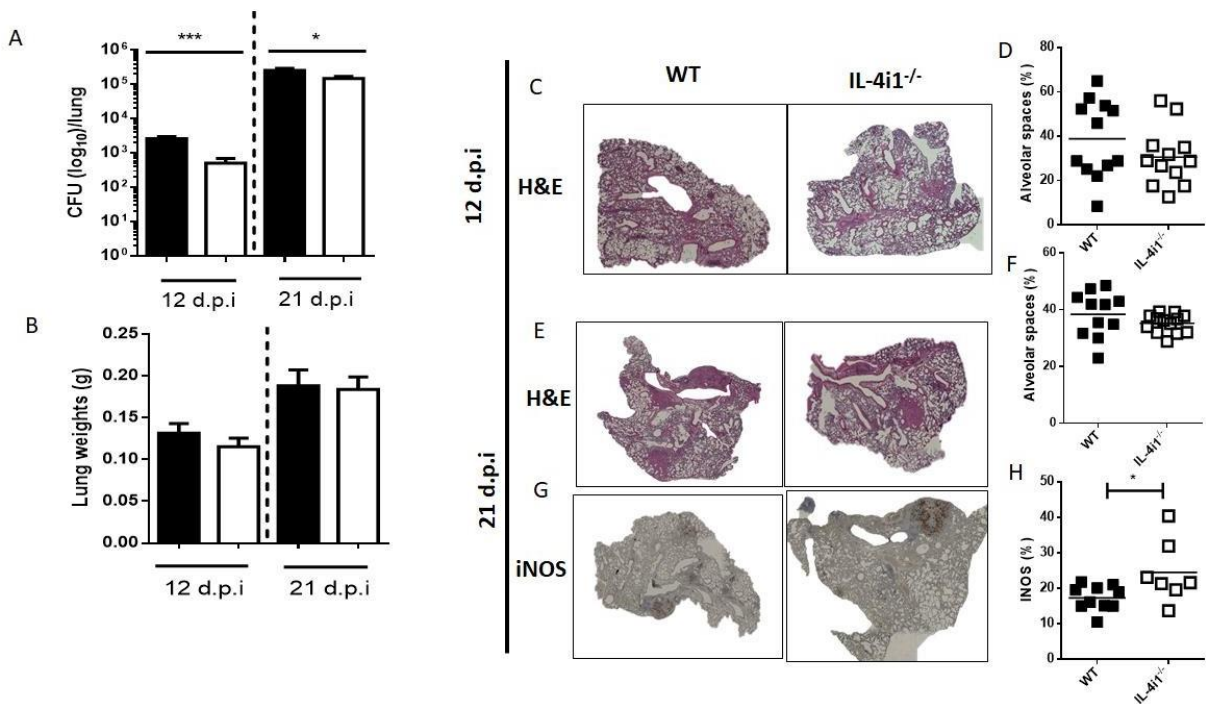


Figure 5.5: IL-4i1 deficient mice were resistant to early HN878-Mtb infection. Control littermate (WT) and IL-4i1 deficient mice (IL-4i1^{-/-}) (n=5) were infected intranasally with 100 hypervirulent H37Rv Mtb strain. Mice were sacrificed at 12 and 21 days post-infection. **A)** Reduced bacterial burden in lungs of infected mice at both 12 and 21 days post-infection. **B)** Lung weights of infected mice. **C)** Representative histopathology sections (×20) at 12 days post infection for H&E sections. **D)** Lung alveolar ventilated airspaces were quantified from 4 deep cuts H&E lung sections per mice (30μM apart) at 12 days post-infection. **E)** Representative histopathology sections (×20) at 21 days post-infection for H&E sections. **F)** Lung alveolar were ventilated airspaces quantified from 4 deep cuts H&E lung sections per mice (30μM apart) at 21 days post-infection **G)** Representative iNOS sections (×20) at 21 days post-infection. **H)** iNOS staining per lung section was quantified from 1–2 deep cut lung sections per mice at 21 days post-infection (30μm apart). Error bars show mean±SEM. Student's *t-test* *P<0.05; ***P<0.001 was used to determine significance.

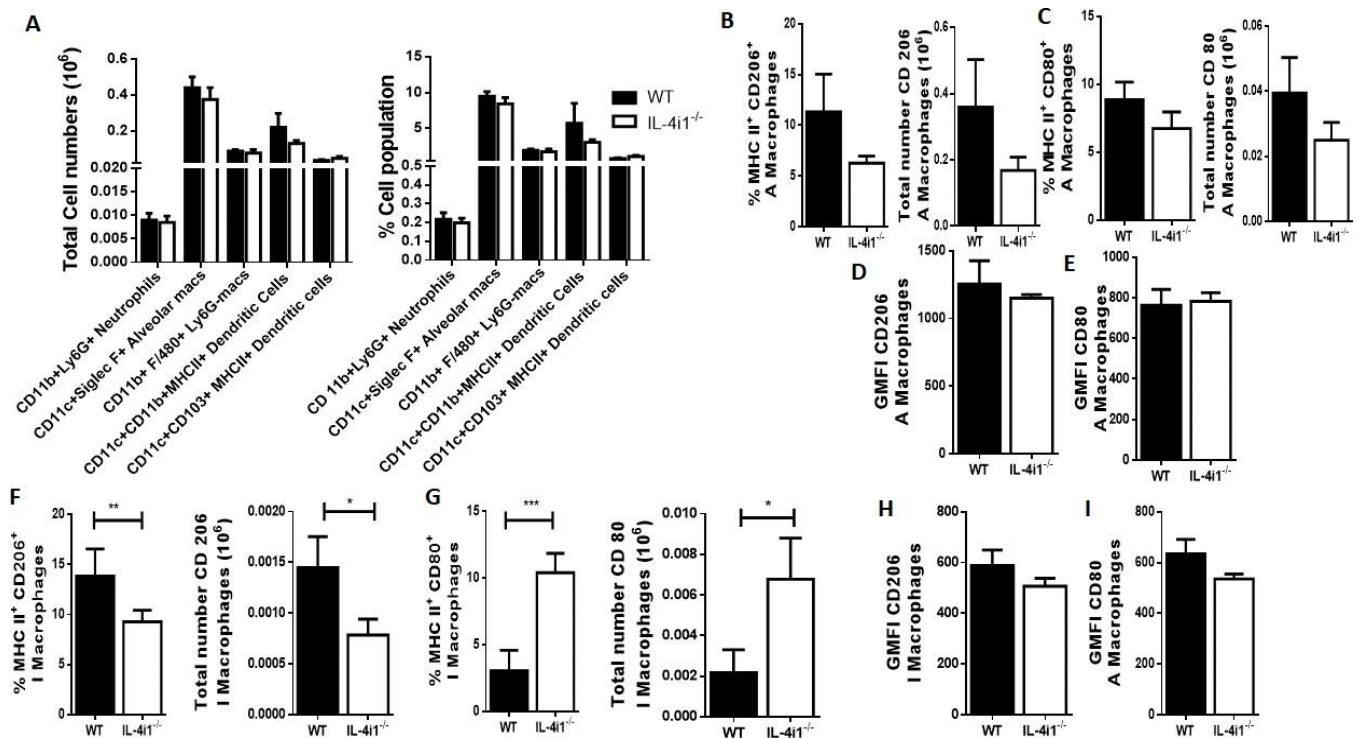


Figure 5.6: IL-4i1 deficiency promotes recruitment of “M1-like” restrictive macrophages at early HN878-Mtb infection. Control littermate (WT) and IL-4i1 deficient mice (IL-4i1^{-/-}) (n=5) were infected intranasally with 100 hypervirulent H37Rv Mtb strain. Mice were sacrificed at 12 post-infection to determine innate immune responses to infection. **A)** Total numbers and percentages of myeloid cell populations (CD11b⁺Ly6G⁺ neutrophils; CD11c⁺SiglecF⁺ Alveolar macrophages; CD11b⁺F4/80⁺ Interstitial macrophages; CD11b⁺CD11c⁺MHCII⁺ Dendritic cells; CD11c⁺CD103⁺MHCII⁺ Migratory dendritic cells) in infected lungs. **B)** Percentage and total numbers of CD11c⁺Siglec F⁺MHCII⁺CD206⁺ alveolar macrophages. **C)** Percentage and total numbers of CD11c⁺SiglecF⁺MHCII⁺CD206⁺ alveolar macrophages. **C)** Percentage and total numbers of CD11c⁺SiglecF⁺MHCII⁺CD80⁺ alveolar macrophages. **D)** GMFI of CD206⁺ in alveolar macrophages. **E)** GMFI of CD80⁺ in alveolar macrophages. **F)** Percentage and total numbers of CD11b⁺F4/80⁺MHCII⁺CD206⁺ interstitial macrophages. **G)** Percentage and total numbers of CD11b⁺F4/80⁺MHCII⁺CD80⁺ interstitial macrophages. **H)** GMFI of CD206⁺ in interstitial macrophages. **I)** GMFI of CD80⁺ in interstitial macrophages. Data are representatives of mean±SEM. Student’s *t-test* *P<0.05; **P<0.01; P<0.001 was used to determine significance.

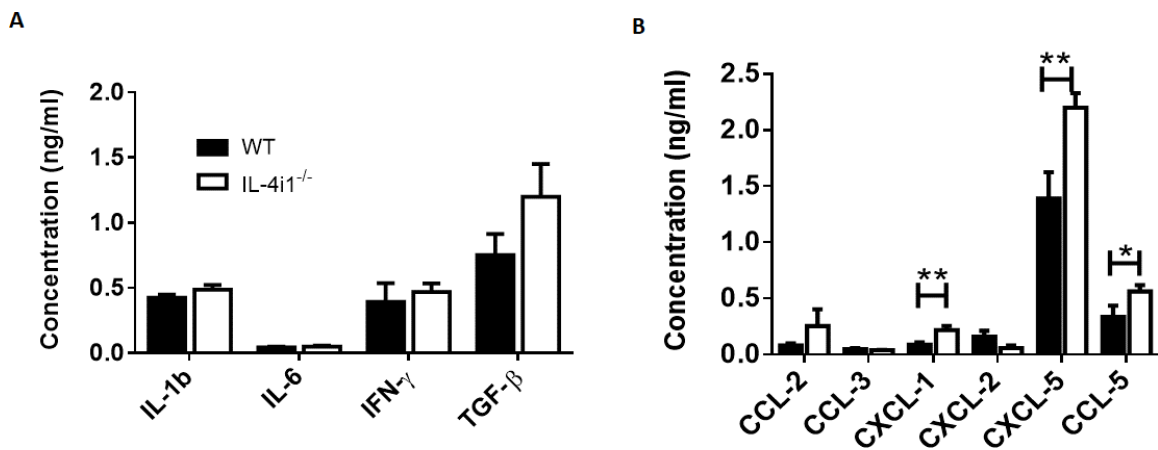


Figure 5.7: IL-4i1 deficiency promotes pro-inflammatory chemokine production. Control littermate (WT) and IL-4i1 deficient mice (IL-4i1^{-/-}) (n=5) were infected intranasally with 100 hypervirulent HN878 Mtb strain. Mice were sacrificed at 12 days post-infection to determine **A)** cytokine, **B)** chemokine production in infected lung homogenates during infection. Data are representatives of mean \pm SEM. Student's *t*-test *P<0.05; **P<0.01 was used to determine significance.

5.6 Summary

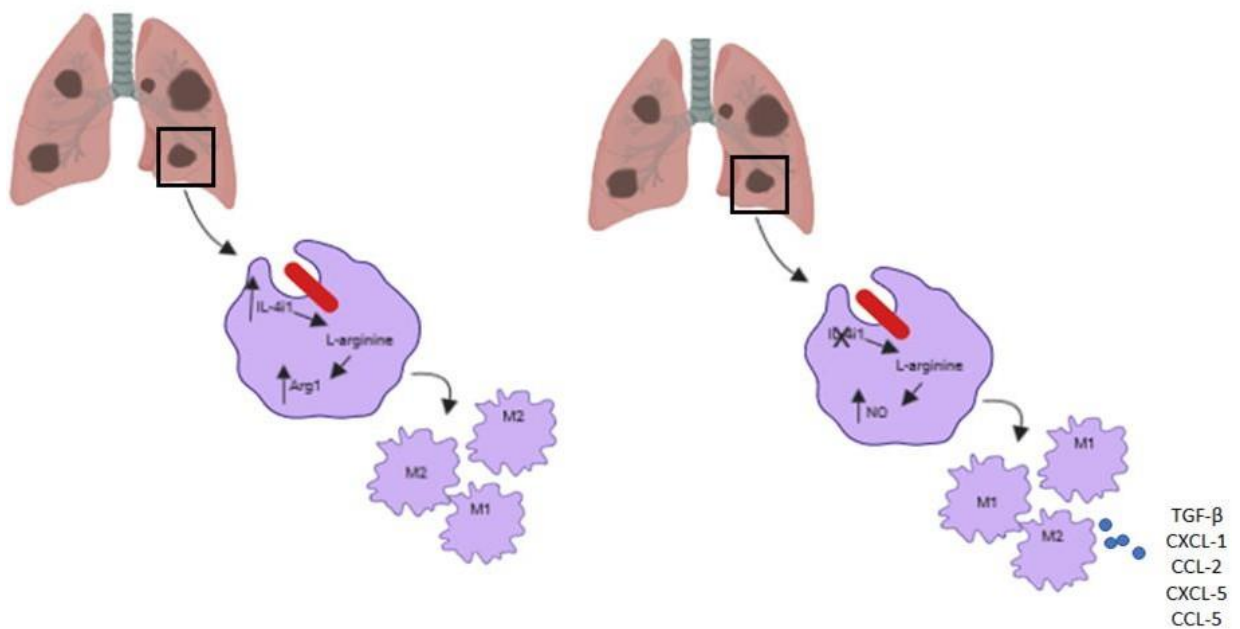


Figure 5.8: Graphical representation of the role of IL-4i1 during early *Mycobacterium tuberculosis* infection.

5.7 Acknowledgements

We thank the UCT Research Animal Facility for maintaining mice, Munadia Ansari for genotyping mice, Zarinah Sondag, Faried Abbass, Marlon Peterson, for their valuable technical assistance. We are grateful to Lizette Fick, for her excellent histology services.

5.8 Funding

The work reported herein was made possible through funding by the South African Medical Research Council through its Division of Research Capacity Development under the SAMRC Internship Scholarship Programme from funding received from the South African National Treasury to LH. The content hereof is the sole responsibility of the authors and do not necessarily represent the official views of the SAMRC or the funders. ICGEB, Cape Town Component with Arturo Falaschi fellowships to MO and JEC. Claude Leon Foundation fellowship to JKN; Sydney Brenner Fellowship from the Academy of Science of South Africa to JKN as well as support by the South African National Research Foundation (NRF) Research Chair initiative (SARChi) to FB and NRF Competitive Program for Unrated Researchers (CSUR) and DST/NRF postgraduate training program to RG. The funders had no role in study design, data collection and analysis, decision to publish, or preparation of the manuscript.

5.9 Transparency Declarations

None to declare

Chapter 6

Conclusions

The aim of the study presented in this thesis was to identify potential drug targets for pathogen- and host-directed therapy for tuberculosis. TB remains a major public health global challenge. The shortage of effective drugs and vaccines, with the emergence of MDR and XDR TB, propels an urgent need for new effective therapeutics. The STOP-TB partnership has set goals to eradicate TB by 2050. Their goals include developing new effective drugs, vaccines, diagnostics and vaccines. It is imperative to develop treatment approaches that focus on both the pathogen and the host. The development of new effective drugs lies primarily on understanding host-pathogen interactions and the possible mechanisms by which the pathogen can invade or subvert host immune system through molecular approaches. These approaches would help identify possible targets that may be used by Mtb to subvert cellular transcriptional landscape especially macrophages which are the first contact for Mtb.

In this study we addressed the role of MGBs that target the AT-rich regions of the minor groove of pathogenic DNA as a potential target for pathogen-directed therapy. We further addressed the importance of using a reliable delivery system (NIVs) for effective treatment. MGBs bind to pathogenic DNA and inhibit DNA replication. The anti-infective activity of Strathclyde MGBs has been previously reported against many pathogens [25, 26, 29-31, 34-36, 106, 113, 116]. The specificity of binding affinity and cell wall permeability for is mostly associated with the structure of the head and tail groups of the compound. From the list of the compounds we screened, we identified hit compounds that were effective against Mtb *in vitro*. Proof of concept studies in mice showed *in vivo* activity of one of the compounds, MGB 364 at low concentrations. The use of NIVs improved the activity of these compounds. From these studies we could conclude on the potential of MGB 364 as a lead compound against Mtb infection. Interestingly we also observed that intranasal administration of MGB-NIV 364 formulation improved immune responses and pathology during Mtb infection. With this we could conclude on the possibility of an adjunct TB therapy while using NIVs. In this case NIVs would be effective in delivering the drug of interest as well as trigger immune activation necessary for killing of the pathogen. However, this would need controlled measures to ensure that the effects are not detrimental to the host. The limitations of the study is the availability of the compound to perform further experiments due to delay in synthesis process. Future studies include testing *in vivo* efficacy of MGB-364 using lower dose of Mtb for infection as well as low (0.5 mg/kg) and high (10 mg/kg) doses of MGB-364 via intranasal and oral routes of administration. We aim to further identify specific targets of these MGB 364 through the

creation of mutant strains and also addressing the possible mechanism by which MGB 364 kills Mtb. The use of extracellular vesicles from Mtb infected macrophages have been reported to carry Mtb RNA that triggers IFN- β signaling pathway as well as improved activity of moxifloxacin when used as an adjunct therapy [48]. It would thus be essential to investigate the signaling pathway triggered by NIVs to elicit an immune response.

To address possible targets for host-directed therapy, the aforementioned CAGE analysis was used to select candidate genes in macrophages that might be used by Mtb to subvert immune responses based on the initial hypothesis. Our initial hypothesis was that Mtb uses or alters M2 transcriptional landscape to hide away from M1 macrophage effector killing. Here we selected IL-4i1, a candidate gene highly upregulated in M2 macrophages. This gene codes for an L-amino acid oxidase and was selected based on its T-cell immunoregulatory properties. We postulated that the enzyme secreted by macrophages, upon release would limit T-cell responses that are responsible for Mtb killing. We used gene deficient mouse models to address the functional role of IL-4i1 during Mtb infection. We first investigated the role of the gene at steady-state and whether gene deletion would not cause any systemic impairments. We used the “reverse F2 strategy” to eliminate the flanking gene confounders. We noticed systemic dysregulation at early generations of mouse breeding which stabilized at F9 congenic background. At F9 we could unprecedentedly show the role of IL-4i1 on activation and proliferation of CD 4 T-cells in spleen and lungs at steady-state *in vivo*. We thus could see that IL-4i1 is important for immune homeostasis and that null mutation or deletion could lead to autoimmunity. These data are indicative of IL-4i1 hypo-mutation as a potential causative of autoimmunity. We then addressed the role of IL-4i1 on infectious immunity during Mtb infection. We showed that IL-4i1 deletion rendered mice resistant to hypervirulent Mtb strain and that the role of IL-4i1 on Mtb infection is at early infection and is associated with macrophage responses not T-cells during acute Mtb infection as initially postulated. We showed that IL-4i1 promotes the recruitment of the M2 macrophage phenotype. These data are in synergy with the previous findings on the role of IL-4i1 in M2 polarization via the IL-4R α signaling and STAT-6 signaling pathways and also the oxidization of L-arginine and L-tryptophan. It has also previously been shown that the M2 macrophage is permissive for Mtb survival. However, it has been shown that the IL-4R α signaling in macrophages *in vivo* has no effect on the outcome of Mtb burden. However, hypervirulent Mtb can induce arginase production to trigger an M2 polarized environment. We thus concluded that Mtb promotes expression of IL-4i1 for its part role in oxidizing L-arginine to produce Arg1 promotes the polarization of M2 phenotype and related immune responses. We thus showed IL-4i1 as

potential target during Mtb infection. Future studies to address the mechanism underlying the role of IL-4i1 during Mtb infection may include transcriptional and metabolomic targeting approaches on the enzymatic activity of IL-4i1 during Mtb infection.

In conclusion, our work provides a framework for possible new drug targets for effective TB therapy, providing a stepping-stone towards the development of new drugs and vaccines. This work thus significantly contributes to combating the world's most prevalent and life-threatening disease, TB.

References

1. WHO. Global Tuberculosis report. 2018.
2. Ismail NA, Mvusi L, Nanoo A, Dreyer A, Omar SV, Babatunde S, et al. Prevalence of drug-resistant tuberculosis and imputed burden in South Africa: a national and sub-national cross-sectional survey. *The Lancet Infectious diseases*. 2018;18(7):779-87.
3. Trofimov V, Costa-Gouveia J, Hoffmann E, Brodin P. Host-pathogen systems for early drug discovery against tuberculosis. *Current opinion in microbiology*. 2017;39:143-51.
4. Guler R, Brombacher F. Host-directed drug therapy for tuberculosis. *Nature Chemical Biology*. 2015;11:748.
5. Laurenzi M, Ginsberg A, Spigelman M. Challenges Associated with Current and Future TB Treatment. *Infectious Disorders - Drug Targets*. 2007;7(2):105-19.
6. Hoagland DT, Liu J, Lee RB, Lee RE. New agents for the treatment of drug-resistant *Mycobacterium tuberculosis*. *Advance Drug Delivery Reviews*. 2016;102:55-72.
7. Zumla A, Nahid P, Cole ST. Advances in the development of new tuberculosis drugs and treatment regimens. *Nature Reviews Drug Discovery*. 2013;12:388.
8. Nicola JM, Gaston KM, Holididy AR. Using Host-Pathogen Functional Interactions for Filtering Potential Drug Targets in *Mycobacterium tuberculosis*. *Mycobacterial Diseases*. 2013;03(02).
9. Mwaba P, McNerney R, Grobusch MP, O'Grady J, Bates M, Kapata N, et al. Achieving STOP TB Partnership goals: perspectives on development of new diagnostics, drugs and vaccines for tuberculosis. *Tropical Medicine & International Health*. 2011;16(7):819-27.
10. Zumla A, Abubakar I, Raviglione M, Hoelscher M, Ditiu L, McHugh TD, et al. Drug-resistant tuberculosis--current dilemmas, unanswered questions, challenges, and priority needs. *Journal of Infectious Diseases*. 2012;205 Suppl 2:S228-40.
11. Brigden G, Hewison C, Varaine F. New developments in the treatment of drug-resistant tuberculosis: clinical utility of bedaquiline and delamanid. *Infection and Drug Resistance*. 2015;8:367-78.
12. Tahlan K, Wilson R, Kastrinsky DB, Arora K, Nair V, Fischer E, et al. SQ109 Targets MmpL3, a Membrane Transporter of Trehalose Monomycolate Involved in Mycolic Acid Donation to the Cell Wall Core of *Mycobacterium tuberculosis*. *Journal Antimicrobial Agents and Chemotherapy*. 2012;56(4):1797-809.
13. Zumla A, Maeurer M, Chakaya J, Hoelscher M, Ntoumi F, Rustomjee R, et al. Towards host-directed therapies for tuberculosis. *Nature reviews Drug discovery*. 2015;14(8):511-2.
14. Zumla A, Consortium ftH-DTN, Maeurer M, Consortium ftH-DTN, Consortium ftH-DTN, Zumla A, et al. Host-Directed Therapies for Tackling Multi-Drug Resistant Tuberculosis: Learning From the Pasteur-Bechamp Debates. *Clinical Infectious Diseases*. 2015;61(9):1432-8.
15. Rangel Moreno J, Estrada Garcia I, De La Luz Garcia Hernandez M, Aguilar Leon D, Marquez R, Hernandez Pando R. The role of prostaglandin E2 in the immunopathogenesis of experimental pulmonary tuberculosis. *Immunology*. 2002;106(2):257-66.
16. Singhal A, Jie L, Kumar P, Hong GS, Leow MK-S, Paleja B, et al. Metformin as adjunct antituberculosis therapy. *Science Translational Medicine*. 2014;6(263):263ra159-263ra159.
17. Parihar SP, Guler R, Khutlang R, Lang DM, Hurdalay R, Mhlanga MM, et al. Statin therapy reduces the mycobacterium tuberculosis burden in human macrophages and in mice by enhancing autophagy and phagosome maturation. *The Journal of infectious diseases*. 2014;209(5):754-63.
18. Mehta S, Mugusi FM, Bosch RJ, Aboud S, Urassa W, Villamor E, et al. Vitamin D status and TB treatment outcomes in adult patients in Tanzania: a cohort study. *BMJ Open*. 2013;3(11):e003703.

19. Kearns MD, Tangpricha V. The role of vitamin D in tuberculosis. *Journal of clinical & translational endocrinology*. 2014;1(4):167-9.
20. Parihar SP, Guler R, Khutlang R, Lang DM, Mhlanga MM, Suzuki H, et al. Statins mediate protection against *Mycobacterium tuberculosis* infection by enhancing phagosomal maturation and autophagy. *Frontiers in Immunology*.
21. Guler R, Mpotje T, Ozturk M, Nono JK, Parihar SP, Chia JE, et al. Batf2 differentially regulates tissue immunopathology in Type 1 and Type 2 diseases. *Mucosal Immunology*. 2018. 12: 390-402.
22. Tamgue O, Gcanga L, Ozturk M, Whitehead L, Pillay S, Jacobs R, et al. Differential Targeting of c-Maf, Bach-1, and Elmo-1 by microRNA-143 and microRNA-365 Promotes the Intracellular Growth of *Mycobacterium tuberculosis* in Alternatively IL-4/IL-13 Activated Macrophages. *Frontiers Immunology*. 2019;10:1-15.
23. Yang X, Yang J, Wang J, Wen Q, Wang H, He J, et al. Microarray analysis of long noncoding RNA and mRNA expression profiles in human macrophages infected with *Mycobacterium tuberculosis*. *Scientific reports*. 2016;6:38963.
24. Khalaf AI, Al-Kadhimi AA, Ali JH. DNA Minor Groove Binders-Inspired by Nature. *Acta chimica Slovenica*. 2016;63(4):689-704.
25. Barrett MP, Gemmell CG, Suckling CJ. Minor groove binders as anti-infective agents. *Pharmacology Therapy*. 2013;139(1):12-23.
26. Suckling CJ, Scott FJ. Selectivity in Anti-infective Minor Groove Binders. 3rd International Electronic Conference on Medicinal Chemistry. 2017.
27. Brown DG, Sanderson MR, Garman E, Neidle S. Crystal structure of a berenilid(CGCAAATTTGCG) complex. *Journal of Molecular Biology*. 1992;226(2):481-90.
28. Barrett M, Gemmel C, Suckling C. Minor groove binders as anti-infective agents. *Pharmacology Therapy*. 2013;139(1):12-23.
29. Scott FJ, Nichol RJO, Khalaf AI, Giordani F, Gillingwater K, Ramu S, et al. An evaluation of Minor Groove Binders as anti-fungal and anti-mycobacterial therapeutics. *European Journal of Medicinal Chemistry*. 2017;136:561-72.
30. Suckling C. From multiply active natural product to candidate drug? Antibacterial (and other) minor groove binders for DNA. *Future Medicinal Chemistry*. 2012;4(8):971-89.
31. Parkinson JA, Scott FJ, Suckling CJ, Wilson G. Exceptionally strong intermolecular association in hydrophobic DNA minor groove binders and their potential therapeutic consequences. *MedChemComm*. 2013;4(7):1105-8.
32. Stead AMW, Bray PG, Edwards IG, DeKoning HP, Elford BC, Stocks PA, et al. Diamidine Compounds: Selective Uptake and Targeting in *Plasmodium falciparum*. *Molecular Pharmacology*. 2001;59(5):1298-306.
33. Werbovets K. Diamidines as antitrypanosomal, antileishmanial and antimalarial agents. *Current Opinions in Investigational Drugs*. 2006;7(2):147-57.
34. Scott FJ, Khalaf AI, Giordani F, Wong PE, Duffy S, Barrett M, et al. An evaluation of Minor Groove Binders as anti-Trypanosoma brucei brucei therapeutics. *European Journal of Medicinal Chemistry*. 2016;116:116-25.
35. Giordani F, Khalaf A, Gillingwater K, Munday J, De Koning H, Suckling C, et al. Novel Minor Groove Binders Cure Animal African Trypanosomiasis in an in Vivo Mouse Model 2019.
36. Scott FJ, Khalaf AI, Duffy S, Avery VM, Suckling CJ. Selective anti-malarial minor groove binders. *Bioorganic and Medicinal Chemistry Letters*. 2016;26(14):3326-9.
37. Del Poeta M, Schell WA, Dykstra CC, Jones S, Tidwell RR, Czarny A, et al. Structure-In Vitro Activity Relationships of Pentamidine Analogues and Dication-Substituted Bis-Benzimidazoles as New Antifungal Agents. *Antimicrobial Agents and Chemotherapy*. 1998;42(10):2495-502.
38. Ge Y, Difuntorum S, Touami S, Critchley I, Burli R, Jiang V, et al. In vitro antimicrobial activity of GSQ1530, a new heteroaromatic polycyclic compound. *Antimicrobial Agents & Chemotherapy*. 2002;46(10):3168-74.

39. Brucoli F, Guzman JD, Maitra A, James CH, Fox KR, Bhakta S. Synthesis, anti-mycobacterial activity and DNA sequence-selectivity of a library of biaryl-motifs containing polyamides. *Bioorganic & Medicinal Chemistry*. 2015;23(13):3705-11.
40. Wilczewska AZ, Niemirowicz K, Markiewicz KH, Car H. Nanoparticles as drug delivery systems. *Pharmacological reports : PR*. 2012;64(5):1020-37.
41. Azad AK, Rajaram MVS, Schlesinger LS. Exploitation of the Macrophage Mannose Receptor (CD206) in Infectious Disease Diagnostics and Therapeutics. *Journal of Cytology & Molecular Biology*. 2014;1(1):1000003.
42. Pandey R, Khuller GK. Antitubercular inhaled therapy: opportunities, progress and challenges. *The Journal of Antimicrobial Chemotherapy*. 2005;55(4):430-5.
43. Silva R, Ferreira H, Cavaco-Paulo A. Sonoproduction of Liposomes and Protein Particles as Templates for Delivery Purposes. *Biomacromolecules*. 2011;12(10):3353-68.
44. Sercombe L, Veerati T, Moheimani F, Wu SY, Sood AK, Hua S. Advances and Challenges of Liposome Assisted Drug Delivery. *Frontiers in Pharmacology*. 2015;6:286-.
45. Movassaghian S, Moghimi HR, Shirazi FH, Koshkaryev A, Trivedi MS, Torchilin VP. Efficient down-regulation of PKC-alpha gene expression in A549 lung cancer cells mediated by antisense oligodeoxynucleotides in dendrosomes. *International Journal of Pharmaceutics*. 2013;441(1-2):82-91.
46. Chono S, Tanino T, Seki T, Morimoto K. Efficient drug targeting to rat alveolar macrophages by pulmonary administration of ciprofloxacin incorporated into mannosylated liposomes for treatment of respiratory intracellular parasitic infections. *Journal of Controlled Release : official journal of the Controlled Release Society*. 2008;127(1):50-8.
47. Pinheiro M, Lucio M, Lima JL, Reis S. Liposomes as drug delivery systems for the treatment of TB. *Nanomedicine (London, England)*. 2011;6(8):1413-28.
48. Cheng Y, Schorey JS. Extracellular vesicles deliver Mycobacterium RNA to promote host immunity and bacterial killing. *EMBO reports*. 2019.
49. Deol P, Khuller GK, Joshi K. Therapeutic efficacies of isoniazid and rifampin encapsulated in lung-specific stealth liposomes against Mycobacterium tuberculosis infection induced in mice. *Antimicrobial Agents & Chemotherapy*. 1997;41(6):1211-4.
50. Pandey R, Sharma S, Khuller GK. Lung specific stealth liposomes as antitubercular drug carriers in guinea pigs. *Indian journal of experimental biology*. 2004;42(6):562-6.
51. Pandey R, Sharma S, Khuller GK. Nebulization of liposome encapsulated antitubercular drugs in guinea pigs. *International journal of antimicrobial agents*. 2004;24(1):93-4.
52. Kumar GP, Rajeshwarrao P. Nonionic surfactant vesicular systems for effective drug delivery—an overview. *Acta Pharmaceutica Sinica B*. 2011;1(4):208-19.
53. Alsaadi M, Italia JL, Mullen A, Kumar MNVR, Candlish AA, Williams R, et al. The efficacy of aerosol treatment with non-ionic surfactant vesicles containing amphotericin B in rodent models of leishmaniasis and pulmonary aspergillosis infection. *Journal of Controlled Release*. 2012;160(3):685-91.
54. Alsaadi M, Italia JL, Mullen AB, Ravi Kumar MN, Candlish AA, Williams RA, et al. The efficacy of aerosol treatment with non-ionic surfactant vesicles containing amphotericin B in rodent models of leishmaniasis and pulmonary aspergillosis infection. *Journal of Controlled Release : official journal of the Controlled Release Society*. 2012;160(3):685-91.
55. Mullen AB, Baillie AJ, Carter KC. Visceral leishmaniasis in the BALB/c mouse: a comparison of the efficacy of a nonionic surfactant formulation of sodium stibogluconate with those of three proprietary formulations of amphotericin B. *Antimicrobial agents and Chemotherapy*. 1998;42(10):2722-5.
56. Akbari V, Abedi D, Pardakhty A, Sadeghi-Aliabadi H. Release Studies on Ciprofloxacin Loaded Non-ionic Surfactant Vesicles. *Avicenna journal of medical biotechnology*. 2015;7(2):69-75.

57. Ernst JD. The immunological life cycle of tuberculosis. *Nature Reviews Immunology*. 2012;12:581.
58. Philips JA, Ernst JD. Tuberculosis Pathogenesis and Immunity. *Annual Review of Pathology: Mechanisms of Disease*. 2012;7(1):353-84.
59. Ahmad S. Pathogenesis, Immunology, and Diagnosis of Latent Mycobacterium tuberculosis Infection. *Clinical and Developmental Immunology*. 2011;2011:17.
60. Silva Miranda M, Breiman A, Allain S, Deknuydt F, Altare F. The Tuberculous Granuloma: An Unsuccessful Host Defence Mechanism Providing a Safety Shelter for the Bacteria? *Clinical and Developmental Immunology*. 2012;2012:14.
61. Cooper AM. Cell-Mediated Immune Responses in Tuberculosis. *Annual Review of Immunology*. 2009;27(1):393-422.
62. Ramakrishnan L. Revisiting the role of the granuloma in tuberculosis. *Nature Reviews Immunology*. 2012;12:352.
63. Rubin EJ. The Granuloma in Tuberculosis — Friend or Foe? *New England Journal of Medicine*. 2009;360(23):2471-3.
64. Kaufmann SHE, Hussey G, Lambert P-H. New vaccines for tuberculosis. *The Lancet*. 2010;375(9731):2110-9.
65. Benoit M, Desnues B, Mege JL. Macrophage polarization in bacterial infections. *Journal of immunology (Baltimore, Md : 1950)*. 2008;181(6):3733-9.
66. Arango Duque G, Descoteaux A. Macrophage Cytokines: Involvement in Immunity and Infectious Diseases 2014. 491 p.
67. Bean AG, Roach DR, Briscoe H, France MP, Korner H, Sedgwick JD, et al. Structural deficiencies in granuloma formation in TNF gene-targeted mice underlie the heightened susceptibility to aerosol Mycobacterium tuberculosis infection, which is not compensated for by lymphotoxin. *Journal of immunology (Baltimore, Md : 1950)*. 1999;162(6):3504-11.
68. Bozzano F, Marras F, De Maria A. Immunology of tuberculosis. *Mediterranean journal of hematology and infectious diseases*. 2014;6(1):e2014027-e.
69. Cooper AM, Dalton DK, Stewart TA, Griffin JP, Russell DG, Orme IM. Disseminated tuberculosis in interferon gamma gene-disrupted mice. *The Journal of Experimental Medicine*. 1993;178(6):2243-7.
70. Cooper AM, Magram J, Ferrante J, Orme IM. Interleukin 12 (IL-12) is crucial to the development of protective immunity in mice intravenously infected with Mycobacterium tuberculosis. *The Journal of Experimental Medicine*. 1997;186(1):39-45.
71. Scanga CA, Mohan VP, Tanaka K, Alland D, Flynn JL, Chan J. The inducible nitric oxide synthase locus confers protection against aerogenic challenge of both clinical and laboratory strains of Mycobacterium tuberculosis in mice. *Infection & Immunity*. 2001;69(12):7711-7.
72. Mattila JT, Ojo OO, Kepka-Lenhart D, Marino S, Kim JH, Eum SY, et al. Microenvironments in tuberculous granulomas are delineated by distinct populations of macrophage subsets and expression of nitric oxide synthase and arginase isoforms. *Journal of Immunology (Baltimore, Md : 1950)*. 2013;191(2):773-84.
73. Garcia I, Guler R, Vesin D, Olleros ML, Vassalli P, Chvatchko Y, et al. Lethal Mycobacterium bovis Bacillus Calmette Guerin infection in nitric oxide synthase 2-deficient mice: cell-mediated immunity requires nitric oxide synthase 2. *Laboratory Investigation; A Journal of Technical Methods and Pathology*. 2000;80(9):1385-97.
74. Carbonnelle-Puscian A, Copie-Bergman C, Baia M, Martin-Garcia N, Allory Y, Haioun C, et al. The novel immunosuppressive enzyme IL41 is expressed by neoplastic cells of several B-cell lymphomas and by tumor-associated macrophages. *Leukemia*. 2009;23(5):952-60.
75. Gordon S. Alternative activation of macrophages. *Nature reviews Immunology*. 2003;3(1):23-35.
76. Lawrence T, Natoli G. Transcriptional regulation of macrophage polarization: enabling diversity with identity. *Nature reviews Immunology*. 2011;11(11):750-61.

77. Gordon S, Martinez FO. Alternative activation of macrophages: mechanism and functions. *Immunity*. 2010;32(5):593-604.
78. Pessanha AP, Martins RA, Mattos-Guaraldi AL, Vianna A, Moreira LO. Arginase- 1 expression in granulomas of tuberculosis patients. *FEMS immunology and medical microbiology*. 2012;66(2):265-8.
79. Pathak SK, Basu S, Basu KK, Banerjee A, Pathak S, Bhattacharyya A, et al. Direct extracellular interaction between the early secreted antigen ESAT-6 of *Mycobacterium tuberculosis* and TLR2 inhibits TLR signaling in macrophages. *Nature Immunology*. 2007;8(6):610-8.
80. Guler R, Parihar SP, Savvi S, Logan E, Schwegmann A, Roy S, et al. IL-4R α -dependent alternative activation of macrophages is not decisive for *Mycobacterium tuberculosis* pathology and bacterial burden in mice. *PloS one*. 2015;10(3):e0121070.
81. The FC, the RP, Clst, Forrest ARR, Kawaji H, Rehli M, et al. A promoter-level mammalian expression atlas. *Nature*. 2014;507:462.
82. Noguchi S, Arakawa T, Fukuda S, Furuno M, Hasegawa A, Hori F, et al. FANTOM5 CAGE profiles of human and mouse samples. *Sci Data*. 2017;4:170112-.
83. Roy S, Schmeier S, Kaczowski B, Arner E, Alam T, Ozturk M, et al. Transcriptional landscape of *Mycobacterium tuberculosis* infection in macrophages. *Scientific reports*. 2018;8(1):6758-.
84. Mason JM, Naidu MD, Barcia M, Porti D, Chavan SS, Chu CC. IL-4-induced gene-1 is a leukocyte L-amino acid oxidase with an unusual acidic pH preference and lysosomal localization. *Journal of Immunology (Baltimore, Md : 1950)*. 2004;173(7):4561-7.
85. Puiffe M-L, Lachaise I, Molinier-Frenkel V, Castellano F. Antibacterial Properties of the Mammalian L-Amino Acid Oxidase IL4I1. *PloS One*. 2013;8(1):e54589.
86. Marquet J, Lasoudris F, Cousin C, Puiffe ML, Martin-Garcia N, Baud V, et al. Dichotomy between factors inducing the immunosuppressive enzyme IL-4-induced gene 1 (IL4I1) in B lymphocytes and mononuclear phagocytes. *European Journal of Immunology*. 2010;40(9):2557-68.
87. Scarlata CM, Celse C, Pignon P, Ayyoub M, Valmori D. Differential expression of the immunosuppressive enzyme IL4I1 in human induced Aiolos⁺, but not natural Helios⁺, FOXP3⁺ Treg cells. *European Journal of Immunology*. 2015;45(2):474-9.
88. Santarlaschi V, Maggi L, Mazzoni A, Capone M, Querci V, Rossi MC, et al. IL-4-induced gene 1 maintains high Tob1 expression that contributes to TCR unresponsiveness in human T helper 17 cells. *European Journal of Immunology*. 2014;44(3):654-61.
89. Boulland ML, Marquet J, Molinier-Frenkel V, Moller P, Guiter C, Lasoudris F, et al. Human IL4I1 is a secreted L-phenylalanine oxidase expressed by mature dendritic cells that inhibits T-lymphocyte proliferation. *Blood*. 2007;110(1):220-7.
90. Lasoudris F, Cousin C, Prevost-Blondel A, Martin-Garcia N, Abd-Alsamad I, Ortonne N, et al. IL4I1: an inhibitor of the CD8⁺ antitumor T-cell response in vivo. *European Journal of Immunology*. 2011;41(6):1629-38.
91. Cousin C, Aubatin A, Le Gouvello S, Apetoh L, Castellano F, Molinier-Frenkel V. The immunosuppressive enzyme IL4I1 promotes FoxP3(+) regulatory T lymphocyte differentiation. *European Journal of Immunology*. 2015;45(6):1772-82.
92. Yue Y, Huang W, Liang J, Guo J, Ji J, Yao Y, et al. IL4I1 Is a Novel Regulator of M2 Macrophage Polarization That Can Inhibit T Cell Activation via L-Tryptophan and Arginine Depletion and IL-10 Production. *PloS One*. 2015;10(11):e0142979-e.
93. Bod L, Douguet L, Auffray C, Lengagne R, Bekkat F, Rondeau E, et al. IL-4-Induced Gene 1: A Negative Immune Checkpoint Controlling B Cell Differentiation and Activation. *Journal of Immunology (Baltimore, Md : 1950)*. 2018;200(3):1027-38.
94. Bod L, Lengagne R, Wrobel L, Ramspott JP, Kato M, Avril MF, et al. IL4-induced gene 1 promotes tumor growth by shaping the immune microenvironment in melanoma. *Oncoimmunology*. 2017;6(3):e1278331.

95. Psachoulia K, Chamberlain KA, Heo D, Davis SE, Paskus JD, Nanescu SE, et al. IL41 augments CNS remyelination and axonal protection by modulating T cell driven inflammation. *Brain : A Journal of Neurology*. 2016;139(Pt 12):3121-36.
96. Scott-Browne JP, Shafiani S, Tucker-Heard Gs, Ishida-Tsubota K, Fontenot JD, Rudensky AY, et al. Expansion and function of Foxp3-expressing T regulatory cells during tuberculosis. *The Journal of Experimental Medicine*. 2007;204(9):2159-69.
97. Molinier-Frenkel V, Mestivier D, Castellano F. Alterations of the immunosuppressive IL41 enzyme activity induced by naturally occurring SNP/mutations. *Genes And Immunity*. 2015;17:148.
98. WHO. Global tuberculosis report 2016. Geneva: World Health Organization.
99. WHO. Global tuberculosis report 2015. Geneva: World Health Organization.
100. Murray S, Mendel C, Spigelman M. TB Alliance regimen development for multidrug-resistant tuberculosis. *The International Journal of Tuberculosis and Lung Disease*. 2016;20(12):S38-S41.
101. Zuniga ES, Early J, Parish T. The future for early-stage tuberculosis drug discovery. *Future Microbiology*. 2015;10(2):217-29.
102. Pai M, Behr MA, Dowdy D, Dheda K, Divangahi M, Boehme CC, et al. Tuberculosis. *Nature Reviews Disease Primers*. 2016;2:16076.
103. Mdluli K, Kaneko T, Upton A. The tuberculosis drug discovery and development pipeline and emerging drug targets. *Cold Spring Harbor Perspectives in Medicine*. 2015;5(6).
104. Pethe K, Bifani P, Jang J, Kang S, Park S, Ahn S, et al. Discovery of Q203, a potent clinical candidate for the treatment of tuberculosis. *Nature Medicine*. 2013;19(9):1157-60.
105. Makarov V, Manina G, Mikusova K, Mollmann U, Ryabova O, Saint-Joanis B, et al. Benzothiazinones kill Mycobacterium tuberculosis by blocking arabinan synthesis. *Science*. 2009;324(5928):801-4.
106. Suckling CJ. Molecular recognition and physicochemical properties in the discovery of selective antibacterial minor groove binders. *Journal of Physical Organic Chemistry*. 2008;21(7-8):575-83.
107. Edwards KJ, Jenkins TC, Neidle S. Crystal structure of a pentamidine-oligonucleotide complex: implications for DNA-binding properties. *Biochemistry*. 1992;31(31):7104-9.
108. Fox KR, Sansom CE, Stevens MFG. Footprinting studies on the sequence-selective binding of pentamidine to DNA. *FEBS Letters*. 1990;266(1-2):150-4.
109. Brown DG, Sanderson MR, Garman E, Neidle S. Crystal structure of a berenilid(CGCAAATTTGCG) complex. *Journal of Molecular Biology*. 1992;226(2):481-90.
110. Paine MF, Wang MZ, Generaux CN, Boykin DW, Wilson WD, De Koning HP, et al. Diamidines for human African trypanosomiasis. *Current Opinion Investigational Drugs*. 2010;11(8):876-83.
111. Scott FJ, Khalaf AI, Giordani F, Wong PE, Duffy S, Barrett M, et al. An evaluation of Minor Groove Binders as anti-Trypanosoma brucei brucei therapeutics. *European Journal of Medicinal Chemistry*. 2016;116:116-25.
112. Tao B, Huang TL, Zhang Q, Jackson L, Queener SF, Donkor IO. Synthesis and anti-Pneumocystis carinii activity of conformationally restricted analogues of pentamidine. *European Journal of Medicinal Chemistry*. 1999;34(6):531-8.
113. Khalaf AI, Bourdin C, Breen D, Donoghue G, Scott FJ, Suckling CJ, et al. Design, synthesis and antibacterial activity of minor groove binders: the role of non-cationic tail groups. *European Journal of Medicinal Chemistry*. 2012;56:39-47.
114. Khalaf AI, Anthony N, Breen D, Donoghue G, Mackay SP, Scott FJ, et al. Amide isosteres in structure-activity studies of antibacterial minor groove binders. *European Journal of Medicinal Chemistry*. 2011;46(11):5343-55.
115. Ravic M, Firmin D, Sahgal O, van den Berg F, Suckling CJ, Hunter IS. A Single-Centre, Double-Blind, Placebo-Controlled Study in Healthy Men to Assess the Safety and Tolerability of Single and Repeated Ascending Doses of MGB-BP-3, a New Class of

Antibacterial Agent. American Society of Microbiology Microbe Meeting, Boston, Massachusetts. 2016.

116. Scott FJ, Nichol RJ, Khalaf AI, Giordani F, Gillingwater K, Ramu S, et al. An evaluation of minor groove binders as anti-fungal and anti-mycobacterial therapeutics. *European Journal of Medicinal Chemistry*. 2017;136:561-72.

117. Gulbay BE, Gurkan OU, Yildiz OA, Onen ZP, Erkekol FO, Baccioglu A, et al. Side effects due to primary antituberculosis drugs during the initial phase of therapy in 1149 hospitalized patients for tuberculosis. *Respiratory Medicine*. 2006;100(10):1834-42.

118. Pelgrift RY, Friedman AJ. Nanotechnology as a therapeutic tool to combat microbial resistance. *Advance Drug Delivery Reviews*. 2013;65(13-14):1803-15.

119. Gaidukevich SK, Mikulovich YL, Smirnova TG, Andreevskaya SN, Sorokoumova GM, Chernousova LN, et al. Antibacterial Effects of Liposomes Containing Phospholipid Cardioplipin and Fluoroquinolone Levofloxacin on Mycobacterium tuberculosis with Extensive Drug Resistance. *Bulletin of Experimental Biology and Medicine*. 2016;160(5):675-8.

120. Sohrabi S, Haeri A, Mahboubi A, Mortazavi A, Dadashzadeh S. Chitosan gel-embedded moxifloxacin niosomes: An efficient antimicrobial hybrid system for burn infection. *International Journal of Biological Macromolecules*. 2016;85:625-33.

121. Imran M, Shah MR, Ullah F, Ullah S, Elhissi AM, Nawaz W, et al. Glycoside-based niosomal nanocarrier for enhanced in-vivo performance of Cefixime. *International Journal of Pharmacology*. 2016;505(1-2):122-32.

122. Mehta SK, Jindal N. Tyloxapol niosomes as prospective drug delivery module for antiretroviral drug nevirapine. *AAPS PharmSciTech*. 2015;16(1):67-75.

123. Hari BN, Chitra KP, Bhimavarapu R, Karunakaran P, Muthukrishnan N, Rani BS. Novel technologies: A weapon against tuberculosis. *Indian Journal of Pharmacology*. 2010;42(6):338-44.

124. Andreu N, Fletcher T, Krishnan N, Wiles S, Robertson BD. Rapid measurement of antituberculosis drug activity in vitro and in macrophages using bioluminescence. *Journal of Antimicrobial Chemotherapy*. 2011;67(2):404-14.

125. Collins LA, Torrero MN, Franzblau SG. Green fluorescent protein reporter microplate assay for high-throughput screening of compounds against Mycobacterium tuberculosis. *Antimicrobial Agents Chemother*. 1998;42(2):344-7.

126. Salie S, Hsu NJ, Semanya D, Jardine A, Jacobs M. Novel non-neuroleptic phenothiazines inhibit Mycobacterium tuberculosis replication. *Journal of Antimicrobial Chemotherapy*. 2014;69(6):1551-8.

127. Schwegmann A, Guler R, Cutler AJ, Arendse B, Horsnell WG, Flemming A, et al. Protein kinase C delta is essential for optimal macrophage-mediated phagosomal containment of Listeria monocytogenes. *Proceedings of the National Academy of Sciences of the United States of America*. 2007;104(41):16251-6.

128. Hughes JP, Rees S, Kalindjian SB, Philpott KL. Principles of early drug discovery. *British journal of pharmacology*. 2011;162(6):1239-49.

129. Changsen C, Franzblau SG, Palittapongarnpim P. Improved green fluorescent protein reporter gene-based microplate screening for antituberculosis compounds by utilizing an acetamidase promoter. *Antimicrobial Agents & Chemotherapy*. 2003;47(12):3682-7.

130. Fuchs JE, Spitzer GM, Javed A, Biela A, Kreutz C, Wellenzohn B, et al. Minor groove binders and drugs targeting proteins cover complementary regions in chemical shape space. *Journal of Chemical Information and Modelling*. 2011;51(9):2223-32.

131. Rajera R, Nagpal K, Singh SK, Mishra DN. Niosomes: a controlled and novel drug delivery system. *Biological and Pharm aceutical Bulletin*. 2011;34(7):945-53.

132. Cortesi R, Romagnoli R, Menegatti E, Esposito E, Cervellati F, Nastruzzi C. Liposomes containing distamycins: preparation, characterization and antiproliferative activity. *Drug Delivery*. 2004;11(2):83-8.

133. Carter KC, Mullen AB, Sundar S, Kenney RT. Efficacies of vesicular and free sodium stibogluconate formulations against clinical isolates of *Leishmania donovani*. *Antimicrobial Agents & Chemotherapy*. 2001;45(12):3555-9.
134. Williams D, Mullen AB, Baillie AJ, Carter KC. Comparison of the efficacy of free and non-ionic-surfactant vesicular formulations of paromomycin in a murine model of visceral leishmaniasis. *Journal of Pharmacy and Pharmacology*. 1998;50(12):1351-6.
135. Nieto J, Alvar J, Mullen AB, Carter KC, Rodriguez C, San Andres MI, et al. Pharmacokinetics, toxicities, and efficacies of sodium stibogluconate formulations after intravenous administration in animals. *Antimicrobial Agents & Chemotherapy*. 2003;47(9):2781-7.
136. Hlaka L, Rosslee MJ, Ozturk M, Kumar S, Parihar SP, Brombacher F, et al. Evaluation of minor groove binders (MGBs) as novel anti-mycobacterial agents and the effect of using non-ionic surfactant vesicles as a delivery system to improve their efficacy. *The Journal of Antimicrobial Chemotherapy*. 2017;72(12):3334-41.
137. Ferguson LR, Denny WA. Genotoxicity of non-covalent interactions: DNA intercalators. *Mutation Research*. 2007;623(1-2):14-23.
138. Bonin AM, Banks TM, Campbell JJ, Glover SA, Hammond GP, Prakash AS, et al. Mutagenicity of electrophilic N-acyloxy-N-alkoxyamides. *Mutation Research*. 2001;494(1-2):115-34.
139. Snyder RD, Brown JE. Evidence for and role of the dimethylamino group in tamoxifen DNA intercalation in intact Chinese hamster V79 cells. *Drug and Chemical Toxicology*. 2002;25(4):473-9.
140. Snyder RD, Hendry LB. Toward a greater appreciation of noncovalent chemical/DNA interactions: Application of biological and computational approaches. *Environmental and Molecular Mutagenesis*. 2005;45(2-3):100-5.
141. Störl K, Störl J, Zimmer C, Lown JW. Minor-groove binders are inhibitors of the catalytic activity of DNA gyrases. *FEBS Letters*. 1993;317(1):157-62.
142. Cho KH, Pezzuto JM, Bolton JL, Steele VE, Kelloff GJ, Lee SK, et al. Selection of cancer chemopreventive agents based on inhibition of topoisomerase II activity. *European Journal of Cancer (Oxford, England : 1990)*. 2000;36(16):2146-56.
143. Nikolova T, Dvorak M, Jung F, Adam I, Kramer E, Gerhold-Ay A, et al. The gammaH2AX assay for genotoxic and nongenotoxic agents: comparison of H2AX phosphorylation with cell death response. *Toxicological sciences : an official journal of the Society of Toxicology*. 2014;140(1):103-17.
144. Banath JP, Olive PL. Expression of phosphorylated histone H2AX as a surrogate of cell killing by drugs that create DNA double-strand breaks. *Cancer Research*. 2003;63(15):4347-50.
145. Wang J, He L, Fan D, Ding D, Wang X, Gao Y, et al. Establishment of a gamma-H2AX foci-based assay to determine biological dose of radon to red bone marrow in rats. *Scientific reports*. 2016;6:30018.
146. Patil J, Devi V, Devi K, Sarasija S. A novel approach for lung delivery of rifampicin-loaded liposomes in dry powder form for the treatment of tuberculosis. *Lung India*. 2015;32(4):331-8.
147. Gelperina S, Kisich K, Iseman MD, Heifets L. The Potential Advantages of Nanoparticle Drug Delivery Systems in Chemotherapy of Tuberculosis. *American Journal of Respiratory and Critical Care Medicine*. 2005;172(12):1487-90.
148. Pandey R, Khuller GK. Solid lipid particle-based inhalable sustained drug delivery system against experimental tuberculosis. *Tuberculosis (Edinburgh, Scotland)*. 2005;85(4):227-34.
149. Bhardwaj A, Grobler A, Rath G, Goyal AK, Jain AK, Mehta A. Pulmonary Delivery of Anti-Tubercular Drugs Using Ligand Anchored pH Sensitive Liposomes for the Treatment of Pulmonary Tuberculosis. *Current Drug Delivery*. 2016;13(6):909-22.
150. Costa-Gouveia J, Pancani E, Jouny S, Machelart A, Delorme V, Salzano G, et al. Combination therapy for tuberculosis treatment: pulmonary administration of ethionamide and booster co-loaded nanoparticles. *Scientific reports*. 2017;7(1):5390.

151. Parihar SP, Ozturk M, Marakalala MJ, Loots DT, Hurdal R, Maasdorp DB, et al. Protein kinase C-delta (PKCdelta), a marker of inflammation and tuberculosis disease progression in humans, is important for optimal macrophage killing effector functions and survival in mice. *Mucosal Immunology*. 2018;11(2):496-511.
152. Tronde A, Norden B, Marchner H, Wendel AK, Lennernas H, Bengtsson UH. Pulmonary absorption rate and bioavailability of drugs in vivo in rats: structure-absorption relationships and physicochemical profiling of inhaled drugs. *Journal of Pharmaceutical Sciences*. 2003;92(6):1216-33.
153. Rosada RS, Torre LGdl, Frantz FG, Trombone AP, Zárate-Bladés CR, Fonseca DM, et al. Protection against tuberculosis by a single intranasal administration of DNA-hsp65 vaccine complexed with cationic liposomes. *BMC Immunology*. 2008;9(1):38.
154. Pandey R, Sharma A, Zahoor A, Sharma S, Khuller GK, Prasad B. Poly (DL-lactide-co-glycolide) nanoparticle-based inhalable sustained drug delivery system for experimental tuberculosis. *The Journal of Antimicrobial Chemotherapy*. 2003;52(6):981-6.
155. Loos U, Musch E, Jensen JC, Mikus G, Schwabe HK, Eichelbaum M. Pharmacokinetics of oral and intravenous rifampicin during chronic administration. *Klinische Wochenschrift*. 1985;63(23):1205-11.
156. Fremont CM, Togbe D, Doz E, Rose S, Vasseur V, Maillet I, et al. IL-1 receptor-mediated signal is an essential component of MyD88-dependent innate response to *Mycobacterium tuberculosis* infection. *Journal of Immunology (Baltimore, Md : 1950)*. 2007;179(2):1178-89.
157. Khader SA, Partida-Sanchez S, Bell G, Jelley-Gibbs DM, Swain S, Pearl JE, et al. Interleukin 12p40 is required for dendritic cell migration and T cell priming after *Mycobacterium tuberculosis* infection. *The Journal of Experimental Medicine*. 2006;203(7):1805-15.
158. Surh CD, Sprent J. Homeostasis of Naive and Memory T Cells. *Immunity*. 2008;29(6):848-62.
159. Bourgeois C, Stockinger B. T cell homeostasis in steady state and lymphopenic conditions. *Immunology Letters*. 2006;107(2):89-92.
160. Boyman O, Krieg C, Homann D, Sprent J. Homeostatic maintenance of T cells and natural killer cells. *Cellular and molecular life sciences : CMLS*. 2012;69(10):1597-608.
161. Murphy KM, Reiner SL. The lineage decisions of helper T cells. *Nature Reviews Immunology*. 2002;2:933.
162. Shen H, Yin C, Gao Y-N, Pei X-Y, Sun X-Y, Ge Q, et al. Recirculating Th2 cells induce severe thymic dysfunction via IL-4/STAT6 signaling pathway. *Biochemical and Biophysical Research Communications*. 2018;501(1):320-7.
163. Andersen MH. The specific targeting of immune regulation: T-cell responses against Indoleamine 2,3-dioxygenase. *Cancer Immunology Immunotherapy*. 2012;61(8):1289-97.
164. Chu CC, Paul WE. Fig1, an interleukin 4-induced mouse B cell gene isolated by cDNA representational difference analysis. *Proceedings of the National Academy of Sciences of the United States of America*. 1997;94(6):2507-12.
165. Aubatin A, Sako N, Decrouy X, Donnadié E, Molinier-Frenkel V, Castellano F. IL4-induced gene 1 is secreted at the immune synapse and modulates TCR activation independently of its enzymatic activity. *European Journal of Immunology*. 2018;48(1):106-19.
166. Eisener-Dorman AF, Lawrence DA, Bolivar VJ. Cautionary insights on knockout mouse studies: the gene or not the gene? *Brain, Behavior, and Immunity*. 2009;23(3):318-24.
167. Wolfer DP, Crusio WE, Lipp H-P. Knockout mice: simple solutions to the problems of genetic background and flanking genes. *Trends in neurosciences*. 2002;25(7):336-40.
168. Lusic AJ, Yu J, Wang SS. The problem of passenger genes in transgenic mice. *Arteriosclerosis, thrombosis, and vascular biology*. 2007;27(10):2100-3.
169. Sekiya T, Yoshimura A. *In Vitro Th Differentiation Protocol* 2015. 183-91 p.

170. Traba J, Miozzo P, Akkaya B, Pierce SK, Akkaya M. An Optimized Protocol to Analyze Glycolysis and Mitochondrial Respiration in Lymphocytes. *Journal of visualized experiments : JoVE*. 2016;(117):54918.
171. Buck MD, O'Sullivan D, Pearce EL. T cell metabolism drives immunity. *The Journal of Experimental Medicine*. 2015;212(9):1345-60.
172. Loftus RM, Finlay DK. Immunometabolism: Cellular Metabolism Turns Immune Regulator. *The Journal of Biological Chemistry*. 2016;291(1):1-10.
173. Howie D, Waldmann H, Cobbold S. Nutrient Sensing via mTOR in T Cells Maintains a Tolerogenic Microenvironment. *Frontiers in Immunology*. 2014;5:409-.
174. Ramsay G, Cantrell D. Environmental and Metabolic Sensors That Control T Cell Biology. 2015;6(99).
175. O'Neill LAJ, Kishton RJ, Rathmell J. A guide to immunometabolism for immunologists. *Nature Reviews Immunology*. 2016;16:553.
176. Marino S, Cilfone NA, Mattila JT, Linderman JJ, Flynn JL, Kirschner DE. Macrophage Polarization Drives Granuloma Outcome during Mycobacterium tuberculosis Infection. *Infection and Immunity*. 2015;83(1):324.
177. Monin L, Griffiths KL, Lam WY, Gopal R, Kang DD, Ahmed M, et al. Helminth-induced arginase-1 exacerbates lung inflammation and disease severity in tuberculosis. *The Journal of Clinical Investigations*. 2015;125(12):4699-713.

Appendix

List of FACS and ELISA antibodies used

Antibody	Conjugate	Type	Company	Catalogue number	Dilution used
CD3	A700	Hamster anti-mouse	BD Biosciences	557984	1:160 of 0.2 mg/ml
CD4	FITC	Rat anti-mouse	BioLegend	100510	1:640 of 0.5mg/ml
CD8	V500	Rat anti-mouse	BD Biosciences	560776	1:320 of 0.2mg/ml
CD11b	V450	Rat anti-mouse	BD Biosciences	560455	1:640 of 0.2mg/ml
CD11c	A700	Hamster anti-mouse	BD Biosciences	560583	1:320 of 0.2mg/ml
F4/80	PE-cy7	Rat anti-mouse	Affymetrix eBioscience	25-4801-82	1:320 of 0.2mg/ml
Siglec-F	APC	Rat anti-mouse	BD Biosciences	562680	1:160 of 0.2mg/ml
Ly6G	APC-Cy7	Rat anti-mouse	Sony Biotechnology Inc	1238120	1:640 of 100µg/ml
IL-4i1	Polyclonal	Rabbit anti-goat	BD Biosciences	553081	1:320 of 0.2mg/ml
Foxp3	APC	Rat anti-mouse	BD Pharmigen	560401	1:50 of 0.5mg/ml
CD19	PercCP-cy 5.5	Rat anti-mouse	BD Pharmigen	551001	1:640 of 0.5mg/ml
CD62L	V450	Rat anti-mouse	BD eBioscience	560507	1:640 of 0.5mg/ml
CD4	PercCP-cy 5.5	Rat anti-mouse	BD Pharmigen	5530252	1:640 of 0.5mg/ml
CD44	FITC	Rat anti-mouse	BD Biosciences	553133	1:640 of 0.5mg/ml
Ki67	PE	Mouse anti-human	BD Biosciences	556027	1:50
MHC II	A700	Anti-mouse	eBiosciences	565321	1:640
CD4	PE	Anti-mouse	eBiosciences	120041-82	1:640

Ly6C	PercCP-cy 5.5	Rat anti-mouse	BD Pharmigen	560525	1:160
CD11c	APC	Hamster anti-mouse	BD Pharmigen	550261	1:320
Siglec F	APC-cy7	Rat anti-mouse	BD Biosciences	565527	1:320
Ly6G	FITC		BD Pharmigen	551460	1:320
Streptavidin	Texas Red		BD Biosciences	562284	1:1000
CD103	PE		BD Biosciences		1:160
NK.1.1	APC-cy7	Mouse anti-mouse	BD Biosciences	560618	1:160
CD 206	FITC	Anti-mouse	Biolegend	141703	
CD11b	PercCP-cy 5.5	Rat anti-mouse	BD Pharmigen	5509993	
CD80	V450		BD Horizon	566285	

Cytokine or antibody		Company	Catalogue number	Dilution used	Clone
IFN-gamma	Primary	Home-made (UCT)		1:500 Of 3.4782 mg/ml	AN18.KL6
	secondary	BD	554410	1:1000 Of 0.5mg/ml	
	Standard	BD	554587	200ng/ml	
TNF-alpha	Primary	BD	551225	1:500 of 0.5mg/ml	
	secondary	PharMingen	1B122D	1:500 Of 0.5mg/ml	
	Standard	BD Bioscience	554589	200ng/ml	
TGF-beta	Primary	BD	555052	1:250 Of 0.5mg/ml	A75-2
	secondary	BD	555053	1:500 Of 0.5mg/ml	A75-3
	Standard	WhitSci	240-B-002	100ng/ml	

IL-1 alpha	Primary	BD	550604	1:250 Of 0.5mg/ml	
	secondary	BD	550606	1:500 Of 0.5mg/ml	
	Standard	WhitSci	400-ML-005	100ng/ml	
IL-1 beta	Primary	R&D systems			
	secondary	R&D systems			
	Standard	R&D systems			
	Primary	Home-made (UCT)		1:500 Of 2.065mg/ml	11B11
IL-4	secondary	BD	554390	1:1000 Of 0.5mg/ml	
	Standard	BD	550067	100ng/ml	
	Primary	BD	554400	:1:250 Of 0.5mg/ml	
IL-6	secondary	BD	554402	1:500 Of 0.5mg/ml	
	Standard	BD Bioscience	554582	100ng/ml	
	Primary	WhitSci	MAB417-500	1:500 Of 500µg	JES052A5
IL-10	secondary	Biocom Biotech	504906	1:1000	
	Standard	WhitSci	417-ML-005	100ng/ml	
	Primary	Biolegend	506902	1/500 Of 500µg	
IL-17	secondary	Biolegend	507022	1/500 Of 50µg	
	Standard	WhitSci	421-ML-025	100ng/ml	
IL-12p40	secondary				
	Standard	R&D systems	49-ML-025		
	Primary				
IL-12p70	secondary				

	Standard	BD	554592		
	Primary				